Natural Dynamics of Spin Chains

Rebecca Juliane Helena Ronke

Submitted for the Degree of

PhD

University of York

Department of Physics

February 2012

Abstract

In this thesis, we discuss the natural dynamics of spin chains with regards to their potential role as information carriers in quantum computers and also standalone uses in a quantum computational context. We discuss a range of spin chain devices, expanding existing results on linear chains and simple branched devices to more complex geometries and circular devices. Over the course of this work, we analyse requirements and feasibility of perfect state transfer using the natural dynamics of spin chains and present an extensive investigation into the effects of a number of perturbations on the dynamics of these devices. This includes both fabrication defects and other sources of perturbations. We also present other potential uses of spin chains, including state storage, and introduce an original protocol for the generation of cluster state ladders using only a single linear spin chain.

Contents

List of Figures

Declarations

I declare that the work presented in this thesis, except where otherwise stated, is based on my own research and has not been submitted previously for a degree in this or any other university. Parts of the work reported in this thesis have been published in:

R. Ronke, T. P. Spiller and I. D'Amico, "Effect of perturbations on information transfer in spin chains", *Phys. Rev. A* **83**, 012325 (2011)

R. Ronke, T. P. Spiller and I. D'Amico, "Long-range interactions and information transfer in spin chains", *J. Phys.: Conf. Ser.* **286**, 012020 (2011)

R. Ronke, I. D'Amico and T. P. Spiller, "Knitting distributed cluster state ladders with spin chains", *Phys. Rev. A* **84**, 032308 (2011)

Signed
Rebecca Ronke

Chapter 1

Introduction

The focus of this thesis is spin chains and their potential for quantum communication and other tasks in quantum computing. In this chapter, we will start by giving a brief introduction to the wider field of quantum information and define the tools used throughout this work as well as the mathematical framework supporting them. We will then introduce spin chains, including the mathematical objects used to describe and define them, as well as the general set-up and the fundamental assumptions made throughout this work. Finally, we will give an outline of this thesis.

1.1 Quantum Information

Quantum information, despite the recent focus on it, is in fact a much older research field than one might think. Dating back to the 1930s, most notably to John von Neumann's fundamental contribution to the mathematical foundations of quantum mechanics [1], quantum information has continually advanced and branched out. Most contemporary work is however based on results from the 1980s onwards (see for example [2] for a concise summary of applications and realisations). There are many different aspects to the wider field of quantum information, ranging from foundations of quantum mechanics and fundamental measurement questions to relatively new subjects, such as quantum money [3] or quantum games [4–6]. Some of the most famous quantum information results are in fact algorithms, such as Shor's algorithm for the factorisation of integer numbers [7], the Deutsch-Jozsa algorithm for black box query problems [8] or Grover's search algorithm [9], to name but a few. Other well-known and even implemented quantum information protocols include quantum teleportation [10], which was demonstrated experimentally as early as 1997 [11–13]. In this work, we are interested in the transport and evolu-

tion of quantum information. We will therefore first of all present some of the background of our work and then define ways of quantifying and measuring information.

1.1.1 Background

The mathematical background of quantum information is varied and vast, encompassing a plenitude of ideas and approaches, as well as many equivalent definitions. As such, it is impossible to give a self-contained and complete account of the results and concepts which were needed to make the present work possible – this is a project vast enough to merit a thesis in its own right. Instead, we will limit ourselves to introducing the tools we will be mentioning in the following chapters of this work and complete the picture where needed.

1.1.1.1 Basic definitions

Throughout this work, we will be dealing with finite dimensional systems only, such that we can neglect any special cases and problems arising in infinite dimensions. In particular, we will be working in a Hilbert space $\mathfrak{H}$, a finite dimensional complex vector space defined with the inner product $\langle \cdot | \cdot \rangle$: If $|\phi\rangle, |\psi\rangle \in \mathfrak{H}$ with $|\phi\rangle = \sum_{i=1}^{2^N} c_i |\phi_i\rangle$ and $|\psi\rangle = \sum_{i=1}^{2^N} d_i |\psi_i\rangle$, then $\langle \phi | \psi \rangle = \sum_{i=1}^{2^N} c_i^* d_i$ [14]. Since we will be dealing with systems containing a finite number N of spin-half particles which represent qubits, we have

$$\mathfrak{H} = \mathbb{C}^{2^N} = \bigotimes_{i=1}^{N} \mathbb{C}^2.$$

The dimension of the full Hilbert space is therefore 2^N. Each of the N copies of $\mathbb{C}^2$ has a basis $\left\{ \begin{pmatrix} 1 \\ 0 \end{pmatrix}, \begin{pmatrix} 0 \\ 1 \end{pmatrix} \right\}$. According to a postulate of quantum mechanics, a pure **state** of a quantum system is described by a unit vector in a Hilbert space $\mathfrak{H}$. In more general terms, any state is represented by an operator $\rho : \mathfrak{H} \to \mathfrak{H}$, such that $tr(\rho) = 1$ and $\langle \phi | \rho \phi \rangle \geq 0$ for all elements $|\phi\rangle \in \mathfrak{H}$. We will also refer to ρ as the **density matrix** representing a state.

1.1.1.2 Types of states

There are different types of states and to distinguish between them, we introduce now some notation commonly used in quantum information. We will write a state $|\phi\rangle$ in the Hilbert space $\mathfrak{H}$ as defined above by using the conventional $|0\rangle \equiv \begin{pmatrix} 1 \\ 0 \end{pmatrix}$ and $|1\rangle \equiv \begin{pmatrix} 0 \\ 1 \end{pmatrix}$, with $|\phi\rangle = |q_1\rangle \otimes |q_2\rangle \otimes \cdots \otimes |q_N\rangle \equiv |q_1 q_2 \cdots q_N\rangle$

and $q_i \in \{0, 1\}$ (see [14] for a definition of the tensor product). In this notation, we will refer to the subscripts i as the **sites** of a device, such that a device contains N sites. If the state of a site i is $|1\rangle$, we will say that this site contains an excitation or that it is excited. An arbitrary state of a spin chain containing a qubit at each site can be written as $|\psi\rangle = \sum_{i=1}^{2^N} c_i |\phi_i\rangle$ (with $c_i \in \mathbb{C}$). We require, without exception, that $|\psi\rangle$ be a unit vector, such that $\langle\psi|\psi\rangle = 1$ or equivalently $\sum_{i=1}^{2^N} |c_i|^2 = 1$ (the normalisation condition) [1]. We will also make the assumption that a chain can always be initialised in a certain pure state, which then evolves, although there has also been research into transfer without initialisation [15–17].

States of quantum mechanical systems such as the ones we will be dealing with have a number of properties, the most important of which we will list below.

- **Pure state:** Using the density matrix ρ (as defined above in section 1.1.1.1) to define a state, we say that this state is pure if and only if $\text{tr}(\rho^2) = 1$. There are many equivalent definitions of pure states, but for our purposes this one is clearest. If the state of a site i is pure, we can write $|\psi_i\rangle = \alpha|0\rangle + \beta|1\rangle$ (with $\alpha, \beta \in \mathbb{C}$ and $|\alpha|^2 + |\beta|^2 = 1$).

- **Mixed state:** If a state is not pure, i.e., $\text{tr}(\rho^2) < 1$, it is said to be mixed. A state is maximally mixed when $\text{tr}(\rho^2)$ achieves a minimum.

- **Superposition of states:** In contrast to mixed states, which are also known as statistical mixtures, superpositions of states are linear combinations of pure states only. As such, any superposition of pure states is also a pure state itself. A famous example is the so-called cat-state (after Schrödinger's cat), $|\psi\rangle = \frac{1}{\sqrt{2}} (|0\cdots0\rangle + |1\cdots1\rangle)$.

- **Product states:** For a system A described by the state $|\psi\rangle_A$ and a system B described by the state $|\psi\rangle_B$, the total state describing both systems is the product state $|\psi\rangle = |\psi\rangle_A \otimes |\psi\rangle_B$. In terms of Hilbert spaces, if $|\psi\rangle_A \in \mathfrak{H}_A$ and $|\psi\rangle_B \in \mathfrak{H}_B$, then $|\psi\rangle \in \mathfrak{H}_{AB} \equiv \mathfrak{H}_A \otimes \mathfrak{H}_B$.

- **Entangled states:** If a state describing two systems A and B cannot be written as a product state (as above), it is entangled.

Entangled states are an important resource in quantum information as they represent the most crucial component in the vast majority of quantum protocols, be it quantum teleportation or any of the algorithms mentioned earlier. As such, we will now present the measures we use to determine the amount of entanglement in a system, but also some other measures that allow us to quantify the quality of information transport and general behaviour of a system.

1.1.2   Measures of information transport quality

Determining the properties of a quantum system is crucial for our aim to quantify the aptitude and capacities of spin chains as quantum computational devices. In the following chapters, we will be interested in the ability of spin chains to reliably transfer information, encoded in states, as well as their ability to generate specific states. As such, we will need some measures to determine to what extend a system is in a desired state, or alternatively some way of indicating what the state of the system is in general.

1.1.2.1   Fidelity

One of the most commonly used measures of information transport quality is the state fidelity. State fidelity, or the fidelity of state vectors, is a comparison of an initial state $|\psi_{initial}\rangle$ and a desired state $|\psi_{desired}\rangle$ after a time t. We therefore define the fidelity F of $|\psi_{initial}\rangle$ with respect to $|\psi_{desired}\rangle$ as [18]

$$F = |\langle \psi_{desired}|e^{-i\widehat{\mathscr{H}}t/\hbar}|\psi_{initial}\rangle|^2 \qquad (1.1)$$

where $\widehat{\mathscr{H}}$ is the time-independent Hamiltonian governing the system, which will be defined in section 1.2.1.1 below. When discussing the dynamics of a system, we will often simply refer to "the fidelity of $|\psi\rangle$", by which we mean the fidelity of the overall state of the system against the state $|\psi\rangle$. Fidelity is therefore a good measure of transport quality if the desired state $|\psi_{desired}\rangle$ which the system will be measured against is known. In scenarios where $|\psi_{desired}\rangle$ is not known or other properties of a system are of interest, we will use other measures.

1.1.2.2   Entanglement entropy

One other aspect that we might be interested in is, for example, how mixed or pure a given state is. To analyse this type of problem, we measure the entropy of a system state, which tells us the degree of mixedness of the system state. There are several types of entropy, but in this work we will only be using the von Neumann entropy [1]. The von Neumann entropy S of a state ρ is defined as follows:

$$S(\rho) = -Tr(\rho \log_2 \rho) \qquad (1.2)$$

If ρ is a pure state, $S(\rho){=}0$, whereas for a maximally mixed state, $S = \log_2(\dim(\mathfrak{H}))$. Since ρ can also represent a state of more than one site in a spin chain, entropy is a useful measure to determine whether a section of a spin chain is entangled

with the rest or not [19]. Suppose for example that we have two systems *A* and *B* with Hilbert spaces $\mathfrak{H}_A$ and $\mathfrak{H}_B$ respectively and a state $|\phi\rangle \in \mathfrak{H}_A \otimes \mathfrak{H}_B$. We can associate this state with the density matrix ρ_ϕ. To gain information about system *A* only, we then trace out system *B* from ρ_ϕ to obtain the reduced density matrix ρ_A: $\rho_A = Tr_B\rho_\phi$. We can then use the entropy *S* to check whether ρ_A describes a pure state: if it does, the systems *A* and *B* are not entangled. Entropy is therefore a useful measure of the purity or mixedness of a state and also indicates whether two systems are entangled, but it does not quantify any entanglement for mixed states. For this purpose, we use the Entanglement of Formation (EoF).

1.1.2.3 Entanglement of Formation

The Entanglement of Formation (EoF) is a bipartite measure of entanglement, formulated by W. Wootters in 1997 [20]. The fact that this is a bipartite measure which only measures the entanglement between two parties is an intrinsic property of this measure which cannot be circumvented. In our case, these two parties could be two separate sections of a spin chain, each comprising one or more spins, but we will focus on entanglement between two individual spins only. Some attempts have been made to find lower bounds [21–23], categorisations [24–26] and other quantifiers [27–40] for multipartite entanglement, but at the time of writing no exact measure of multipartite entanglement exists. To quote R. Facchi et al.: "We find that the problem exhibits frustration." [32]. In cases where we want to evaluate the amount of entanglement between more than two parties, we will therefore fall back on measuring the fidelity instead, which means that we can only do this when we know the multipartite entangled state we are aiming for. An outline for the computation of the EoF of a density matrix $\rho_{A,B}$ describing the state of two sites *A* and *B* is given in algorithm 1. Even though there are other measures of entanglement (see for

---

Algorithm 1 Computing the EoF of a density matrix $\rho_{A,B}$ describing the state of two sites *A* and *B*.

1: Compute $\rho_{A,B}\widetilde{\rho_{A,B}} = \rho_{A,B}(\sigma_y^A \otimes \sigma_y^B)\rho_{A,B}^*(\sigma_y^A \otimes \sigma_y^B)$, where $\rho_{A,B}^*$ is the complex conjugate of $\rho_{A,B}$ and σ_y is the *y* Pauli spin matrix: $\sigma_y = \begin{pmatrix} 0 & -i \\ i & 0 \end{pmatrix}$. $\rho_{A,B}\widetilde{\rho_{A,B}}$ has eigenvalues ε_i
2: Compute $\lambda_i = \sqrt{\varepsilon_i}$ and arrange λ_i in decreasing order
3: Compute $\tau = (max\{\lambda_1 - \lambda_2 - \lambda_3 - \lambda_4, 0\})^2$
4: Compute $x = (1 + \sqrt{1-\tau})/2$
5: Finally obtain $\text{EoF}(\rho_{A,B}) = -x\log_2(x) - (1-x)\log_2(1-x)$

---

example [41]), we will only be using EoF for this purpose in this thesis and therefore also simply refer to it as "entanglement".

1.1.2.4 Site occupation probability

Since we will be dealing with spin chains consisting of a finite number N of sites, we will occasionally be interested in the probability of an individual site being "occupied", meaning containing an excitation or being in state $|1\rangle$. While this is not an indicative measure of information transport quality and generally gives no information about either entropy or entanglement in a system, it is very educational in certain scenarios where it provides insight into the natural dynamics of spin chains (as shown in [42]). To compute the occupation probability of a site j, let us first of all do a decomposition of the state $|\psi\rangle$ of the spin chain and write $|\psi\rangle = \sum_{i=1}^{2^N} c_i |\phi_i\rangle$ (where $\{|\phi_i\rangle\}$ are the 2^N basis vectors of the Hilbert space $\mathfrak{H}$). As previously noted, $|\phi_i\rangle = |q_1 q_2 \cdots q_N\rangle$ with $q_i \in \{0, 1\}$. To find the occupation probability of a site j ($1 \leq j \leq N$), we are only interested in those basis vectors which make a contribution to the site j being occupied, i.e., those with $q_j = 1$. Let us label these vectors $|\phi_{i,j}\rangle$ and their corresponding coefficients $c_{i,j}$. The occupation probability of the site j is now given by $\sum_{i=1}^{q} |c_{i,j}|^2$ with q the number of contributing vectors. Note that a vector $|\phi_i\rangle$ might contribute to the occupation probability of more than one site. The sum of the occupation probabilities of all sites of a chain is then also equal to the average number of excitations in the chain – this will be further discussed in section 1.2.1.2 below.

1.2 Spin chains

Let us now describe how the background and mathematical tools mentioned so far apply to the objects of interest in this thesis, namely spin chains. Broadly speaking, any set of two-state quantum systems could be considered to be a spin chain, although it is commonly also assumed that the individual two-level systems represent sites which are coupled to nearest neighbours. In this work, we will go beyond a simple linear chain but limit ourselves to a particular type of model, which we will now introduce, along with an outlook on potential hardware. For a broader review of spin chains in the context of quantum communication, see for example [43] and references therein or [19].

1.2.1 Definitions

Before being able to describe our spin chain model in more detail, we need to define some basic parameters of our systems. First of all, we will fix the energy scale of all spin chains we will consider by imposing an upper bound on
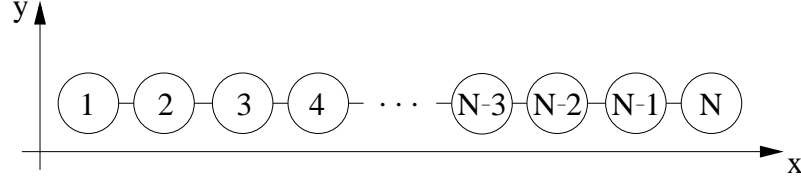
Figure 1.1: Diagram of a linear chain with site labels and terminology used.

the coupling strengths in the chain. We call this maximal coupling J_{max} and throughout our investigations, we will use an indicative value of $J_{max} = 1meV$, regardless of the number of sites in the chain or any other properties. This value of $1meV$ is based on energy values for quantum dots, a prominent candidate for spin chains (see section 1.2.3.2). For other hardware implementations, this value will have to be adjusted accordingly. J_{max} sets the energy scale of the systems and as such is crucial to ensure realistic behaviour of the systems: Without an upper limit, it would be possible for couplings to take entirely unphysical values of several eV.

Each chain also has a characteristic energy scale or characteristic coupling, which we designate by J_0. The exact form of J_0 is determined by conditions which we will impose on the couplings of the chain to achieve so-called perfect state transfer, which will be introduced in section 1.2.2. Since J_{max} is fixed and equal for all chains, J_0 will vary with the number of sites N and also depend on the parity of the chain. For linear chains obeying all perfect state transfer conditions, as shown in figure 1.1, J_0 can be deduced from the length of the chain (N) and J_{max} [44,45]: For even chains, $J_0 = \frac{2J_{max}}{N}$ and for odd chains $J_0 = \frac{2J_{max}}{N\sqrt{1-\frac{1}{N^2}}}$. This typical energy scale J_0 influences the fundamental dynamics of a spin chain and depends on the length of the chain, which for linear chains is also the number of site, N.

For non-linear chains, we cannot define J_0 via the number of spins since this number is not equal to the length of the device. Instead, we introduce the **Effective Chain Length** (ECL), which characterises the system. For linear chains, the ECL is equal to the number of spins N. We will define the ECL for non-linear devices as they are introduced in the following sections.

1.2.1.1 System Hamiltonian

Having defined the most fundamental system parameters J_{max} and J_0, we are now able to write out the system Hamiltonian, which governs the natural dynamics of a spin chain. In order to ensure that this operator represents physical observables of our systems, we require it to be hermitian (or self-adjoint). We

will initially assume again that we are describing a linear spin chain and as mentioned before, only allow for nearest-neighbour interaction, such that two adjacent sites are connected by a coupling $J_{i,i+1}$. We now have:

$$\widehat{\mathscr{H}} = \sum_{i=1}^{N-1} \varepsilon_i |1\rangle\langle 1|_i + J_{i,i+1}[|1\rangle\langle 0|_i \otimes |0\rangle\langle 1|_{i+1} + |0\rangle\langle 1|_i \otimes |1\rangle\langle 0|_{i+1}]. \qquad (1.3)$$

One of the elemental assumptions we will make now is that the single-site excitation energies ε_i are site-independent (or are tuned to be so). This allows us to concentrate on the second term of equation (1.3) only, although we will revisit the influence of the first term in chapter 5.2. This time-independent Hamiltonian $\widehat{\mathscr{H}}$ is used to evolve the system computationally according to algorithms 3 and 4 given in appendix A, which corresponds to using a first order approximation to solve the time-dependent Schrödinger equation at every finite time step. Alternatively, it is possible to use the eigenstates $|\phi_i\rangle$ and eigenvalues E_i of the Hamiltonian $\widehat{\mathscr{H}}$ to compute the state of the system $|\psi\rangle$ at any given time t: At $t = 0$, we have $|\psi(0)\rangle = \sum_i c_i(0)|\phi_i\rangle$ with $\widehat{\mathscr{H}}|\phi_i\rangle = E_i|\phi_i\rangle$. At time t, the state $|\psi\rangle$ has then evolved into $|\psi(t)\rangle = \sum_i c_i(0)|\phi_i\rangle e^{-iE_i t/\hbar}$ [18]. However, in particular for systems with large Hamiltonians (i.e., high dimensional Hilbert spaces), finding the eigenvalues is computationally very expensive, making this method not very efficient.

1.2.1.2 Information encoding

Since every site of a spin chain corresponds to a two-level quantum system, these sites can also be thought of as qubits, the quantum analogue to classical bits. As mentioned in section 1.1.1.2, any such qubit can be in a variety of states (which can be visualised using a Bloch sphere [18, 46]), and a spin chain state can be spread over several qubits. As the hardware support for a qubit is not necessarily spin, the term spin chain can be somewhat misleading. For example, if a site of a chain or a qubit is implemented via a singly charged quantum dot pair [47], the logical states of the qubit correspond to the position of the electron in the pair, rather than its spin.

To better understand the differences in transport between different types of states, we will often take into account the number of excitations a state contains. This number can easily be read off for basis vectors, as the number of excitations is equal to the number of sites or qubits in state $|1\rangle$, but for more complicated states we require a slightly more sophisticated approach. We therefore

define the hermitian excitation number operator $\widehat{\mathscr{T}}$:

$$\widehat{\mathscr{T}} = \sum_{i=1}^{N} |1\rangle\langle 1|_i. \tag{1.4}$$

The total number of excitations T in a state $|\psi\rangle$ is now given by the expectation value of $\widehat{\mathscr{T}}$ in $|\psi\rangle$. $\widehat{\mathscr{T}}$ commutes with $\mathscr{H}$, which implies that T is conserved. We can now also see that the eigenspaces of $\widehat{\mathscr{T}}$ provide a decomposition of the Hilbert space $\mathfrak{H}$ into excitation subspaces: $\mathfrak{H} = \bigoplus_{T=0}^{N} \mathfrak{H}_T$, where $\mathfrak{H}_T$ is the subspace spanned by all states containing T excitations. Any subspace $\mathfrak{H}_T$ contains therefore $^{N}C_T$ orthogonal states (where $^{N}C_T$ is the binomial coefficient indexed by N and T).

1.2.2 Perfect state transfer

One of our main concerns with spin chains is their ability to reliably transfer information. Since we encode this information in quantum states, we are therefore looking for so-called Perfect State Transfer (PST) (see [48,49] for a review). In this section, we will look at the necessary conditions for PST, as well as the resulting transfer timing.

1.2.2.1 Perfect State Transfer couplings

The obvious spin chain parameter to adjust in order to achieve PST are the couplings $J_{i,i+1}$ between the sites of the spin chain. It was shown by Christandl et al. in [44] that unmodulated chains, meaning those where $J_{i,i+1} = J_{max}$, for all $1 \leq i \leq N-1$, can only achieve PST for $N < 4$. For longer chains in this regime, only various degrees of approximation to PST can be achieved [50,51], although other possibilities are opened up [33,52–54]. In order to achieve PST for any length of chain, Christandl et al., and simultaneously Nikolopoulos et al., derived the following nearest-neighbour couplings $J_{i,i+1}$ [44,55,56]:

$$J_{i,i+1} = J_0 \sqrt{i(N-i)}. \tag{1.5}$$

A spin chain set up with these parameters will now achieve PST simply through its natural unitary dynamics. In contrast to this general formula, explicit couplings have also been derived for a number of specific devices [57–59], but we will not consider these special cases in this work. Furthermore, there have been a number of extensions to Christandl's and Nikolopoulos' results [49,60–68], as well as similar, more graph-theoretical approaches [69–73]. If the couplings
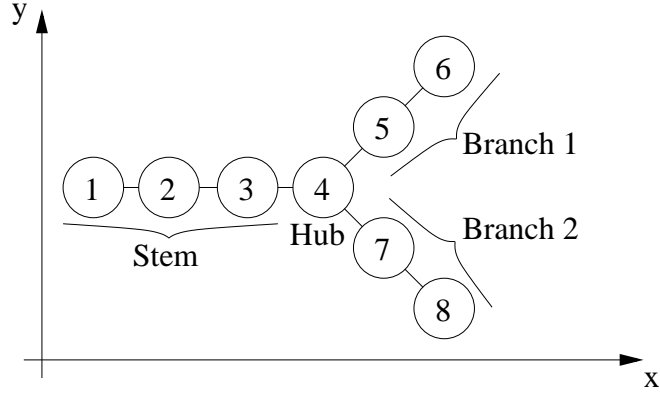
Figure 1.2: Diagram of a Y-type chain with $N = 8$ with site labels and terminology used. The stem length is 3 and the branch length is 2.

of a device have been set up according to equation (1.5), any state will be perfectly transferred along the chain (and back), without the need for any further external intervention, for example any adjustment of these couplings.

It is also worth noting that a chain set up with PST couplings displays symmetric couplings, i.e., $J_{i,i+1} = J_{(N-i),(N-i+1)}$ (see figure 1.1 for site labelling). As such, linear chains are symmetric by geometry as well as by couplings, which means that the direction of labelling along their x-axis is entirely interchangeable. Throughout this thesis, we will assume that any devices we investigate have been set up according to this PST rule and are therefore, under ideal conditions, capable of PST.

Since the PST couplings $J_{i,i+1}$ depend on J_0, they also depend on the ECL. This is particularly important for non-linear devices, where an added complication arises. Let us consider a simply branched Y-type chain, as shown in figure 1.2. Unlike linear chains, where the order of labelling makes no difference to the system, Y-type chains do not have a symmetric geometry along the x-axis and we have to be more careful with the site labels. We impose a direction on the device by orienting it such that the linear part (the "stem") is on the left hand side and the branches on the right hand side. The leftmost site is then site 1 and we continue with the labelling along the stem to the hub site (site 4 in figure 1.2) and along the uppermost branch to its end (site 6 in figure 1.2). We continue with the labelling from the first spin of the next branch (i.e., the one connected to the hub spin), going along the branch to its end, and proceed this way until all spins are labelled. The ECL for this type of device is now the length of the stem plus 1 (the hub) plus the length of the longest branch. As we will see in chapter 2, we actually require all branches to be of the same length in order to ensure PST, such that the ECL is equal to the label of the last spin of the topmost branch 1 (in figure 1.2, the ECL is 6).

In order to represent the couplings of non-linear chains in the Hamiltonian $\widehat{\mathcal{H}}$, we have to ensure that the first site b in any branch is coupled to the hub site h (so terms $J_{h,b}$ have to be added) and also that the last site of any branch is only connected to a single site (so some existing couplings have to be removed). When altering the Hamiltonian in this way, care must be taken to maintain the hermiticity of $\widehat{\mathcal{H}}$ to ensure representation of a physical system. In a general Y-type device, the hub site h is now connected to the stem of the device and B branches (in figure 1.2, $B = 2$). This disrupts the usual dynamics, as in linear chains any site other than sites 1 and N is connected to exactly two neighbouring sites. To compensate for this disruption, we implement the so-called **hub rule** [74]: For a Y-type chain with B branches, the coupling between the hub site h and the first site b in any of the B branches is given by

$$J_{h,b} = J_0 \sqrt{h(N' - h)} / \sqrt{B} \qquad (1.6)$$

where N' refers to the ECL of the device, not the total number of spins N. For example, in figure 1.2 we have $J_{4,5} = J_{4,7} = J_0 \sqrt{4(6 - 4)} / \sqrt{2}$.

1.2.2.2 Transfer timing

The characteristic energy or coupling constant J_0 of a system is not only needed to fix the PST couplings according to equation (1.5), it also determines the time scale of the system. A meaningful measure of system time is the transfer timing; the time it takes to transfer a state from one end of the chain to the other, given PST conditions. We will call this time t_M. As noted by Christandl, t_M scales with N [44], which is in agreement with physical intuition: The longer a chain, the longer it takes to transfer a state across it. Using J_0 (and therefore indirectly using J_{max}), we can give the transfer time as

$$t_M = \frac{\pi \hbar}{2 J_0}. \qquad (1.7)$$

It is crucial for any physical implementations to have as accurate a knowledge of t_M as possible, since a state that is not extracted at its destined output site at the correct time will either suffer fidelity loss (see chapter 6.2 for a full discussion) or simply continue its evolution in the chain and return to its initial state after $2t_M$, which is the time of a full system period.
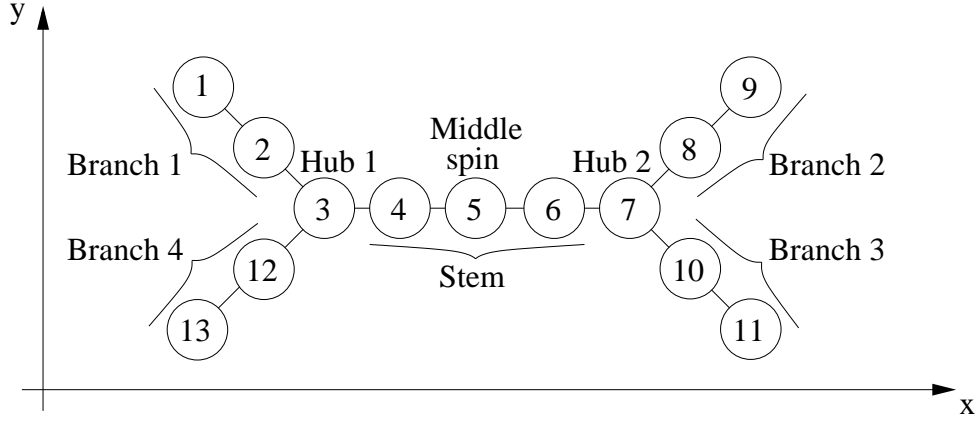
Figure 1.3: Diagram of a double branched chain with $N = 13$ with site labels and terminology used. The stem length is 3 and the branch length is 2.

1.2.3 Device types and potential hardware

There are a number of different approaches to investigating the properties and natural dynamics of spin chains. Aside from the aforementioned unmodulated chains, there are also designs requiring control over the end coupling(s) only [15, 75–78] or efforts to control the dynamics via magnetic fields [79–84], as well as many others [85–96]. Depending on the task that the spin chain is envisaged to fulfill, there has also been research on a range of different geometries, such as parallel chains [97, 98] or star-type networks [99–103], as well as others [76, 86, 104–120], although the vast majority of these designs do not use PST couplings. In this work, we will limit ourselves to spin chains with couplings set up for PST and a small range of geometries, which we will now outline. We will then present an outlook on potential hardware implementations.

1.2.3.1 Types of spin chains to be analysed

So far we have discussed linear spin chains, which are the main focus of this thesis, and Y-type branched chains (see figure 1.2) which require adjustment of some couplings according to the hub rule in order to ensure PST. We propose double branched chains as an extension to Y-type chains, as shown in figure 1.3. This type of device is somewhat more complex, as there are multiple symmetries (both along the x-axis and the y-axis). In order to be able to allocate the correct PST couplings, we need to first of all find the ECL. In the case of double branched chains, the stem of the device consists of those spins connecting the two hubs. As with Y-type chains, we will assume that all branches have the same length, so that the ECL of the double branched chain is now twice the branch length plus the stem length plus 2 (for the two hubs). For the device

shown in figure 1.3, the ECL is therefore $2 * 2 + 3 + 2 = 9$. In order to adjust the Hamiltonian $\widehat{\mathscr{H}}$ as little as possible, we label the device so that the ECL runs along branches 1 and 2 and then continue to label the branches outwards from the hubs and in clockwise order. Since we now have two hubs, we need to apply the hub rule on both hubs separately. The orientation of the device is again crucial as the symmetry of double branched chains folds around the centre of the stem, which is the gap between the two central spins of the stem for devices with even N and the middle spin (as labelled in figure 1.3) for chains with odd N. As such, we will again adjust the couplings between the hubs and the branches they are connected to according to the hub rule (equation 1.6), but not the couplings between the hubs and the stem. We make sure to represent these adjustments to the couplings in the Hamiltonian $\widehat{\mathscr{H}}$ by adding and removing entries as appropriate, keeping $\widehat{\mathscr{H}}$ hermitian.

Beyond linear, Y-type and double branched chains, we will also be looking at circular chains in chapter 4, which are a simple extension of linear chains. It is of course possible to imagine other types of geometries, each with their own advantages, but in an effort to not stray too far from what is currently experimentally feasible, we will not look into any other architectures of spin chains.

1.2.3.2 Outlook on potential hardware implementations

We have already alluded to the fact that a spin chain is not necessarily comprised of sites carrying spin, but can be implemented using any two-level system that can be coupled to their nearest neighbours (or a number of nearest neighbours in the case of branched devices). Another transport method is flying spin qubits [121], which have the advantage of allowing for longer-range communication and are considered a requirement for various quantum applications [122]. Some research has also been done regarding using spin-1 chains instead of the spin-half chains that we are considering [123], most notably using the AKLT model [124], but these are very different devices that we will not consider here. As mentioned earlier, a singly charged quantum dot pair is a possible system to build spin chains, but there are many other suitable potential hardware implementations. Systems encoding information using spin are, for example, nanometer-scale magnetic particles [125, 126], strings of fullerenes [127, 128] or nuclear spins in a molecule [129], to name but a few. It is also possible to use soliton-like packets of excitations to represent a two-level system [118], photons [130], or simulate particular types of spin chains via coupled cavity arrays [131]. Single quantum dots containing electrons or

excitons [55, 132] are also a very popular implementation [133–135], as are devices based on liquid nuclear magnetic resonance. In particular, spin chains set up with PST conditions as per equation (1.5) using liquid nuclear magnetic resonance have both been simulated [136] and implemented [137]. Proposals for quantum registers made using defects in carbon materials (particularly in diamond, where the defect is usually a substitutional nitrogen atom in the diamond lattice) have also seen a recent surge in popularity, especially as they allow for manipulation at room temperature [76, 138]. However, all these implementations require a certain degree of control, which is one of their most important limitations [139].

Quantum dots are arguably one of the most prominent candidates for spin chain hardware at the time of writing [45,55,140]. These quasi-zero-dimensional quantum systems are also referred to as artificial atoms and implementations include for example graphene dots [141], which we will also discuss in chapter 6. One of the issues we need to take into account with spin chain implementations is that of addressability, or in other words the ability to inject or extract information (encoded as quantum states) from the hardware. As we will often be considering quantum dots as an example of a possible implementation, we will consider two main protocols to address a chain: SWAP operations and Rabi flopping. In the case of Rabi flopping, a so-called π-pulse is used on a specific site i, according to the Hamiltonian $\widehat{\mathcal{H}_R} = \Omega(t)|0\rangle\langle 1|_i + \Omega^*(t)|1\rangle\langle 0|_i$, where Ω is the Rabi frequency. A SWAP operation can be implemented by a quantum gate of the form

$$SWAP = \begin{pmatrix} 1 & 0 & 0 & 0 \\ 0 & 0 & 1 & 0 \\ 0 & 1 & 0 & 0 \\ 0 & 0 & 0 & 1 \end{pmatrix}$$

and has for example been demonstrated by Bertoni et al. [142]. As we will commonly use SWAP operations to inject or extract information from a spin chain, in the case of quantum dots we will also be injecting or extracting particles. These particles will be transported along waveguides [143], which are usually either electromagnetic or optical. Optical waveguides themselves have also been used as an implementation of spin chains, where the sites of the chain are represented by parallel waveguides [144].

The possibilities for implementing spin chains are very varied, with a multitude of different hardware realisations, but each with their own limitations and restrictions. We will therefore keep our investigations on the natural dynamics of spin chains as general as possible, without making any further assumptions that would lead to constraints in the physical implementations.

1.3   Thesis outline

The rest of this thesis will be structured as follows: In chapter 2, we will show how the elemental assumptions we have laid out here do indeed lead to PST and discuss what additional conditions are necessary to ensure PST in non-linear chains, in particular with respect to the transfer of entangled states. We will also investigate possibilities for creating entangled states using only the natural dynamics of the chains, as well as some aspects of state storage. Focussing on the further aptitudes of linear chains, chapter 3 will outline work also presented in [42] and analyse the potential of spin chains to create distributed cluster states, again using only the existing natural dynamics of the system. To this end, we will first of all motivate this work and present some additional observations on spin chains before detailing and finally demonstrating the working algorithm of our proposed protocol. Chapter 4 will focus on an extension to linear chains which has not been discussed here so far, namely circular chains. Again we will establish the necessary conditions for PST and outline any limitations to then expand our view on this family of devices, discussing potential for applications as well as constraints. Having considered the natural dynamics of spin chains under ideal conditions, chapters 5 and 6 focus on the effects of a number of perturbations on the workings of spin chains, as partially presented in [42, 145, 146]. While chapter 5 focusses on the effects of fabrication defects, such as energy fluctuations and random noise, chapter 6 discusses the influence of unwanted long-range interactions as well as timing errors. In both chapters, we discuss the magnitude of the effects of the perturbations on the natural spin chain dynamics for different types of states to analyse the strengths and weaknesses of the devices. Finally, we give a summary in chapter 7 as well as an outlook with respect to future work to be done in this field.

Chapter 2

Information transfer and storage in spin chain devices

Having laid out the major tools and assumptions we will be using in this thesis, in this chapter we will now perform an investigation into the possibilities and limitations of information transfer in spin chains. To this end, we will start by analysing the transfer of unentangled states of one or more excitations in the three major types of spin chains we are considering: linear, Y-type and double branched spin chains. We will then move on to consider the more challenging transfer of entangled states. Finally, possibilities for state storage will be discussed and demonstrated. This chapter contains both previously known and original results: in particular, any discussion involving double branched chains is original work, as is the presentation of state storage using linear chains.

2.1 Transfer of unentangled states

The coherent transfer of unentangled states is one of the most fundamental problems in quantum information. It represents a basic building block for any quantum protocol and is thus the first thing to be checked when we are investigating whether a device is suitable for PST, and under what conditions.

2.1.1 Linear spin chains

As discussed in section 1.2.2, the couplings between the individual spins of a linear spin chain can be tuned to ensure PST using equation (1.5) [44, 55, 56]. PST achieved this way and under the conditions outlined in chapter 1 (such
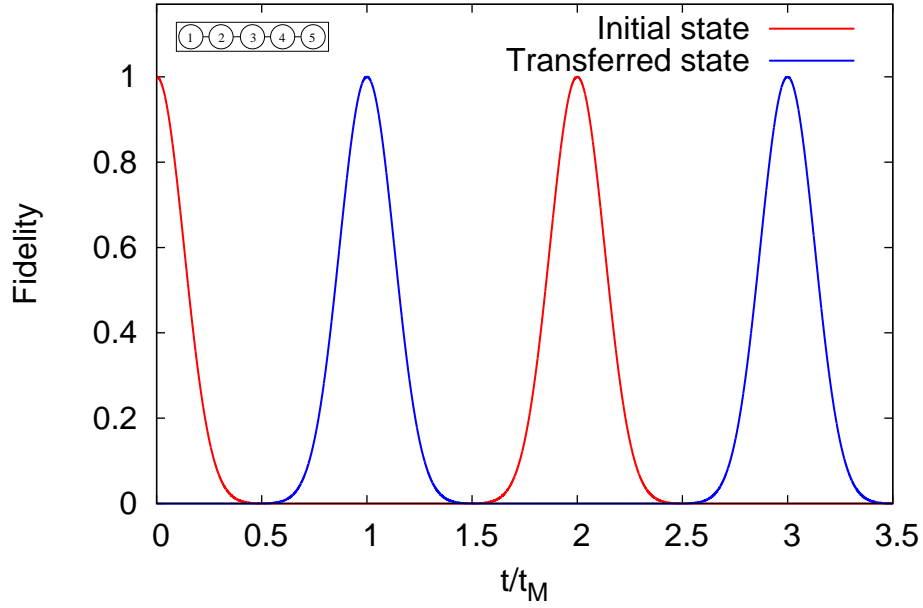
Figure 2.1: Transfer of initial state $|11000\rangle$ to its mirror twin, the transferred state $|00011\rangle$, vs. rescaled time t/t_M.

as site-independent energies) has been demonstrated experimentally [137,147] and widely discussed (see section 1.2.2.1), in particular in the context of single excitations, but also holds for multiple excitations. In figure 2.1, we see how the unentangled two-excitation initial state $|11000\rangle$ of a 5-spin chain is transferred to the opposite end of the chain (shown as $|00011\rangle$) at t_M (and all odd multiples thereof) and subsequently recovered in its original form at $2t_M$ (and multiples thereof). This phenomenon is independent of the parity of the chain, as well as the number of spins it contains. It is also worth noting that a state comprising a number of excitations greater than half the number of spins in a chain is also perfectly transferred. For example, if the above spin chain was injected with initial state $|00111\rangle$, this would transfer to $|11100\rangle$ at t_M and back to the initial state at $2t_M$. It is important to understand that the state as a whole is transferred, not just the excitations represented by a "1" in our notation. While PST and revival of any initial state are independent of the chain length, the fidelity peak width decreases with the number of spins N of the chain. This decrease can be approximated by scaling in $1/\sqrt{N}$, which we also presented in [42], and is illustrated in figure 2.2.

Additionally, Albanese [148] noted that PST in spin chains follows the so-called "mirroring rule" (see also [149] for a non-PST discussion). The mirroring rule states that any state injected into a linear spin chain set up for PST according
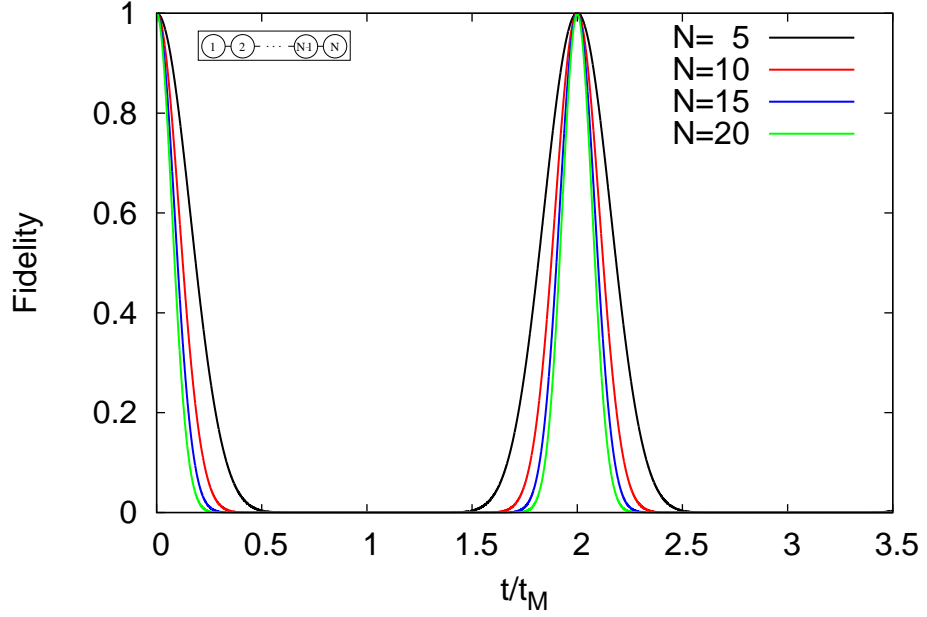
Figure 2.2: Peak widths of the revived initial state $|10\cdots0\rangle$ for four values of N as labelled vs. rescaled time t/t_M.

to equation (1.5) will be reflected about the midpoint of this chain at t_M. For chains with an even number of spins ("even chains"), this is the gap between spins $N/2$ and $(N/2)+1$ whereas for spin chains with an odd number of spins ("odd chains"), this is spin $(N+1)/2$. Let us define the mirror operator $\widehat{M}$:

$$\widehat{M}[|a\rangle_1|b\rangle_2\cdots|y\rangle_{N-1}|z\rangle_N] = |z\rangle_1|y\rangle_2\cdots|b\rangle_{N-1}|a\rangle_N \qquad (2.1)$$

where $a,b,y,z \in \{0,1\}$. In non-linear devices, where the excitation of the transferred state might be split over multiple sites (see section 2.1.2), $\widehat{M}|\psi\rangle$ will have to be adapted accordingly. Note that $\widehat{M}$ and the Hamiltonian $\widehat{\mathscr{H}}$ (equation (1.3)) commute, so that any energy eigenstates of the system are also eigenstates of $\widehat{M}$. We will refer to the state $\widehat{M}|\psi\rangle$ of an initial state $|\psi\rangle$ as its "mirror twin". In the above example, $|11100\rangle$ is the mirror twin of $|00111\rangle$. If a state happens to be identical to its mirror twin, such that $\widehat{M}|\psi\rangle = |\psi\rangle$, this state will be revived at every multiple of the time t_M, as shown in figure 2.3: Here, we see that the initial input state $|10101\rangle$ is perfectly revived at times $t_M, 2t_M, 3t_M$ etc.
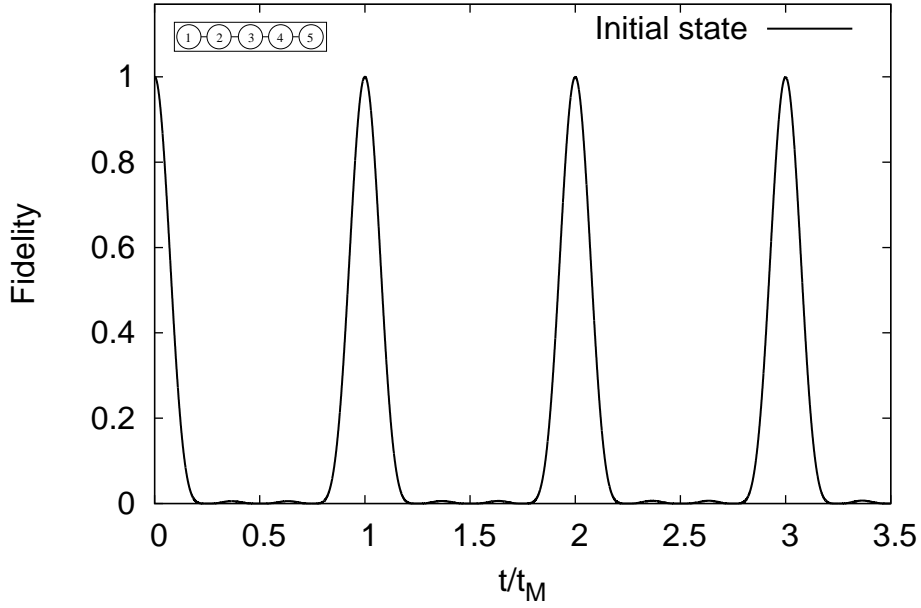
Figure 2.3: Transfer of the initial state $|10101\rangle$ vs. rescaled time t/t_M.

2.1.2   Y-type spin chains

The transfer of unentangled states in Y-type branched chains is somewhat more involved than in linear chains due to the asymmetry of the device along its x-axis. It was shown in [74] that input of a single excitation in the leftmost (first) spin of the stem does indeed allow for PST, where the mirror twin is an entangled state (see section 1.1.1.2). This is demonstrated in the example of a 5-spin chain of branch length 1 in figure 2.4, where the initial state $|10000\rangle$ is transferred to the other end of the chain as $1/\sqrt{2}(|00010\rangle + |00001\rangle)$ at t_M before reverting to $|10000\rangle$ at $2t_M$. We defer the discussion of entanglement as a resource in spin chains to section 2.2. As is shown in figure 2.5, input of a single excitation anywhere (here in spin number 2) in the stem of an 8-spin Y-type chain with stem length 3 and branch length 2 also leads to PST (see section 1.2.3.1 for the site numbering). This corresponds to input in the part of the chain which is symmetric about the y-axis (the stem, see figure 1.2). If on the other hand a single excitation is injected in any spin of the branches, so the part of the device which is asymmetric with respect to the y-axis, PST does not happen. Even if the stem and each of the branches are made of the same number of spins (which results in a perfectly symmetrical looking device), the different couplings at the hub mean that the device is not perfectly symmetrical and cannot be considered as such: input in the stem and at the branches results in different dynamics. For example, the initial state $|00000001\rangle$ in the above 8-
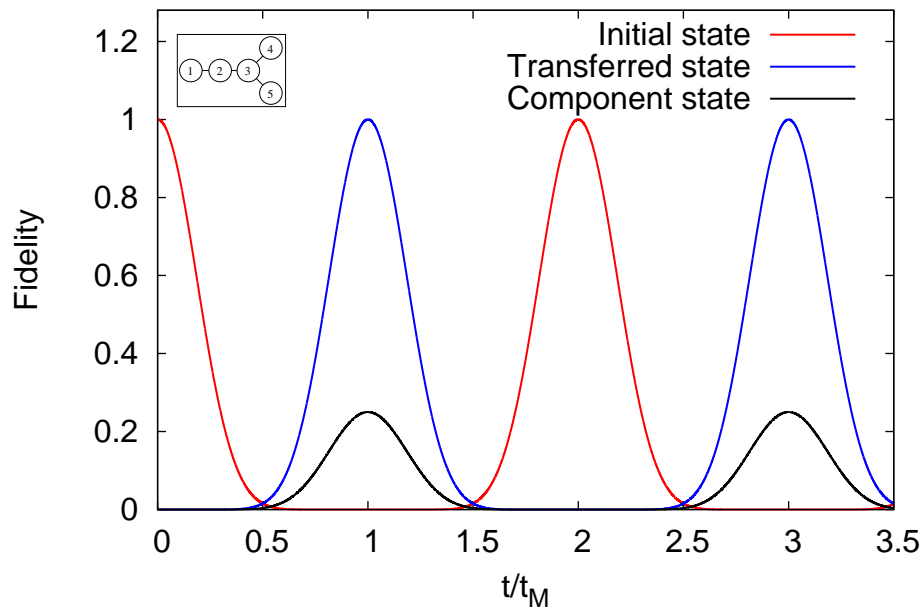
Figure 2.4: Transfer of the initial state $|10000\rangle$, its mirror twin, the transferred state $1/\sqrt{2}(|00010\rangle + |00001\rangle)$, and a component of the transferred state ($|00001\rangle$) vs. rescaled time t/t_M.
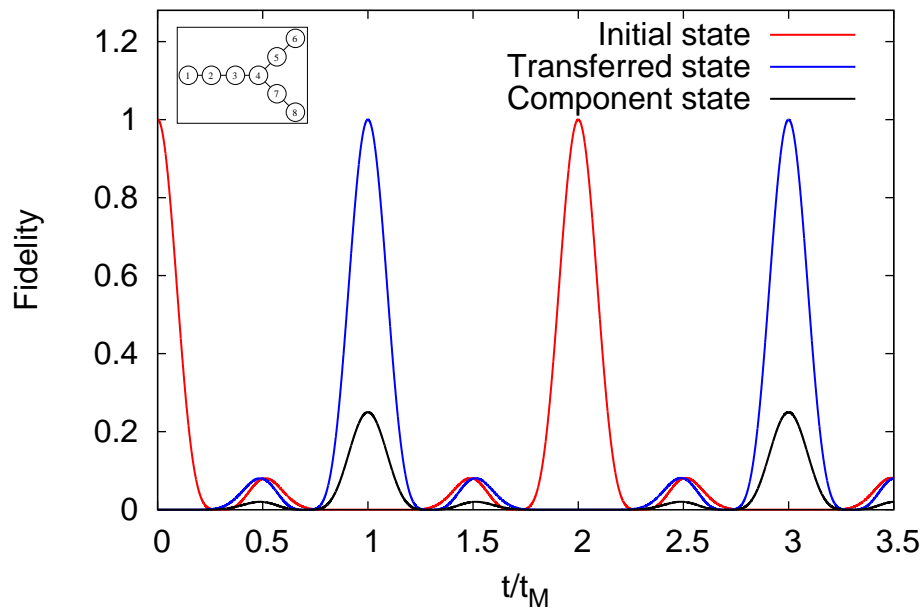
Figure 2.5: Transfer of the initial state $|01000000\rangle$, the transferred state (its mirror twin) $1/\sqrt{2}(|00001000\rangle + |00000010\rangle)$ and a component of the transferred state ($|00000010\rangle$) vs. rescaled time t/t_M.
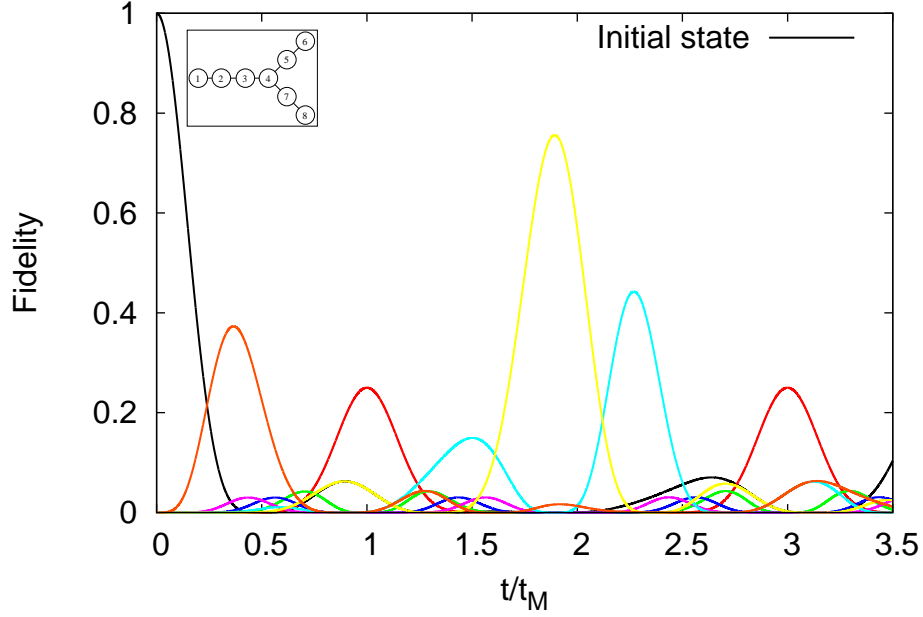
Figure 2.6: Evolution of all basis vectors $|\phi_k\rangle$ after injection of initial state $|00000001\rangle$ (other vectors not labelled) vs. rescaled time t/t_M.

spin device is not transmitted to $|10000000\rangle$ at t_M and is subsequently also not perfectly recovered. Instead, the injected excitation is "spread out" across the device, with no particular state ever becoming periodically prominent (see figure 2.6). This trend becomes more pronounced with time and speeds up with an increase in number of spins in the device due to the larger spatial freedom of the excitation.

It is tempting to think that multiple excitations would allow for initial input states which involve the branches and are symmetric with respect to the y-axis, thus giving PST, (for example $|00011\rangle$ in a 5-spin Y-type chain with branch length 1) but this is not the case. As each spin can only contain a single excitation, and the excitations cannot hop over one another, there is interference when they reach the hub (having started off in the branches) and one of the excitations is inevitably reflected into the branch it was injected into. This leads to a breaking of the initially imposed symmetry, meaning that the initial state is never recovered, nor is another state achieved perfectly or periodically. Similarly, input of more than one excitation in the stem (such as $|11000\rangle$ in the above example) or a mix of excitations in stem and one or both of the branches encounters the same problem and does not achieve PST. Instead, the excitations are spread out along the chain, with devices consisting of more spins being subject to this more quickly.
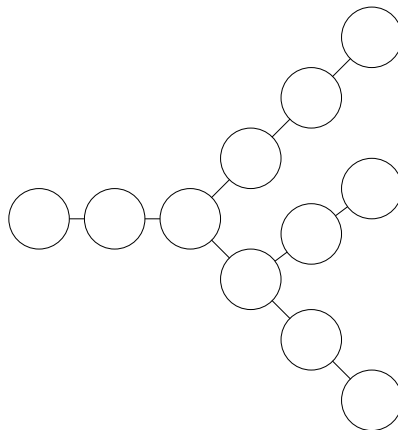
Figure 2.7: Diagram of an irregularly branched spin chain which allows for PST of single excitation states with the excitation either in the stem or the leftmost hub.

2.1.3   Double branched spin chains

The results in this section are original work. When considering branched chains, we are not restricted to a single hub, nor indeed to a hub splitting a chain into two branches. As long as the hub rule (equation (1.6)) is obeyed and the branches of any one hub have the same ECL (as defined in section 1.2.1), input of a single excitation in the stem will result in PST, analogously to results in section 2.1.2. This means that even asymmetric looking devices such as displayed in figure 2.7 are suitable for single excitation PST, allowing for potentially widely distributed networks [74].

Let us consider double branched chains (see figure 1.3). Double branched chains can be thought of as a Y-type chain where each terminal spin of the branches becomes another hub for two branches, resulting in four branches in total. If the stem length is then set to zero, the resulting device is a double branched chain with an odd number of spins, with the first hub making up the middle spin. However, as this spin does not actually function as a hub anymore, the couplings have to be adjusted to be in line with equation (1.5) and not with the hub rule (1.6). For numbering details, see section 1.2.3.1. Much like multiply branched Y-type chains, odd double branched chains allow for PST of a single excitation injected into the middle spin. This is demonstrated in figure 2.8 for a double branched chain with $N = 7$ and branch length 1. However, double branched chains with an even number of spins, which lack a natural pivot spin, do not allow for PST.

Double branched chains, much like Y-type chains, also do not allow for PST of unentangled input states with more than one excitation. In fact, if an even double branched chain consisting of two separate Y-type chains that have individ-
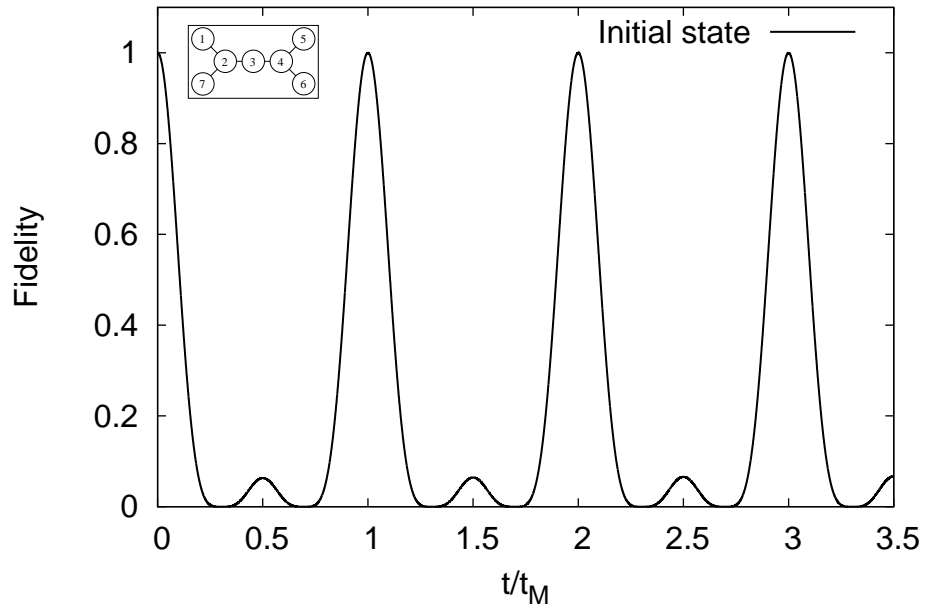
Figure 2.8: Evolution the initial vector $|0010000\rangle$ vs. rescaled time t/t_M for a double branched chain with $N = 7$ and branch length 1.
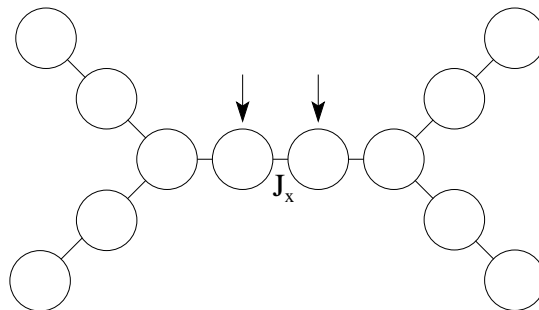
Figure 2.9: Diagram of a double branched spin chain with flexible central coupling J_x. The arrows identify the two excitation injection sites in this set-up.

ually been set up for PST is injected with two excitations as shown in diagram 2.9 and the middle (connecting) coupling J_x is subject to external manipulation, the device will only allow for PST if $J_x = 0$, so if the double branched chain is split into two Y-type devices with one excitation in the stem each. Otherwise, the larger J_x, the worse the state transfer. Again, the more spins the device consists of, the faster the loss of any state fidelity occurs.

2.2   Transfer of entangled states

We have already seen in section 2.1.2 that input of a single excitation in the stem of a Y-type spin chain leads to an entangled state at time t_M. Entanglement is one of the key resources in quantum computing, and is crucial to most quantum cryptography protocols, including quantum teleportation [10]. Multipartite entanglement can for example be generated using single-qubit rotations of electrons in spin chains made of quantum dots [150]. Being able to reliably transfer entanglement from one site to another is therefore a core interest in quantum information transfer and also in distributed quantum computing. In this section, we will discuss entanglement creation and transfer in spin chains in general, considering all three main classes of spin chains. Again, we will simply require the aforementioned PST set-up without any additional constraints, as mentioned also in [60].

2.2.1   Linear spin chains

Let us first of all consider linear spin chains, which serve as building block for the other types of spin chain devices that we will investigate. To gain an understanding of entanglement transfer in linear chains, we notice first of all that any entangled state can be written as a superposition of states from a basis. We know that the set of states $\{|i_1, i_2, \cdots i_N\rangle\}$ with $i_j \in \{0, 1\}$ is a basis for any basis expansion of any (pure) state that the chain can be in, including any entangled states. Let us call this set $\{|\phi_m\rangle\}$, with $1 \leq m \leq k$. k denotes the number of basis vectors, which depends on the chain length N and the number of excitations n present in the chain:

$$k = \sum_{i=0}^{n} \binom{N}{i} \tag{2.2}$$

We can therefore describe an arbitrary state Ψ of the system as follows:

$$|\Psi\rangle = \sum_{k} c_k |\phi_k\rangle \tag{2.3}$$
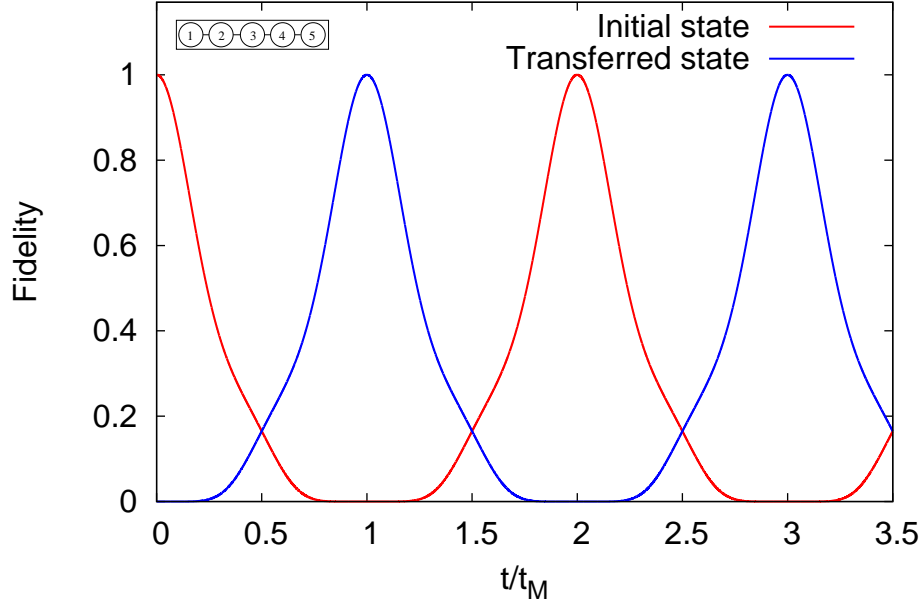
Figure 2.10: Perfect entanglement transfer in a 5 spin chain as described in equation (2.4): $|\psi_{in}\rangle = \frac{1}{\sqrt{2}}(|10000\rangle + |01000\rangle)$ alternates perfectly with its mirror twin, the transferred state $|\psi_{out}\rangle = \frac{1}{\sqrt{2}}(|00001\rangle + |00010\rangle)$, fidelity vs. rescaled time t/t_M.

where $\sum_k |c_k|^2 = 1$ to ensure normalisation.

However, as we have shown in section 2.1.1, any of the states $|\phi_k\rangle$ obey the mirroring rule under the operator $\widehat{M}$ (see equation (2.1)). Therefore we also have $\widehat{M}|\Psi\rangle = \widehat{M}[\sum_k c_k|\phi_k\rangle] = \sum_k c_k \widehat{M}|\phi_k\rangle = \sum_k c_k|\phi_{k;twin}\rangle$ where $|\phi_{k;twin}\rangle$ is the mirror twin of $|\phi_k\rangle$. This implies that any state and in particular any entangled state is transferred to its mirror twin at t_M and recovered at $2t_M$.

An example of this is shown in figure 2.10. Here, the entangled input state

$$|\psi_{in}\rangle = \frac{|0_1 1_2\rangle + |1_1 0_2\rangle}{\sqrt{2}}|0_3 0_4 0_5\rangle = \frac{1}{\sqrt{2}}(|10000\rangle + |01000\rangle) \qquad (2.4)$$

is perfectly transferred to the corresponding mirror twin

$$|\psi_{out}\rangle = |0_1 0_2 0_3\rangle\frac{|0_4 1_5\rangle + |1_4 0_5\rangle}{\sqrt{2}} = \frac{1}{\sqrt{2}}(|00001\rangle + |00010\rangle) \qquad (2.5)$$

at t_M. This is also true for entanglement of the type $\frac{|1_a 1_b\rangle \pm |0_a 0_b\rangle}{\sqrt{2}}|0\cdots0\rangle = |\psi_{in_2}\rangle$ (see figure 2.11) and also for entanglement between more sites, for instance $\frac{|11000\rangle + |10100\rangle + |01100\rangle}{\sqrt{3}} = |\psi_{in_3}\rangle$ (see figure 2.12), as well as generalizations to N spins and excitations. Note how in figure 2.11 the fidelity of the $|0\cdots0\rangle$ com-
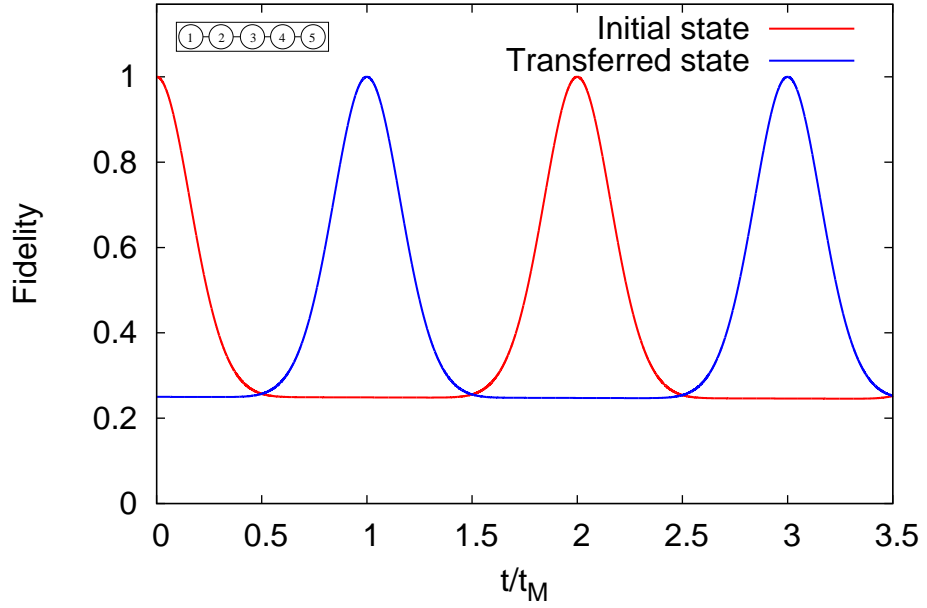
Figure 2.11: Perfect entanglement transfer for a 5 spin chain of $\frac{|1_1 1_2\rangle \pm |0_1 0_2\rangle}{\sqrt{2}} |0_3 0_4 0_5\rangle = |\psi_{in_2}\rangle$ and its mirror twin, the transferred state $|0_1 0_2 0_3\rangle \frac{|1_4 1_5\rangle \pm |0_4 0_5\rangle}{\sqrt{2}} = |\psi_{out_2}\rangle$, vs. rescaled time t/t_M.

ponent in the system must remain constant at 0.25 as it is the only element in its subspace, meaning the fidelity of both $|\psi_{in_2}\rangle$ and $|\psi_{out_2}\rangle$ stays at or above 0.25.

2.2.2 Y-type spin chains

As we have seen in section 2.1.2, Y-type spin chains are capable of generating entanglement (see [99] for an extensive discussion). If the branches are longer than the stem, this phenomenon occurs regardless of where in the stem (or the hub) the single excitation is initially injected: In this case, if we label the two terminal spins of the branches A and B, an initial state $|0 \cdots 1_i \cdots 0\rangle$ is mirrored into $\frac{1}{\sqrt{2}} (|0 \cdots 1_{A-i+1} \cdots 0\rangle + |0 \cdots 1_{B-i+1} \cdots 0\rangle)$. By symmetry of the mirroring rule, this also implies that a state $\frac{1}{\sqrt{2}} (|0 \cdots 1_{A-i+1} \cdots 0\rangle + |0 \cdots 1_{B-i+1} \cdots 0\rangle)$ (where sites $A - i + 1$ and $B - i + 1$ are entangled) is transferred into the unentangled state $|0 \cdots 1_i \cdots 0\rangle$ at time t_M.

If the branches of a Y-type spin chain are exactly the same length as the stem, any input in the stem will lead to entanglement, but as the device is perfectly symmetrical in this case and the hub is now the pivotal spin, a state with an excitation in the hub is its own mirror twin and as such will not be entangled
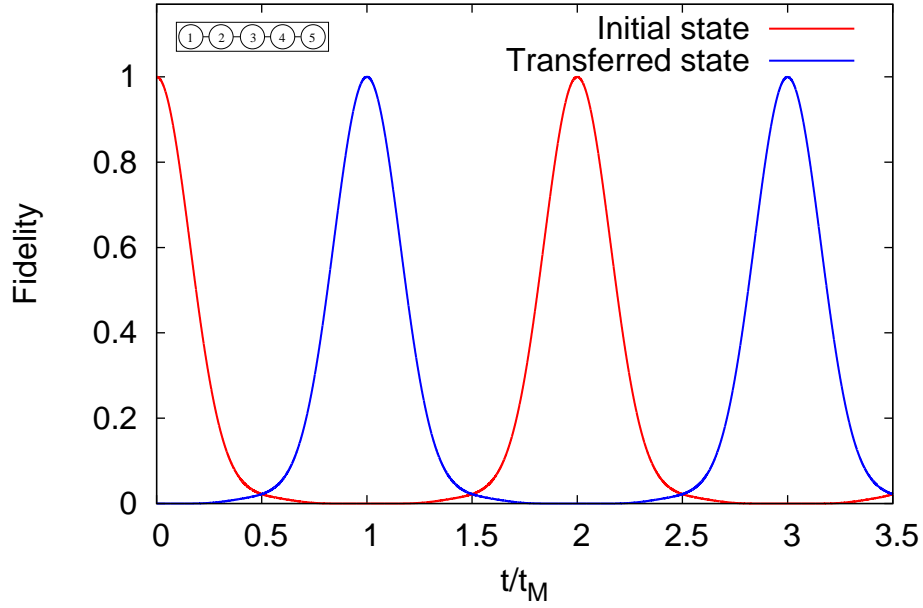
Figure 2.12: Perfect entanglement transfer of the three-site entanglement $\frac{|11000\rangle+|10100\rangle+|01100\rangle}{\sqrt{3}} = |\psi_{in_3}\rangle$ to the transferred (mirror twin) state $\frac{|00011\rangle+|00101\rangle+|00110\rangle}{\sqrt{3}} = |\psi_{out_3}\rangle$ vs. rescaled time t/t_M.

at any time.

Similarly, if the branches are shorter than the stem, the possible input positions for entanglement generation are further restricted. Imagine for example a Y-type chain with branch length 1. If the initial state is $|10\cdots0\rangle$ (where the spins in the middle are all zero), then the mirror twin $1/\sqrt{2}(|00\cdots01\rangle + |00\cdots10\rangle)$ will be entangled. However, in all other cases of a single excitation in the stem (or hub), the resulting mirror state will not be entangled: For example, $|01\cdots0\rangle$ would simply become $|00\cdots100\rangle$ at t_M (so the excitation is now in the hub spin in this case).

It is also possible to perfectly transfer a state which entangles two or more spins in the stem. In figure 2.13, we see that an initial state entangling the first two spins in the stem of a 5-spin Y-type device with branch length 1 is perfectly transferred to its mirror twin at time t_M: $|\psi_{initial}\rangle = \frac{1}{\sqrt{2}}(|10000\rangle + |01000\rangle)$ is transferred to $\psi_{twin} = \frac{1}{\sqrt{3}}(|00100\rangle + |00010\rangle + |00001\rangle)$.

Much as PST does not occur in Y-type spin chains for unentangled states with more than one excitation, entangled states involving more than one excitation do not achieve PST either. Observing this is slightly less straightforward, as there are multiple possibilities imaginable for the entangled mirror twin: see figure 2.14 for an illustration.
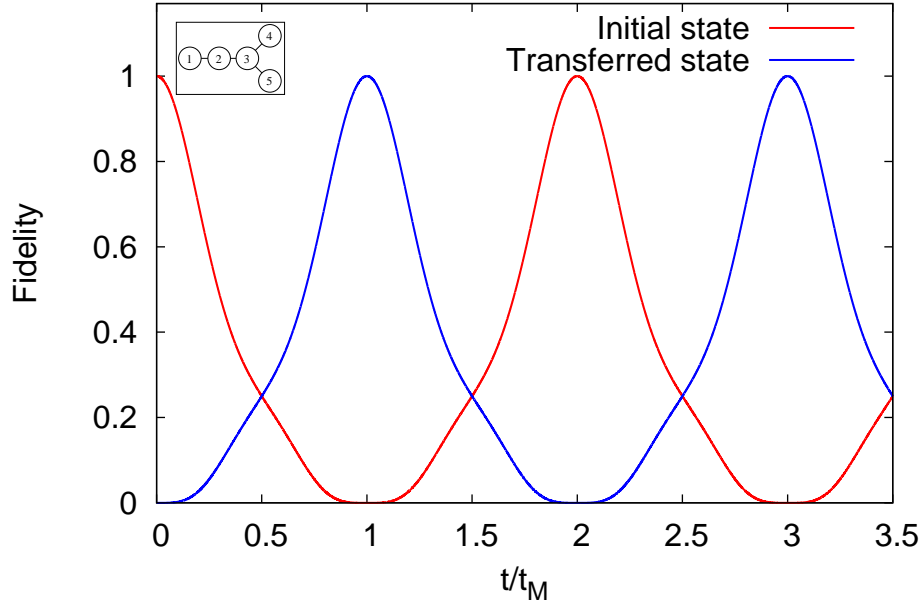
Figure 2.13: Evolution of initial state $|\psi_{initial}\rangle = \frac{1}{\sqrt{2}}(|10000\rangle + |01000\rangle)$ and the mirror twin, the transferred state $|\psi_{twin}\rangle = \frac{1}{\sqrt{3}}(|00100\rangle + |00010\rangle + |00001\rangle)$, vs. rescaled time t/t_M in a 5-spin Y-type chain with branch length 1.
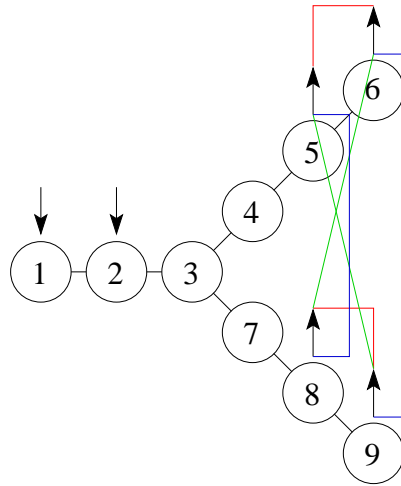
Figure 2.14: Diagram of a Y-type device with 2 excitation input: Injected excitations are shown by black downwards arrows, expected output sites are shown by black upwards arrows. Possible scenarios for an expected entangled mirror twin are shown in red, blue and green, where each colour corresponds to one separate scenario and lines connect arrows of sites that are entangled:

Red: $\frac{1}{\sqrt{2}}(|000011000\rangle + |000000011\rangle)$

Blue: $\frac{1}{\sqrt{2}}(|000010010\rangle + |000001001\rangle)$

Green: $\frac{1}{\sqrt{2}}(|000010001\rangle + |000001010\rangle)$
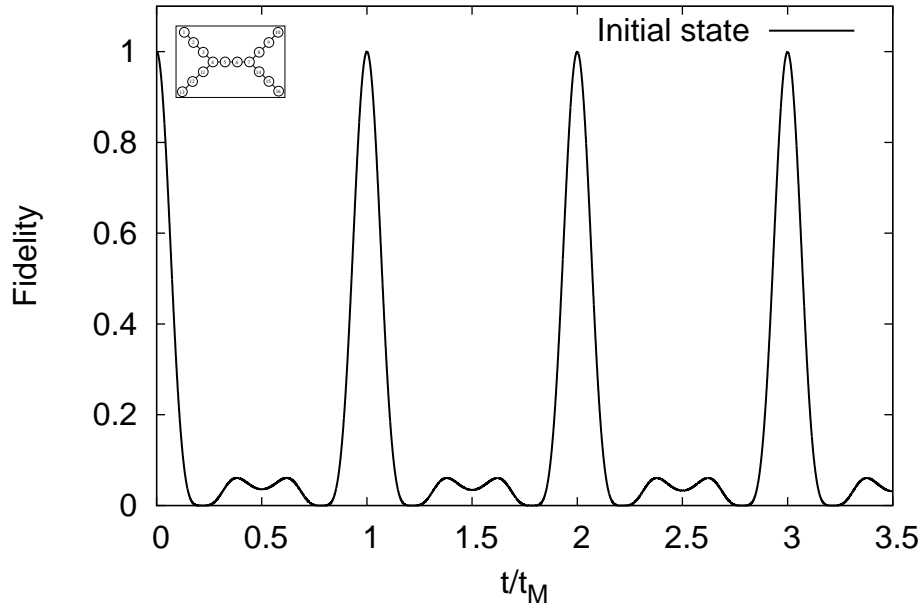
Figure 2.15: Evolution of the initial single excitation state entangling the second to last terminal spin in each of the four branches of a 16-spin double branched chain of branch length 3 vs. rescaled time t/t_M.

2.2.3 Double branched spin chains

It was shown in section 2.1.3 that amongst unentangled states only those consisting of a single excitation at the central spin (which is only possible for odd chains) allow for PST in double branched chains. However, these states are their own mirror twins, so they never result in perfect transfer to an entangled state. Nonetheless, an initial state consisting of a single excitation split evenly over the terminal spins of the four branches, so a fourpartite entanglement, does allow for PST. Again, this state is its own mirror twin, so that the PST is in fact a perfect revival, without any noteworthy intermediate states occurring.

Similarly, an initially entangled state consisting of one excitation split evenly over all four branches such that all four spins of the same distance to their respective terminal spins are entangled is recovered perfectly at times $t_M, 2t_M, \cdots$ as it is its own mirror twin (independent of the parity of the device). See figure 2.15 for an illustration of this, where the four second to last terminal spins are initially entangled.

Within the realms of entangled single-excitation states, further possibilities arise. For example, one could think of an entangled state between the terminal spins of branches 1 and 4 as an initial state. This state does allow for PST, independent of an even or odd number of spins in the device, and is per-
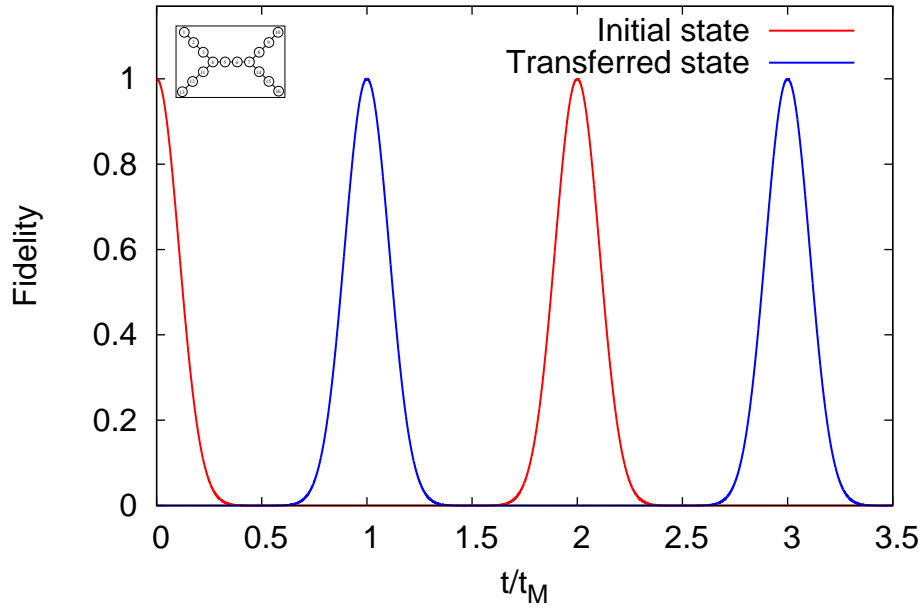
Figure 2.16: Evolution of the initial single excitation state entangling the terminal spins of branches 1 and 4 of a 16-spin double branched chain of branch length 3 and its mirror twin, the transferred state entangling the terminal spins of branches 2 and 3, vs. rescaled time t/t_M.

fectly transferred to its mirror twin, the state entangling the terminal spins of branches 2 and 3, at time t_M (see figure 2.16).

Expanding this type of initially entangled input to multiple excitations does however not result in PST as it encounters the same problems as described in section 2.1.2. For example, a double branched chain with input such that the terminal spins of branches 1 and 4 are entangled (in any way) and the terminal spins of branches 2 and 3 are entangled (meaning two excitations present in the system overall) never reverts with 100% fidelity to this original state, although the timing of the dynamics is conserved - as the input is symmetric we would expect it to be its own mirror twin. For a demonstration, see figure 2.17.

These observations hold for both odd and even chains, with any length of stem and branches, as well as an odd or even number of excitations greater than one. Similar to the set-up described in section 2.1.3 (figure 2.9), the lack of PST in double branched chains, despite favourable, symmetric conditions for multiple excitations, shows that double branched chains cannot be thought of as the sum of two Y-type devices with a linear part forming the stem, but they must indeed be considered as a different class of devices.

Very small double branched chains, with a short stem and typically with branch length 1, take a somewhat special place when considering two excitation en-
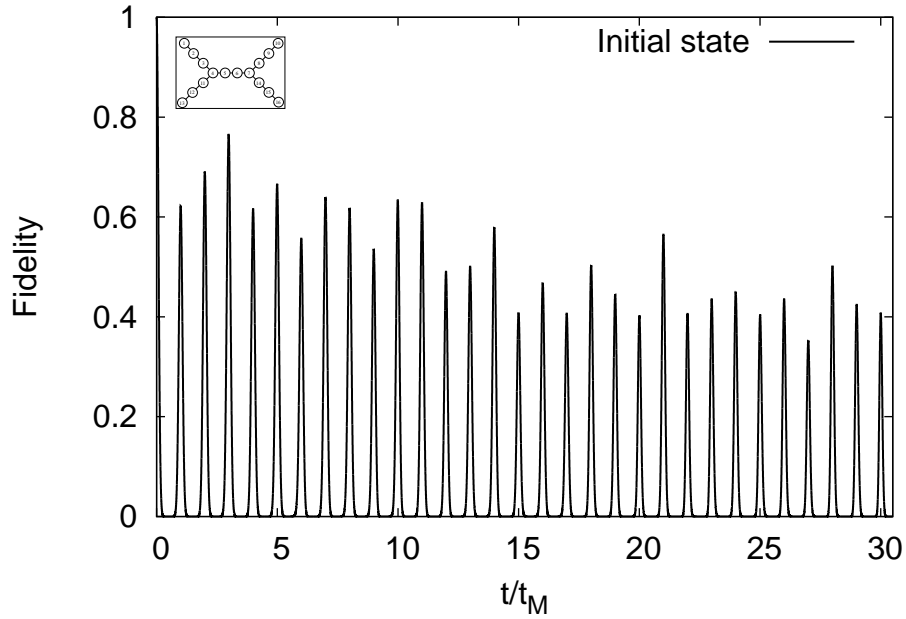
Figure 2.17: Evolution of the initial two excitation state entangling the terminal spins of branches 1 and 4 and the terminal spins of branches 2 and 3 of a 16-spin double branched chain of branch length 3 vs. rescaled time t/t_M.

tangled input (where the entanglement is split evenly) as described above for figure 2.17. Due to the restricted spatial freedom in the device, it appears as though after an initial period of state fidelity decay, the fidelity of the initial state is eventually nearly perfectly recovered at irregular intervals during the time scale which we have considered, although the period of the dynamics is preserved (see figure 2.18). While it might be tempting to deduce that this makes double branched chains suitable for entangled state transfer of more than one excitation, it has to be kept in mind that such long time scales are experimentally very unrealistic due to decoherence effects etc. [151, 152]. In addition, the recovered fidelity decays rapidly with the size of the device. In particular, branches longer than a single spin will result in fast loss of any state fidelity, both short term and long term.

Other entangled multi-excitation inputs, for example involving entanglement between the stem and one or more of the branches, does also not lead to PST.

2.3   State storage

After having thoroughly investigated the possibilities of information transfer in spin chains, we will now look into mechanisms for conserving information
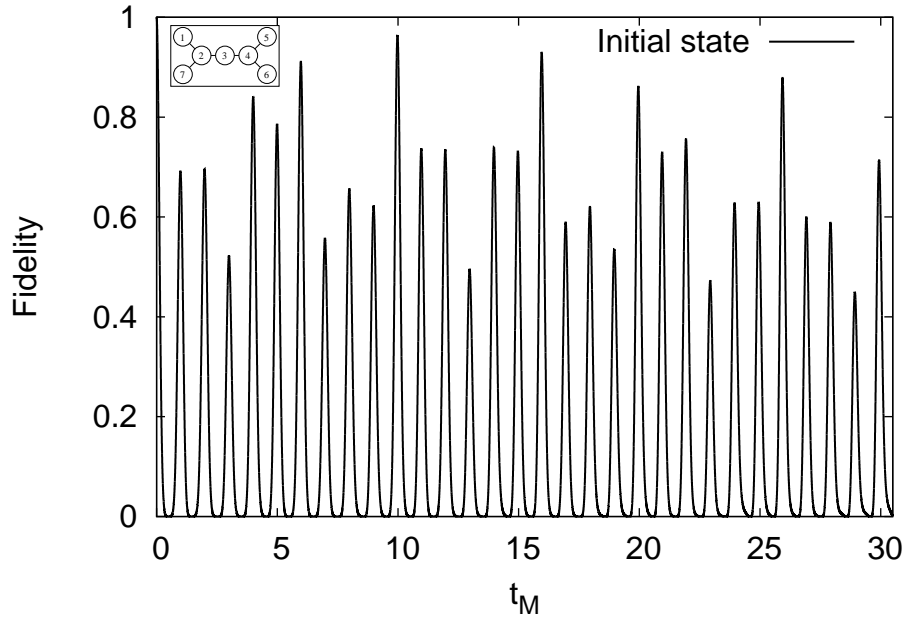
Figure 2.18: Evolution of the initial two excitation state entangling the terminal spins of branches 1 and 4 and the terminal spins of branches 2 and 3 of a 7-spin double branched chain with branch length 1 vs. rescaled time t/t_M.

within spin chain devices, a procedure known as "state storage", as discussed for example in [153–156]. Quantum state storage is a further application of spin chains as information carriers which is specific to the quantum domain. The benefits of such storage possibilities are many. Certainly in distributed networks the ability to "hold" information for short intervals of time, while other computations are effected or the target register is being prepared, would be extremely useful.

2.3.1   Linear spin chains

The results in this section are original work. Linear chains are perhaps the most difficult devices to use for state storage, assuming that extremely intrusive mechanisms such as a complete switching off of the couplings between the spins (and subsequent switching back on when the storage period is over) are not allowed or feasible. Under this assumption, the only possibility for state storage is to achieve a state that is an eigenstate of the Hamiltonian $\widehat{\mathscr{H}}$ (equation (1.3)). This state does then not evolve any further, up to a global phase. We can find these eigenstates numerically, but as we are aiming for minimum intervention to achieve state storage, we are in particular hoping to find an eigenstate that is close to a meaningful input state or its twin.

A very good example of this can be demonstrated on a 4-spin chain. First of all, note that a 4-spin chain containing two excitations has (amongst others) the following eigenstate:

$$|\psi_{Eigen}\rangle = \frac{1}{2}[-|1100\rangle + |0011\rangle + |1010\rangle - |0101\rangle] \tag{2.6}$$

which can be factorised as $|\psi_{Eigen}\rangle = \frac{1}{2}([|0_2 1_3\rangle - |1_2 0_3\rangle] \otimes [|0_1 1_4\rangle + |1_1 0_4\rangle])$. This is remarkably close to a state consisting of two Bell states $\frac{1}{\sqrt{2}}(|10\rangle \pm |01\rangle) = |\pm\rangle$. In particular, this means that if we inject one such state $|+\rangle$ onto spins 2 and 3 and another onto spins 1 and 4, we can store these two Bell states as an eigenstate of the Hamiltonian describing system simply by "flipping" the phase of spin 2 or 3, a very minor intervention. A phase flip gate would implement the gate $|0\rangle \rightarrow |0\rangle$ and $|1\rangle \rightarrow -|1\rangle$ and should be implemented on a short time scale compared to the other spin dynamics. As we know the time scale of perfect revival, if state storage immediately after injection is not possible we still know exactly when to effectuate the phase flip (after $2t_M, 3t_M, 4t_M$ etc.). The original input state can then be retrieved by performing the same phase flip gates again.

A demonstration of this is given in figure 2.19. The initial state $|\psi_{Bell}\rangle = \frac{1}{2}([|1_2 0_3\rangle + |0_2 1_3\rangle] \otimes [|1_1 0_4\rangle + |0_1 1_4\rangle])$, which results from the injection of one Bell state $|+\rangle$ in spins 2 and 3 and another one in spins 1 and 4, revives at time t_M, at which stage the phase of spin 2 is flipped, transforming $|\psi_{Bell}\rangle$ into $|\psi_{Eigen}\rangle$. From this point in time, the state is stored: Its fidelity stays constant at 1 with no further evolution of the system.

Unfortunately, longer chains with two or more excitations do not have eigenstates that can be factorised into forms similar to equation (2.6), allowing us to utilise a single phase flip to store a common system state. Naturally, one can always construct a suitable input state when an eigenstate is known, but this seems much more artificial than the storage of Bell states, which are a common resource in quantum computation protocols. Linear chains with more spins and excitations have increasingly complicated eigenstates with many terms, making the possibility of factorisations as in equation (2.6) increasingly unlikely. Numerical investigations up to 8 spins with 4 excitations revealed no such eigenstates. The only device up to this chain length with an eigenstate that can be factorised into Bell states is a 6-spin chain with 2 excitations, where
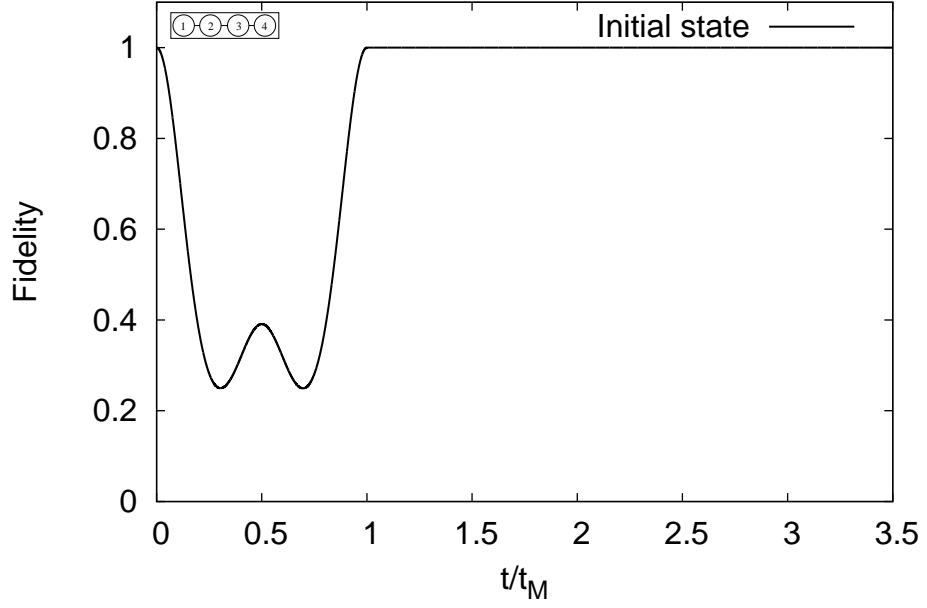
Figure 2.19: Evolution of the initial state $|\psi_{Bell}\rangle = \frac{1}{2}([|1_2 0_3\rangle + |0_2 1_3\rangle] \otimes [|1_1 0_4\rangle + |0_1 1_4\rangle])$ vs. rescaled time t/t_M. At t_M, the phase of spin 2 is flipped, resulting in storage of $|\psi_{Bell}\rangle$.

the factorisation is as follows:

$$
\begin{aligned}
|\psi_{Eigen}\rangle = & 0.18[|0_3 0_4\rangle[|1_2 0_5\rangle - |0_2 1_5\rangle][|1_1 0_6\rangle + |0_1 1_6\rangle]] + \\
& 0.38[|0_2 0_5\rangle[|1_3 0_4\rangle - |0_3 1_4\rangle][|1_1 0_6\rangle + |0_1 1_6\rangle]] + \\
& 0.28[|0_1 0_6\rangle[|1_3 0_4\rangle - |0_3 1_4\rangle][|1_2 0_5\rangle + |0_2 1_5\rangle]].
\end{aligned}
\tag{2.7}
$$

$$
\tag{2.8}
$$

However, due to the different coefficients in this sum, we cannot use the same phase flip method as we did for state storage in a 4-spin chain, which thus remains the only device capable of storing Bell states.

2.3.2 Y-type spin chains

As we have seen in previous sections, the dynamics of Y-type chains are far more complex than those of linear chains. For purposes of state storage, this can be turned into a major advantage [132, 157, 158]. As we have however shown that PST in Y-type chains is only possible for states (entangled or otherwise) containing a single excitation, we will restrict the following discussions to single excitation states also.

Let us now consider an input state in a Y-type chain of branch length 1 such

that there is an excitation in the first spin (see for example figure 2.4). As we have seen in section 2.1.2, at time t_M this state results in a mirror twin where the two branch spins are entangled. Let us label these two branch spins A and B: The mirror twin is then the state

$$|\psi_{Twin}\rangle = \frac{1}{\sqrt{2}}[|0\rangle_A|1\rangle_B + |1\rangle_A|0\rangle_B] = |+\rangle_{AB}. \tag{2.9}$$

This is very similar to an eigenstate of the Hamiltonian describing the system, $|\psi_{Eigen}\rangle = \frac{1}{\sqrt{2}}[|0\rangle_A|1\rangle_B - |1\rangle_A|0\rangle_B] = |-\rangle_{AB}$ (the remaining spins, i.e., the stem and hub spins, are all in state $|0\rangle$ in this state), irrespective of the length of the stem. We can therefore use a phase flip gate (as in section 2.3.1) on either spin A or B to change $|\psi_{Twin}\rangle$ into $|\psi_{Eigen}\rangle$ at t_M (or any odd multiple thereof). $|\psi_{Eigen}\rangle$, as an eigenstate of the Hamiltonian describing the system, will then not partake in the dynamics anymore: The state is now stored [132, 157, 158].

For example, consider a 5-spin Y-type chain with branch length 1 with input state $|\psi_{in}\rangle = |10000\rangle$, the normal state evolution of which we have shown in figure 2.4. Spins A and B correspond to spins 4 and 5 in this case. Figure 2.20 shows that a phase flip of spin 5 at time t_M results in the storage of $|\psi_{out}\rangle = 1/\sqrt{2}(|00010\rangle + |00001\rangle)$: Its fidelity stays constant at 1. Moreover, we see in this figure that the individual components of $|\psi_{out}\rangle$, such as $|00001\rangle$ in figure 2.20, also do not evolve any further.

This idea can further be used for state storage of more distributed Y-type chains, i.e., those with longer branches. As we have seen in section 2.1.2, Y-type chains are capable of PST of single excitation states even when more than one hub is used, provided that the hub rule is obeyed and the branch lengths remain symmetrical (see figure 2.7). If we now wish to store an entangled state in a Y-type device with longer branches after input in the first stem spin, we simply perform a further splitting of the two branches, turning both terminal spins into hubs and adding two branches of length 1 to each of those new hubs (see figure 2.21) [132, 157]. We then proceed as before, except that we now have to utilise two phase flip gates. Using the labelling of figure 2.21, an excitation injected into spin 1 will transfer to the mirror twin $|\psi_{Twin}\rangle = \frac{1}{2}[|1_A0_B0_C0_D\rangle + |0_A1_B0_C0_D\rangle + |0_A0_B1_C0_D\rangle + |0_A0_B0_C1_D\rangle]$ at t_M. In order to store this fourpartite entanglement, it is sufficient to flip the phase of one spin of the pair (A, B) and one spin of the pair (C, D), so that the system will then be in an eigenstate such as $|\psi_{Eigen}\rangle = \frac{1}{2}[|1_A0_B0_C0_D\rangle - |0_A1_B0_C0_D\rangle + |0_A0_B1_C0_D\rangle - |0_A0_B0_C1_D\rangle]$ (in this particular eigenstate, spins B and D were flipped).

This state is now stored and can either be retrieved and used as a resource in further (distributed) networking or alternatively the same spins can be sub-
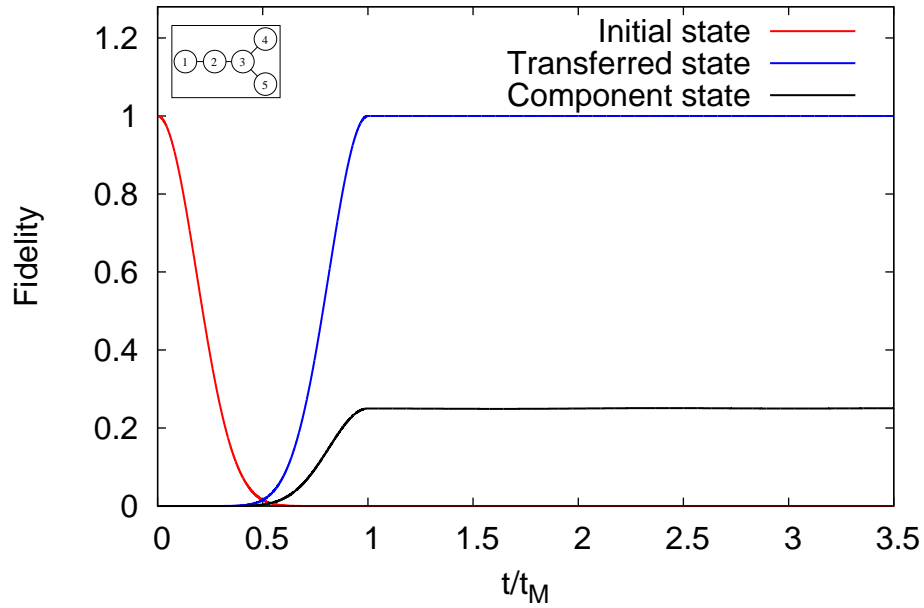
Figure 2.20: Transfer of the initial state $|10000\rangle$, its mirror twin, the transferred state $1/\sqrt{2}(|00010\rangle + |00001\rangle)$, and a component of the transferred state ($|00001\rangle$) vs. rescaled time t/t_M. After a phase flip of spin 5 at t_M, the transferred state is stored: Both it and its component state evolve no further.
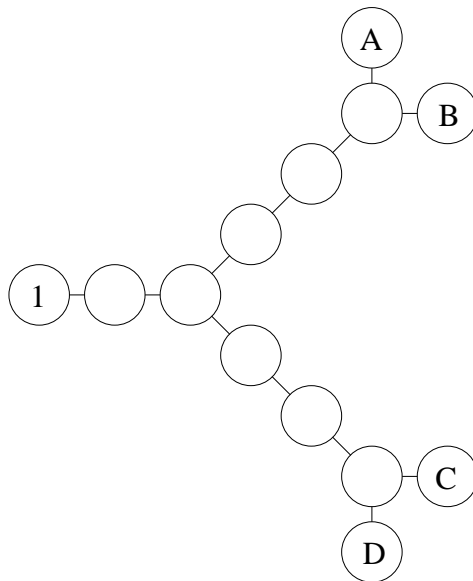
Figure 2.21: Diagram of a Y-type chain with three hubs that can be used to store a state in spins A, B, C and D after injection of an excitation in spin 1.

jected to another phase flip in order to resume the natural system dynamics [132, 157]. The advantage of being able to store a state before its extraction is apparent, in that the potentially more complex extraction protocol does not have to take effect exactly at t_M but is allowed much more temporal freedom.

2.3.3   Double branched spin chains

Having analysed the storage possibilities of a Y-type chain with an additional pair of hubs as in figure 2.21, state storage in double branched chains follows naturally. The work presented here, while based on the previous section, is however original. An advantage over a Y-type chain with three hubs lies in the spatial separation of the two pairs (A, B) and (C, D), which might bring an essential advantage for experimental implementations and in particular the implementation of the phase gate. Physical realisations might also be helped by the fact that more spatial separation is achieved with fewer spins. On the other hand, there are of course severe limitations on possible input sites for the initial excitation, as well as initial input states. As we have seen in figure 2.8, input in the central spin of an odd double branched chain results in perfect revival at every t_M due to the input state being its own mirror twin. Unfortunately, this means that this type of input does not transfer to a perfect fourpartite entanglement and is thus not suitable for simple state storage. Nonetheless, we have also seen in section 2.2.3 that an initial fourpartite entangled state does allow for PST under certain conditions. We can therefore demonstrate state storage on the example of a 7-spin chain of branch length 1, as shown in figure 2.22: At time t_M, the phases of spins 1 and 6 are flipped (corresponding to one spin of the two left hand branch spins and one of the two right hand branch spins), resulting in perfect storage of the initial fourpartite input state.

Again in analogy with Y-type chains, state storage in double branched chains with branches longer than a single spin is in theory also possible. This time, we require an additional four hubs in our device to split each of the original four branches and to then attach two single spin branches to each of the four new hubs. We will then also need to put four phase gates into effect in order to store the achieved state, which at this point will be eight-fold entangled. As this amount of hubs and required phase gates is experimentally extremely challenging, such a distributed double branched chain will probably remain a hypothetical tool for the time being.
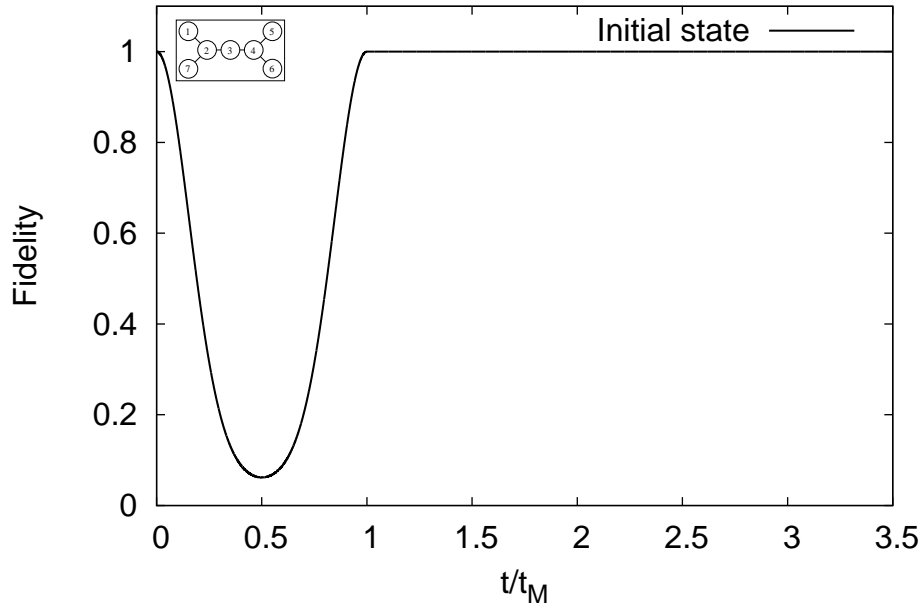
Figure 2.22: Evolution of the initial single excitation state entangling the four branch spins of a 7-spin double branched chain of branch length 1 vs. rescaled time t/t_M. After flipping the phases of spins 1 and 6 at time t_M, the initial state is stored at perfect fidelity.

2.4 Conclusions

In this chapter, we set out to investigate the possibilities and limitations of information transfer in spin chains, as well as state storage. We conclude that only linear chains are capable of PST of arbitrary input states, both unentangled and entangled, and containing any number of excitations. Both Y-type and double branched chains are only capable of perfectly transferring single excitation states, and only under circumstances where specific, symmetry dependent rules are observed. However, both these types of devices are also capable of perfectly transferring entangled states (restrictions by symmetry and to single excitations apply).

Y-type and double branched chains do however have one major advantage over linear spin chains, namely when it comes to state storage. While it is extremely rare for linear chains to be endowed with a system eigenstate which is similar to a meaningful input state (such as a Bell state), and we have only observed a single system where this is the case, branched devices can, in theory, be made to store states with relative ease. They are once more restricted to single excitation states and care must be taken with regards to the symmetry of the input, but nonetheless a much wider range of simple states, initially

either unentangled or entangled, can be stored than for linear chains. With increasing spatial distribution, branched devices are however also becoming increasingly challenging to realise experimentally, and therein lies their most elemental limitation.

Chapter 3

Using spin chains to "knit" cluster states

In this chapter, we will discuss a very diverse use of spin chains, namely their ability to generate, or "knit", distributed cluster states. For this purpose, we will only discuss linear chains, as no further dynamics as provided by branched devices are needed. Linear spin chains have previously been used to generate other entangled states [159], but the algorithm we propose in section 3.2.3 is original work which was also published in [42]. We will first of all introduce cluster states and make some general observations about spin chains, before discussing the specific algorithm used to produce or "knit" cluster states.

3.1 Idea and concept

Before going into any detail about how to fabricate cluster states with spin chains, let us first of all give a brief introduction to the nature of cluster states and outline why it might be desirable to be able to construct them. As we will see, one of the crucial components in the generation of any type of cluster states are quantum gates and so we will also take note of the ability of spin chains to effect such gates before moving on to the cluster state "knitting" algorithm.

3.1.1 Cluster states: definition

Cluster states were first introduced by Briegel and Raussendorf [160] as a particular type of graph state. In their work, it is detailed how a cluster state, which they require to satisfy a number of conditions, is constructed from a set of qubits on a d-dimensional lattice ($d = 1, 2, 3$), see figure 3.1 or [161] for
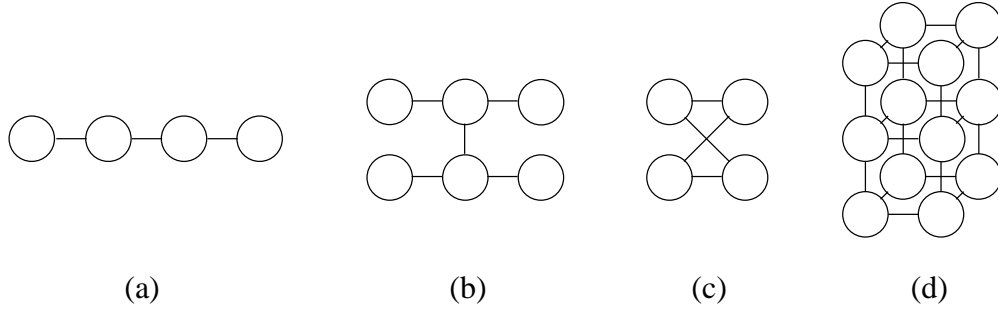
Figure 3.1: Examples of cluster states for (a) $d = 1$, (b) $d = 2$, (c) $d = 2$ and (d) $d = 3$. Circles represent sites, lines represent vertices.

examples. This lattice represents the particular graph state structure that this concept is based on. A cluster state can be shown to be a pure state based on this graph state structure, satisfying maximum connectedness (meaning that any two distinct qubits of a set of qubits can be projected into a pure Bell state by local measurements on a subset of the other qubits) and properties of persistency (the minimum number of measurements needed to completely disentangle a qubit from the cluster state) [160]. Thanks to these properties, a cluster state differs significantly from other entangled quantum states, such as W states [162] or GHZ states [163], in that it is much more difficult to destroy entanglement, for example by accidental or inaccurate projective measurements. Both GHZ states as well as cluster states have been realised experimentally, for example using six photons [130]. The qubits (vertices) of these special types of graph states can be connected by edges via control-Z interactions if they are initially in a $|+\rangle = \frac{1}{\sqrt{2}}(|0\rangle + |1\rangle)$ state. We therefore define the operator

$$\widehat{CZ} = \begin{pmatrix} 1 & 0 & 0 & 0 \\ 0 & 1 & 0 & 0 \\ 0 & 0 & 1 & 0 \\ 0 & 0 & 0 & -1 \end{pmatrix} \tag{3.1}$$

which acts on two previously unentangled qubits (each in state $|+\rangle$) of the cluster state to entangle them, creating an edge between them.

3.1.2   Uses of cluster states

The most prominent use of cluster states can be found in one-way quantum computation, where cluster states are considered quantum computers in their own right [164–167]. In this context of measurement-based quantum computation, the encoding of information and programming of algorithms to be computed is then done purely via the nature and sequence of one-qubit measure-

ments effected on the cluster state, where measurement outcomes determine the nature of following measurements. In fact it can be shown that any quantum logic circuit can be implemented in this way [165] and some research has also been done to relax the single spin control requirement [168]. One-way quantum computing allows for quantum error correction techniques and can be used for any quantum algorithms such as quantum teleportation, dense coding, Shor's algorithm etc.

Cluster states have recently seen a lot of attention in optical quantum computing [144, 169]. One of the possible implementations of large cluster states lies in the use of optical lattices, where individual atoms are trapped in wells using electro-magnetic potentials. Unfortunately, such systems have problems on two scales: First of all, the size of such lattices is limited by construction and decoherence. This is less of a problem in one-way quantum computing, where computations requiring bigger cluster states than are available can be split over multiple states. Secondly however, the lattice spacing is very close in wavelength to the wavelength of the lasers used to manipulate the well heights, thereby creating unwanted entanglement or effecting unwanted measurements, which leads to a high level of errors. When we are aiming to generate cluster states using spin chains, these are factors to be kept in mind, in that a very low level of control over the system, i.e., requiring access to as few sites as possible, is desirable.

3.1.3 Quantum gates in spin chains

In order to understand the natural link between spin chains and quantum gates, we need to take a step back. Quantum gates form an intrinsic part of quantum information processing needed in any quantum algorithm and in fact entire models for quantum computation have been based on them [104, 170]. In this work, we will be interested in quantum gates only in the context of spin chains, so let us consider an arbitrary initial state of a spin chain, $|\psi_{ini}\rangle$. Any state can be decomposed into its even and odd parts under the mirror operator $\widehat{M}$ (equation 2.1), so that if we set $|\psi_{\pm ini}\rangle = \frac{1}{\sqrt{2}}(|\psi_{ini}\rangle \pm \widehat{M}|\psi_{ini}\rangle)$, we can write

$$|\psi_{ini}\rangle = \frac{1}{\sqrt{2}}(|\psi_{-ini}\rangle + |\psi_{+ini}\rangle). \tag{3.2}$$

Similarly, the eigenstates of $\widehat{\mathcal{H}}$ can be decomposed into odd and even energy eigenstates so that $|\psi_{\pm ini}\rangle \equiv \sum_{\pm k} c_{\pm k}|\varepsilon_{\pm k}\rangle$. At t_M, we require the evolved state of

$|\psi_{ini}\rangle$, $|\psi_{t_M}\rangle$, to have unit fidelity against $\widehat{M}|\psi_{ini}\rangle$ and so we must have

$$|\psi_{t_M}\rangle = \frac{e^{-i\theta}}{\sqrt{2}}\left(\sum_{+k} c_{+k}|\varepsilon_{+k}\rangle - \sum_{-k} c_{-k}|\varepsilon_{-k}\rangle\right). \tag{3.3}$$

We see from this that at t_M, the spin chain has picked up a phase factor of $e^{-i\theta}$ which is potentially disruptive but can be easily predicted via the chain length N, as in the single excitation subspace $e^{-i\theta} = (-i)^{N-1}$ [44]. As we are assuming that we are aware of the number of spins in the chain, having set it up for PST according to equation (1.5), we can now consider this phase a controllable feature of the spin chain [171–174]. In particular, the phase factor is unity when $(N-1)$ is a multiple of 4. The fact that every spin chain has a built-in quantum gate distinguishes them from most other quantum systems, where gates have to be achieved via other means [175], which means that more effort has to be put into minimising the number of gates needed [176].

Let us now consider the case where the initial state of a spin chain involves excitations only in spins 1 and N. In the most general case, this initial state must be a superposition of vectors in the excitation subspaces $T = \{0, 1, 2\}$ (see section 1.2.1.2) so it can be expressed in term of the basis $\{|0\rangle_1|0\rangle_N, |0\rangle_1|1\rangle_N, |1\rangle_1|0\rangle_N, |1\rangle_1|1\rangle_N\}$. At time t_M, a chain with this type of input, $|+\rangle_1|+\rangle_N \otimes |0_2 \cdots 0_{N-1}\rangle =$
$= \frac{1}{2}(|0\rangle_1|0\rangle_N + |0\rangle_1|1\rangle_N + |1\rangle_1|0\rangle_N + |1\rangle_1|1\rangle_N) \otimes |0_2 \cdots 0_{N-1}\rangle$, will have effected the following gate:

$$\widehat{G} = \begin{pmatrix} 1 & 0 & 0 & 0 \\ 0 & 0 & (-i)^{N-1} & 0 \\ 0 & (-i)^{N-1} & 0 & 0 \\ 0 & 0 & 0 & (-1)^N \end{pmatrix}. \tag{3.4}$$

This gate is explained by Yung and Bose [171, 172], as well as Clark et al. [173, 174] in their respective works. The effective phase flip underlying these gates stems from the $T = 2$ excitation subspace. As the excitations in a spin chain can be treated as non-interacting fermions, two excitations will anticommute as they pass through each other. If we now set N such that $(N-1)$ is a multiple of 4, we notice that the resulting case of $\widehat{G}$, which we will call $\widehat{G'}$, is the product of a SWAP gate $\widehat{S}$ and a CZ-gate $\widehat{CZ}$ as introduced in equation (3.1):

$$\widehat{G'} = \begin{pmatrix} 1 & 0 & 0 & 0 \\ 0 & 0 & 1 & 0 \\ 0 & 1 & 0 & 0 \\ 0 & 0 & 0 & -1 \end{pmatrix} = \begin{pmatrix} 1 & 0 & 0 & 0 \\ 0 & 0 & 1 & 0 \\ 0 & 1 & 0 & 0 \\ 0 & 0 & 0 & 1 \end{pmatrix}\begin{pmatrix} 1 & 0 & 0 & 0 \\ 0 & 1 & 0 & 0 \\ 0 & 0 & 1 & 0 \\ 0 & 0 & 0 & -1 \end{pmatrix} = \widehat{S}\widehat{CZ} = \widehat{CZ}\widehat{S}.$$
$$\tag{3.5}$$
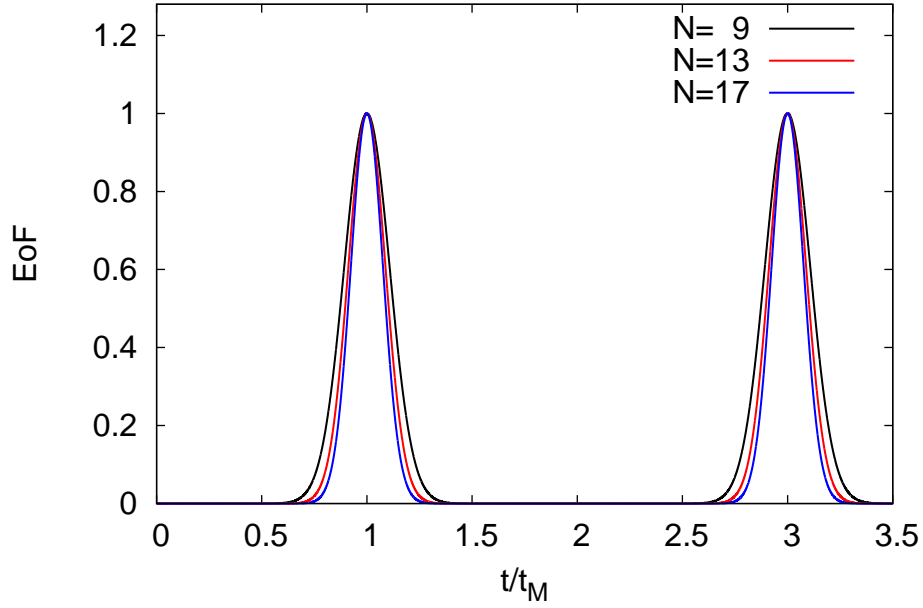
Figure 3.2: Evolution of Entanglement of Formation (EoF) between spins 1 and N for $N = 9, 13, 17$ after injection of $|+\rangle$ states at 1 and N vs. rescaled time t/t_M. Figure adapted from [42].

This can be understood as showing that every time two excitations pass through each other in such a spin chain, they undergo a SWAP operation and also become entangled. The maximum entangling effect of $\widehat{G}'$ is illustrated in figure 3.2, where two $|+\rangle = \frac{1}{\sqrt{2}}(|0\rangle + |1\rangle)$ states have been injected at spins 1 and N of chains of length $N = 9, 13, 17$. As we expected, at t_M the end spins 1 and N have become maximally entangled. As the system dynamics evolves, the end spins become completely unentangled again at $2t_M$ (as $\widehat{G}'\widehat{G}' = \widehat{I}_4$), reach maximum entanglement again at $3t_M$ and so on and so forth. The width of the EoF peak (as defined in section 1.1.2.3) at t_M (and odd multiples thereof) decreases with N (see figure 3.2). For the range of spin chains explored, this decrease scales approximately as $1/\sqrt{N}$, meaning that a potential recovery of entangled spins should be possible even for very long chains.

3.2   Working algorithm

So far we have (i) established the basic ideas behind cluster states and their uses in quantum information processing and (ii) demonstrated that spin chains are capable through their natural dynamics alone of entangling spins via a built-in CZ-gate; we are now going to lay out the working algorithm of a knitting protocol for cluster state ladders.
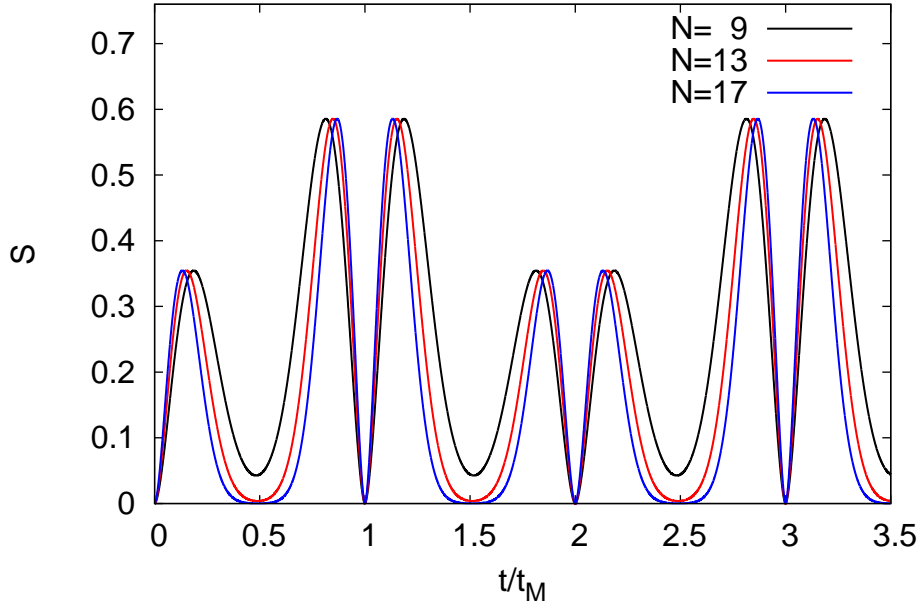
Figure 3.3: Evolution of von Neumann entropy S of spins 1 and N with respect to the rest of the chain, for $N = 9, 13, 17$, and after injection of $|+\rangle$ states at 1 and N vs. rescaled time t/t_M. Figure adapted from [42].

3.2.1 Spin chain entanglement entropy

One of the key observations in the cluster state knitting protocol stems from the entanglement entropy S of the spin chain, as defined in section 1.1.2.2. In this case, we consider the following bipartition of the system: the two end spins (spins 1 and N) and the rest of the chain (spins $2, \cdots, N-1$). For an initial state described as above, with $|+\rangle$ states injected at sites 1 and N and under the action of the intrinsic gate $\widehat{G}'$, the entropy S related to this bipartition evolves as shown in figure 3.3. As is to be expected, the entropy is zero at $t = 0$ (representing the fact that upon injection, there are only excitations in the two end spins while the rest of the chain is empty and thus disentangled) and also zero at t_M (representing the fact that the two end spins are maximally entangled with each other, meaning that they are perfectly disentangled from the middle spins of the chain.). This pattern repeats then at every t_M, as discussed in section 3.1.3. Again, the width of the dips at $t_M, 2t_M, 3t_M \cdots$ scales approximately as $1/\sqrt{N}$.

An important feature of figure 3.3 is the dip of S at $0.5t_M$: We observe that for increasingly long chains, the dip at this point in the evolution tends to zero, meaning that the end spins 1 and N are decoupled from the rest of the chain once more. In particular, this means that for a chain of sufficient length, where S will be low enough to have effective good decoupling, we can inject a

second pair of $|+\rangle$ states into spins 1 and N without perturbing the state of the system. At $0.5t_M$, we see from the dip in S that the excitations contained in the chain are localised in spins 2 to $(N-1)$, allowing for this second injection. As the minimum dip widens with increasing N, the precise timing of this second injection becomes less crucial for longer chains.

Discovering this entropy dip is a crucial observation without which we could never produce more than one entangled pair of qubits. As we can now inject another pair, thus obtaining a total of four excitations in the chain which will all undergo fermionic crossing, we can start building up a cluster state ladder.

3.2.2   Error correction after imperfect injection

Injecting excitations into a spin chain can be done via various mechanisms. The nature of the injection mechanism becomes relevant when we are considering the potentially imperfect or perturbed injection of excitations, such as for example errors in the injection of a second pair of excitations into a spin chain already containing a pair, as suggested in section 3.2.1. There will be a more in-depth discussion of injection errors in section 6.2, but for the purpose of cluster state knitting we will only consider injection by SWAP operation (see section 1.2.3.2). In order to effect a SWAP operation, we require the use of two auxiliary qubits, which contain the $|+\rangle$ states which we are intending to inject. Under the assumption that the SWAP operation itself is not subject to errors, we can then immediately after injection perform a measurement of the auxiliary qubits in order to destroy any unwanted entanglement with the chain. In particular for short chains such as $N = 9$, we have seen that the disentanglement of spins 1 and N from the rest of the chain at the time of the second injection ($t = 0.5t_M$) is not perfect (see figure 3.3). After injection, this would lead to an unwanted entanglement between the spin chain and the auxiliary qubits. We can eliminate this entanglement by measuring the auxiliary qubits: Since we are close to perfect disentanglement, we expect the outcome of this measurement to be zero for both qubits. If the outcome is not zero, we know that the injection has at least partially failed, so that we might have to reset the system. This unentangling of the auxiliary qubits does not alter the state of the spin chain beyond renormalisation (as in the case where we measure zero on the auxiliary qubits A and B, the chain will be collapsed into the state $|0\rangle_A \otimes |0\rangle_B \otimes |\psi_1\rangle$). The probability that the injection of the second pair of $|+\rangle$ states is successful is very high (we define the success probability as 1-(occupation probability of spins 1 and N), see definition in section 1.1.2.4), even for $N = 9$ where the probability is 0.9885 (see figure 3.4), and increases further
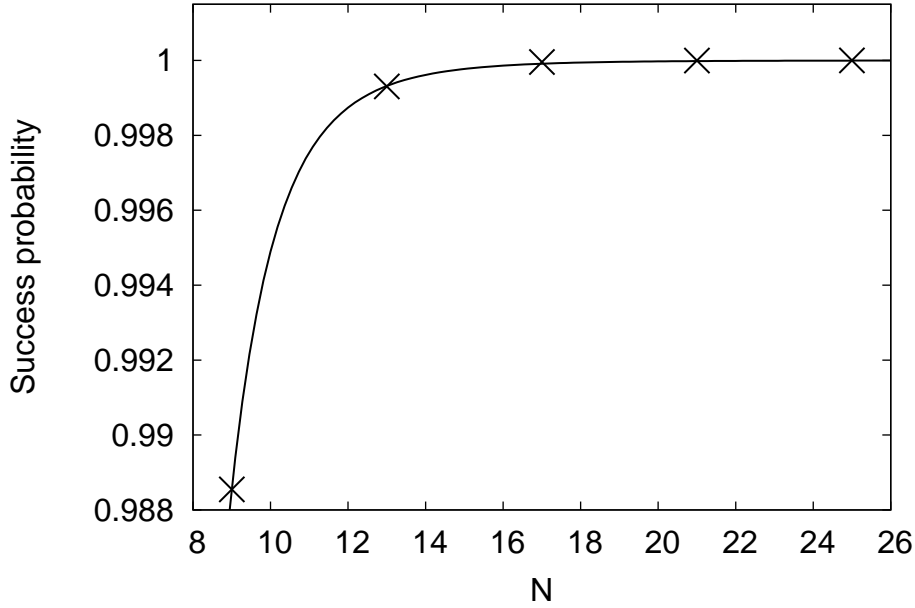
Figure 3.4: Probability of successfully injecting a second pair of $|+\rangle$ states into spins 1 and N at $0.5t_M$ vs. chain length N. Figure published in [42].

with N.

Even with such high success probabilities, it is possible that measuring the auxiliary qubits results in the detection of one or two excitations, in which case we can deduce that the injection has failed. If two excitations are present, we have extracted all excitations which were present in the chain before the SWAP operation, which means that we have reset the chain and can continue with our protocol as if $t = 0$. If instead one excitation only is found, we cannot draw any conclusions about the state of the remaining chain. In this case, the system will have to be reset and the protocol attempted afresh.

3.2.3 "Knitting" algorithm

Let us first of all consider the fabrication of the smallest cluster state of dimension $d = 2$, which requires the use of four qubits (see figure 3.1(c)). As explained in section 3.2.1, the dip in entanglement entropy at $0.5t_M$ allows us to inject a second pair of $|+\rangle$ states into spins 1 and N without perturbing the dynamics of the system (beyond renormalisation). We have now four excitations which will undergo fermionic crossing, thus being entangled due to the action of $\widehat{G}'$ (equation 3.5). Figure 3.5(a) shows a schematic description of the various crossings and figure 3.5(b) the resulting effect on the four qubits, although the excitations can of course not be thought of as being permanently
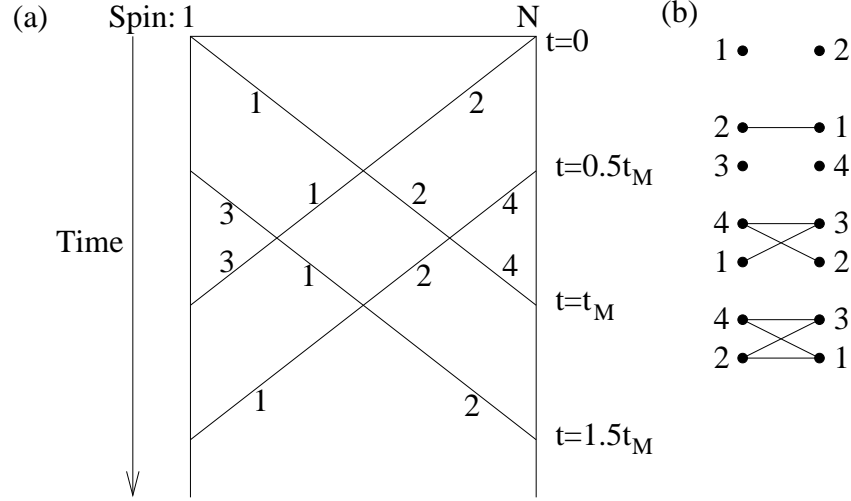
Figure 3.5: Schematic evolution of excitations involved in building of a four qubit cluster state (a) and diagram following build-up of the resulting state (b). Figure adapted from [42].

localised as depicted. Every time a crossing occurs, the crossing excitations become entangled (represented by an edge between them on the right-hand side) and undergo a SWAP operation (as $\widehat{G'} = \widehat{CZ}\widehat{S} = \widehat{S}\widehat{CZ}$ (equation 3.5)), so their labels are switched. After a first extraction at t_M of the states of spins 1 and N (via SWAP operation, swapping in a zero state) and a second extraction at $1.5t_M$, we obtain thus a maximally entangled crossed square cluster state (see final diagram of right-hand side of figure 3.5). The entire algorithm can therefore be completed in only $1.5t_M$, which is less than a full system cycle and therefore very quick. An alternative option for hardware implementation of this protocol besides actual chains of spins are microwave cavity quantum electrodynamics with Rydberg atoms and atomic beams, which have been experimentally achieved [177, 178].

Restricting the necessary manipulation of a spin chain set up for PST to injection and extraction by SWAP gate at two fixed sites, we have thus managed to "knit" a four qubit crossed square cluster state out of $|+\rangle$ states. However, the cluster knitting protocol can easily be extended beyond four qubits. If instead of swapping in a zero state at the first extraction a t_M, we swap in another (third) pair of $|+\rangle$ states, this pair will also become entangled with the remaining pair of excitations in the spin chain. This mechanism can, in theory, be repeated at intervals of $0.5t_M$ after t_M until a cluster state ladder of the desired length has been achieved (see figure 3.6). The actual size of the state will be limited by the qubits' decoherence time (which is dependent on the physical system). It will also be limited by a build-up of error after injection / extraction as refocussing of the system for final states with more than four excitations is
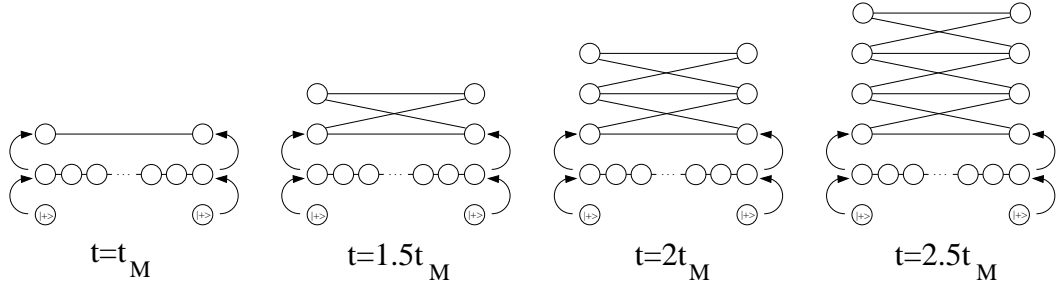
Figure 3.6: Schematic evolution of the progressive build-up of a cluster state ladder (of potentially unlimited size). Each injected spin is in a $|+\rangle$ state.

not possible without destroying parts of the achieved cluster state. Nonetheless, the very positive results from figure 3.4 show a high probability that we may be able to "knit" relatively long chains without any significant errors due to injection.

3.2.4 Demonstration of the working algorithm

We will now demonstrate that the cluster knitting protocol as described above does indeed work and allows us to produce a crossed square cluster state using only a PST spin chain of $(4n+1)$ spins ($n \in \mathbb{N}$) on the example of the four qubit cluster state. To measure the quality of the achieved cluster state, we can unfortunately not use the EoF anymore (as we did to measure the quality of the two qubit gate in section 3.1.3) as this measure is only defined for bipartite systems, so two qubits (see section 1.1.2.3). Instead, we will measure the fidelity of the final state of the four qubits used to store the cluster state against the expected cluster state to judge the quality of the achieved state. As we know the exact state which we are aiming for (the perfect crossed square cluster state), measuring the fidelity of the achieved state against the ideal state provides us with an adequate and reliable quality measure. Figure 3.7 shows the evolution of the fidelity of the ideal state for three different chain lengths. We know from figure 3.3 that the entropy of spins 1 and N with respect to the rest of the chain does not perfectly drop to zero at $0.5t_M$ for a chain with 9 spins only ($N = 9$), which is reflected by a discontinuity at $0.5t_M$ in the fidelity plot for $N = 9$ in figure 3.7. This discontinuity arises from the renormalisation that is effected immediately after the injection at $0.5t_M$: As after successful injection the wavefunction is collapsed into the state $|0\rangle_A \otimes |0\rangle_B \otimes |\psi_1\rangle$ (where A and B are the auxiliary qubits used to inject). If the coefficient of this state was very close to 1 before injection, as is the case for long spin chains, the renormalisation that follows injections has little effect on the new state coefficient and so
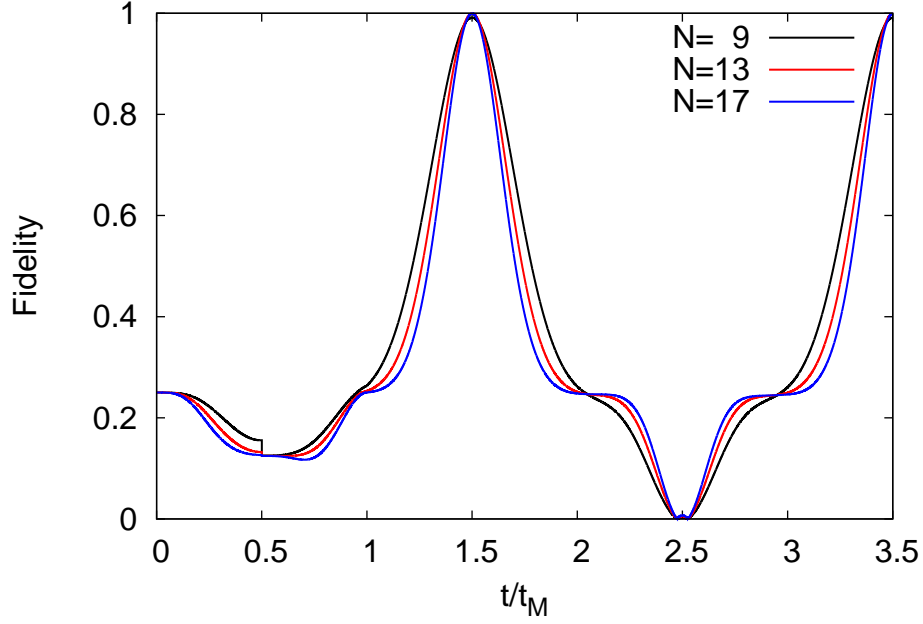
Figure 3.7: Fidelity of the ideal knitted four qubit crossed square cluster state for $N = 9, 13, 17$ vs. rescaled time t/t_M. Figure adapted from [42].

the fidelity of the ideal cluster state remains continuous. Conversely, for short spin chains where the coefficient of the state that the system collapses into was not as close to 1, renormalisation leads to a bigger change in the new system state coefficient, leading to the observed discontinuity in the fidelity of the desired cluster state. Nonetheless, the figure also shows that perfect fidelity is very nearly reached at $1.5t_M$ for $N = 9$ (fidelity reaches 0.9915). For longer spin chains, such as $N = 13$ or $N = 17$, the entropy of spins 1 and N with respect to the rest of the chain at $0.5t_M$ is already sufficiently close to zero that there is no visible discontinuity in the fidelity of the cluster state during the second injection at $0.5t_M$. As expected, perfect fidelity is then also reached at $1.5t_M$. In figure 3.7, the first extraction at t_M is effected but at $1.5t_M$ no extraction is done to observe whether the system continues to evolve in a predictable manner, allowing us to potentially effect the second extraction at a later point in time. As we see in figure 3.7, this is indeed the case: Beyond $1.5t_M$, the system continues to evolve periodically, with the cluster state fidelity dropping to zero at $(2.5 + 2n)t_M$, for all $n \in \mathbb{N}$ (corresponding to the excitations at spins 1 and N having crossed again so that they are completely disentangled), and achieving perfect fidelity at every $(1.5 + 2n)t_M$, making these suitable extraction times. The discontinuity at $0.5t_M$ for $N = 9$ is also reflected by a very small irregular "bump" at $2.5t_M$. Again, the width of the fidelity peaks scales as $1/\sqrt{N}$, in keeping with figure 2.2.
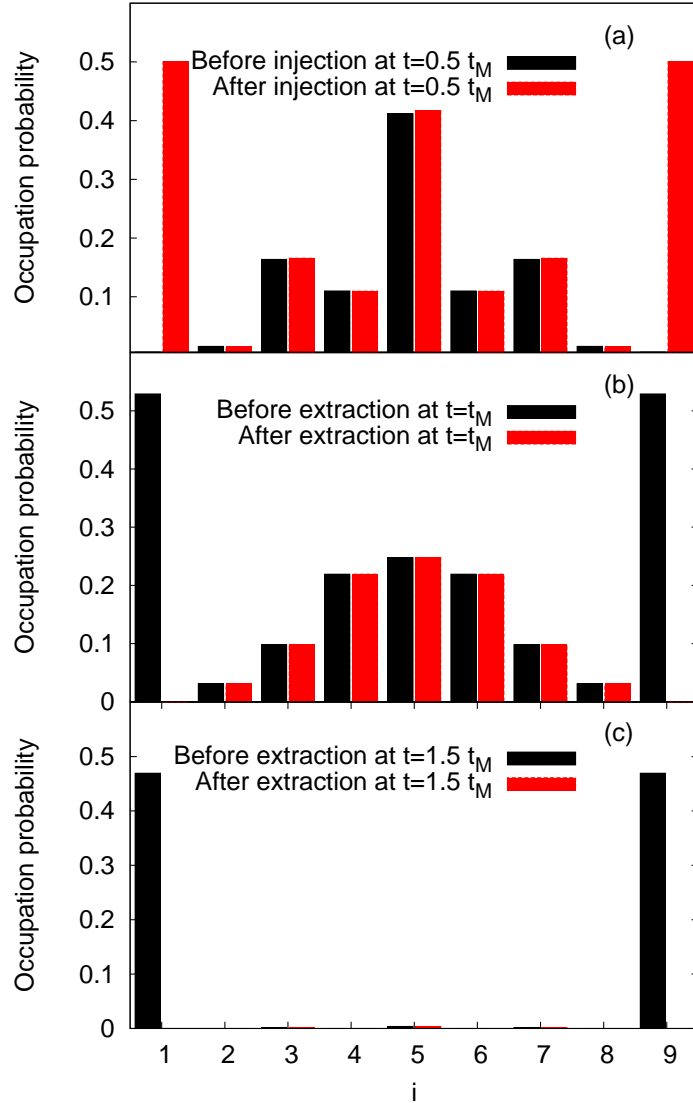
Figure 3.8: Occupation probabilities of the sites i of a 9-spin chain at injection and extraction times of the cluster state knitting protocol for a four qubit cluster state. Figure adapted from [42].

If the second extraction does take place at $1.5t_M$, the chain is left empty and is thus immediately ready to be used again (be it for cluster knitting or other quantum computation tasks). To illustrate this, we use the occupation probability of the sites of a spin chain, as defined in section 1.1.2.4. Figure 3.8 shows a histogram displaying the occupation probabilities for a 9-spin chain at the three crucial stages of the cluster state knitting protocol, $t = 0.5t_m, t_m, 1.5t_M$. Even for $N = 9$, where we have observed that the relatively short length of the chain leads to some inaccuracies in the protocol, the remaining occupation probability of the chain is extremely low, as is shown in figure 3.8, frame (c). Figure 3.8 shows clearly that for a 9-spin chain, spins 1 and 9 are empty before injection at $0.5t_M$ and their occupation probability is 0.5 after injection as
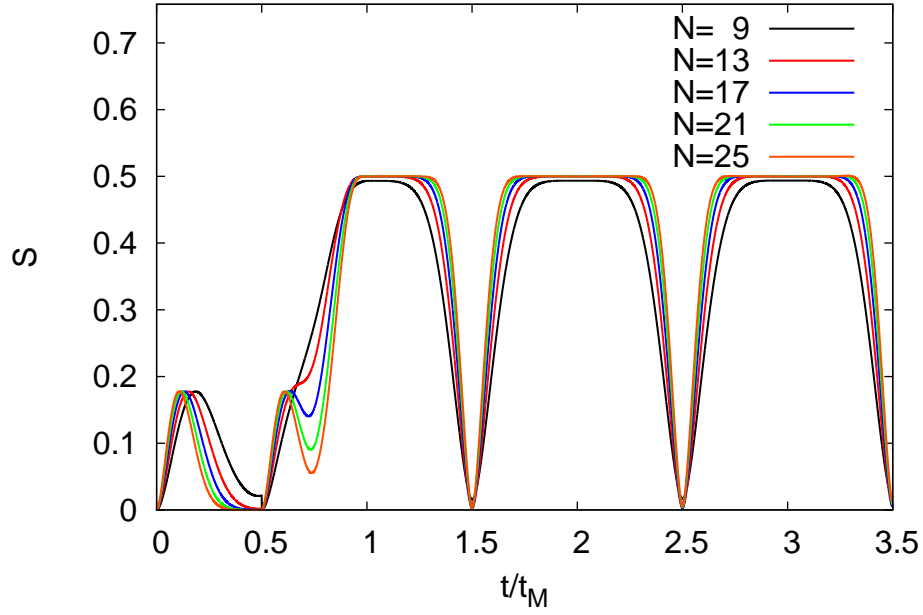
Figure 3.9: Von Neumann Entropy S of the ideal knitted four qubit crossed square cluster state for $N = 9, 13, 17, 21, 25$ vs. rescaled time t/t_M. Figure adapted from [42].

it should be (frame (a)). The occupation probability of spins 1 and 9 at the first extraction at t_M is instead larger than 0.5 (frame (b)). This is also reflected at the second extraction at $1.5t_M$, where the occupation probability of spins 1 and 9 is now less than 0.5 (frame (c)). Nonetheless, figure 3.7 showed that the achieved state is very nearly the cluster state we were aiming to produce, indicating that the protocol is very robust against the indicated inaccuracies.

The observed discontinuity of the fidelity of the $N = 9$ plot at $0.5t_M$ is also reflected in the von Neumann entropy evolution (see figure 3.9). This is now calculated according to the bipartition of (the four spins containing the desired cluster state) and (the rest of the chain). To do this, we compute the four-qubit density matrix of spins $1, N, A$ and B (where A and B are the two spins used for storage after extraction at t_M), tracing out spins $2 - (N-1)$. Just as the fidelity does not perfectly reach unity at $1.5t_M$ for $N = 9$, S also does not perfectly drop to zero at this time, indicating a very small amount of entanglement left between spins 1 and 9 and the rest of the chain. Again, in figure 3.9 the second extraction at $1.5t_M$ was not effected to allow observation of the subsequent periodicity of the system. Chains of $N = 13$ and longer, which do reach perfect fidelity at $1.5t_M$, also have the von Neumann entropy of spins 1 and N with respect to the rest of the chain drop to zero at $(0.5 + n)t_M$, $n \in \mathbb{N}$.

In analogy with figure 3.3, the width of the entropy dips in figure 3.9 scales
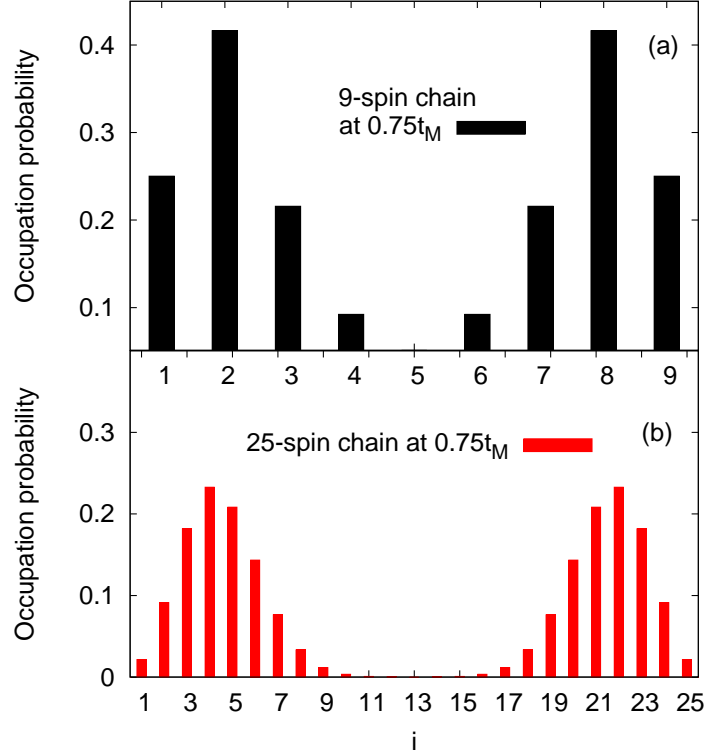
Figure 3.10: Occupation probabilities of the sites *i* of a 9-spin chain (a) and of a 25-spin chain (b) at $t = 0.75t_M$ during the cluster state knitting protocol for a four qubit cluster state. Panel (a) of figure published in [42].

as $1/\sqrt{N}$. For long chains however, another feature emerges from the entropy plots: Virtually invisible for $N = 9$, we observe the appearance of an additional dip in S at approximately $0.75t_M$, which approaches zero for increasingly long chains. This corresponds to an additional decoupling of spins 1 and N from the rest of the chain and it is worth noting that this phenomenon is not repeated in the system dynamics after the first extraction at t_M has taken place. Figure 3.10 shows a comparison of the occupation probabilities at $0.75t_M$ of a very short chain ($N = 9$, frame (a)) and a long chain ($N = 25$, frame (b)). The entanglement of spins 1 and N with respect to the rest of the chain can be deduced in frame (a) from the very high occupation probability. For $N = 25$ (frame (b)) the decoupling trend of spins 1 and N from the rest of the chain has already become very visible, despite some non-zero amount of occupation probability, and thus entanglement of spins 1 and N with the rest of the chain, remaining. This implies that for sufficiently long chains, where the decoupling of spins 1 and N at approximately $0.75t_M$ becomes perfect, we could inject another (third) pair of $|+\rangle$ states into these spins without perturbing the ongoing evolution of the system. The state which would result from such an altered protocol is shown in figure 3.11 but as the simulation of the required chain lengths is be-
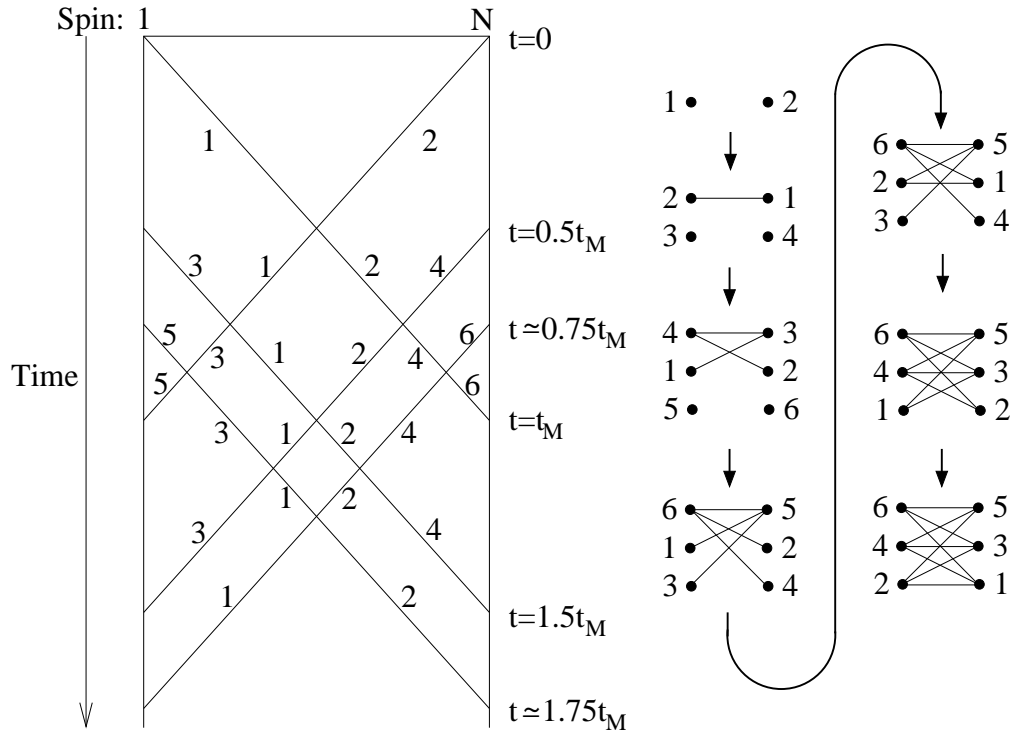
Figure 3.11: Schematic evolution of excitations involved in building of a six qubit cluster state (left-hand side) and diagram following build-up of the resulting state (right-hand side).

yond the reach of current computational means, an illustration of the fidelity and entropy evolutions is omitted in this case.

Having explained and demonstrated the working algorithm of the cluster state knitting protocol, we have found it to yield overall excellent results and also discovered possibilities for altering the algorithm to achieve cluster states of a different shape.

3.3   Conclusions

In conclusion, we have shown how linear spin chains can be used to knit cluster state ladders of arbitrary length. Starting from the premise that the number of access sites as well as the operation complexity should be kept to a minimum, we have achieved a protocol requiring access to the two extremal spins of a chain only and no further requirements from the spin chain itself other than the usual PST conditions. The overall construction time of a $2n$-spin cluster state is $0.5t_M(1+n)$ for all n, making this a quick procedure. We were able to develop this protocol thanks to the built-in quantum gates in spin chains, choosing values for N such that these gates do not lead to any additional phase

in the dynamics of the excitations we inject into the system. By studying the natural dynamics of the system, in particular the von Neumann entropy of the two end spins with respect to the rest of the chain, we found that there are ideal times to inject further pairs of excitations into the chain. Under ideal conditions, this leads to no perturbation of the existing dynamics. This allows us to build a maximally entangled cluster state ladder, whose actual length is limited by fabrication defects and decoherences only. The only other limitation is a small risk of imperfect injection in short chains (such as $N = 9$), where unwanted entanglement with auxiliary qubits can be resolved when a four-qubit cluster state is produced, but not for larger cluster states. However, the probability of this happening is less than 2% for $N = 9$ and decreases further as $1/N$, so that any cluster state resulting from our proposed protocol can be considered to be a suitable resource for applications in quantum information, especially for one-way quantum computing.

The work presented in this chapter has been computationally challenging and has also imposed limits on the type of system we could investigate, both with respect to the number of spins in a chain as well as the number of excitations. Without or with less restrictive computational limits than what is possible at the time of writing, it would be interesting to discuss further possibilities for spin chains to knit cluster states, such as a demonstration of the protocol suggested in figure 3.11 for example. It is likely that a wider range of cluster state topologies can be constructed, especially if access to further sites (such as the central spin) is permitted. For instance, figure 3.10 highlights that the occupation probability of the central spin (spin 5 for $N = 9$ in frame (a), spin 13 for $N = 25$ in frame (b)) is zero at $0.75t_M$, regardless of the chain length. This might allow for injection into the central spin without causing perturbation to the system. As future work, it would be particularly interesting to analyse how this central excitation will interact and become entangled with the other excitations in the chain.

Chapter 4

Circular spin chain devices

Having analysed the transport properties of linear spin chains as well as their potential as cluster state knitting devices, we will now turn our attention to circular spin chain devices. Unlike branched devices, as discussed in sections 2.1.2 and 2.1.3, circular spin chains do not abide by the established rules for PST but display more complex dynamics [104, 156], particularly when more than a single excitation is involved. In this chapter, we will discuss the possibilities and limitations of PST in simple circular devices before considering more complex constructs of circular spin chains with branches or consisting of multiple circles. The discussion expanding the simple one-excitation set-up as well as the following sections are original work.

4.1   Basic circular spin chains

Let us first of all consider the most basic circular spin chain, which consists of a single circle of spins, i.e., a linear spin chain where spin N is connected again to spin 1. We will establish the necessary conditions to achieve PST in such a device and also discuss its limitations.

4.1.1   Set-up for Perfect State Transfer

While some work has been done on circular spin chains without PST couplings [179], we will consider circular chains as an extension of our previous work and therefore aim for PST by appropriate adjustment of the couplings $J_{i,j}$. The simplest way of achieving PST in a circular chain is by treating it as two separate spin chains of equal length, set up for PST, which have a common first and last spin. The ECL of the overall circle device will therefore be the same as that of the two chains. This is shown in figure 4.1, where spins 1
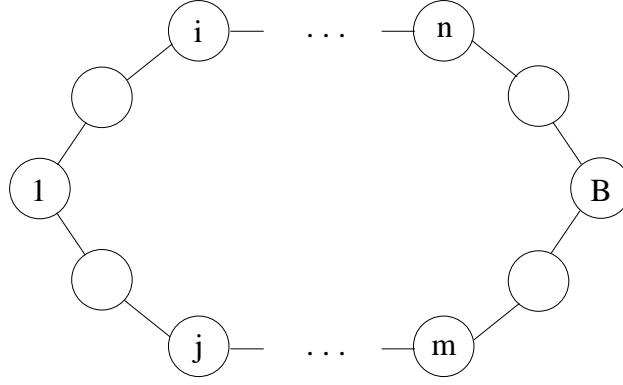
Figure 4.1: Diagram of a circular spin chain with two hubs, 1 and *B*.

and *B* are the two common spins. As per natural spin chain dynamics, these two sites are now natural "extremal" points in the circular device, but they are also hubs between two chains and must therefore obey the hub rule: Instead of their couplings to their two neighbouring sites being J_1 (or $J_{N-1} = J_1$), the couplings have to be adjusted to be $J_1/\sqrt{2}$. In this case, PST of one excitation from spin 1 to spin *B* or vice versa can be achieved, as was mentioned in [104]. In analogy to "mirror twin" transport in linear chains, an excitation split over a vertical pair of qubits (for example the two qubits *i* and *j* in figure 4.1) as $\frac{1}{\sqrt{2}} \left(|1_i 0_j\rangle + |0_i 1_j\rangle \right)$ can also be transferred perfectly to its "mirror twin" pair (in this case qubits *n* and *m*).

The authors of [104] do however also note that this set-up of a circular spin chain only allows for PST of single excitations. In higher excitation subspaces, the crossing of excitations leads to altered dynamics, which do not lead to PST (see figure 4.2). In the device described by diagram 4.1, let us for example assume that we would like to transfer a state with two excitations *p* and *q*, one in spin 1 and one in spin *B*. There are two possible paths ("channels") between 1 and *B*, which we will denote by α and β - as the channels are identical, the actual labelling is irrelevant. The excitations *p* and *q* will split over the channels α and β in an equal superposition, such that the state $|\psi_1\rangle$ of the circle just after injection (but before any crossings of *p* and *q*) can be thought of as

$$|\psi_1\rangle = \frac{1}{2} \left(|0\rangle_{p\alpha} |1\rangle_{p\beta} + |1\rangle_{p\alpha} |0\rangle_{p\beta} \right) \left(|0\rangle_{q\alpha} |1\rangle_{q\beta} + |1\rangle_{q\alpha} |0\rangle_{q\beta} \right).$$

Here each ket represents one or several spin sites, meaning that we are assuming a degree of localisation of *p* and *q*. This assumption is justified since we have also previously observed various degrees of localisation of excitations in spin chains, see for example chapter 3. Due to their fermionic nature, *p* and *q* pick up a π phase, so a minus sign, when they cross through each other, so that after crossing in both path α and path β has occurred, the state of the system
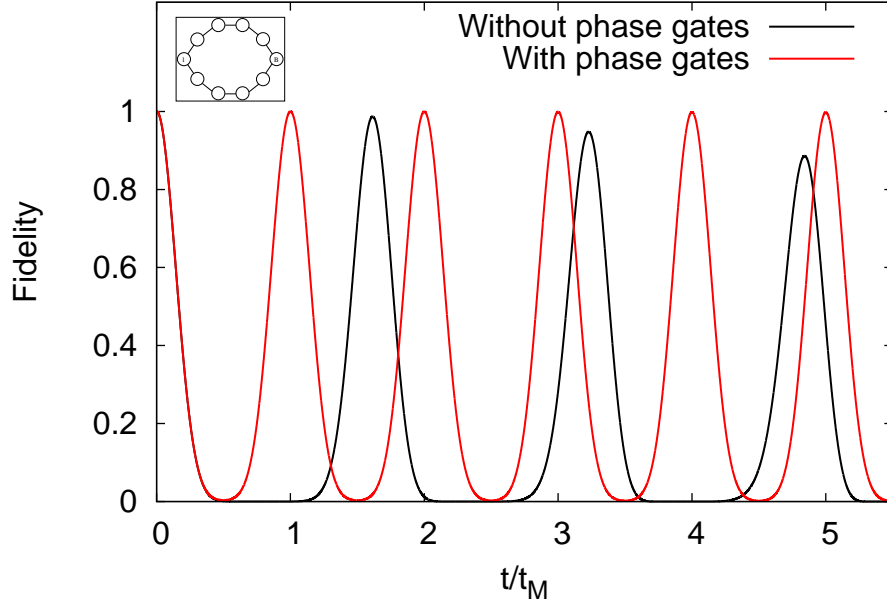
Figure 4.2: Comparison of the evolution of the fidelity of the two excitation initial state $|\psi\rangle = |1_1 0 \cdots 1_B \cdots 0\rangle$ against itself in a 10-spin circular chain (see inset for a diagram) with and without phase gates vs. rescaled time t/t_M.

$|\psi_2\rangle$ can be thought of as

$$
\begin{aligned}
|\psi_2\rangle &= \frac{1}{2}\left(-|0\rangle_{p\alpha}|1\rangle_{p\beta}|0\rangle_{q\alpha}|1\rangle_{q\beta} + |0\rangle_{p\alpha}|1\rangle_{p\beta}|1\rangle_{q\alpha}|0\rangle_{q\beta}\right.\\
&\quad \left. +|1\rangle_{p\alpha}|0\rangle_{p\beta}|0\rangle_{q\alpha}|1\rangle_{q\beta} - |1\rangle_{p\alpha}|0\rangle_{p\beta}|1\rangle_{q\alpha}|0\rangle_{q\beta}\right)\\
&= \frac{1}{2}\left(|0\rangle_{p\alpha}|1\rangle_{p\beta} - |1\rangle_{p\alpha}|0\rangle_{p\beta}\right)\left(-|0\rangle_{q\alpha}|1\rangle_{q\beta} + |1\rangle_{q\alpha}|0\rangle_{q\beta}\right).
\end{aligned}
$$

The factorised form of $|\psi_2\rangle$ illustrates why PST of two excitations cannot be achieved with the given set-up: Where a single excitation, which would not have experienced any crossing and would therefore also not have picked up a minus sign in its state, will just recombine at the opposite hub, the state $|\psi_2\rangle$ of the two excitation case experiences interference at both hubs instead of smooth recombination and so PST fails.

It is possible to solve this problem by introducing artificial phases to the circular spin chain, for example by inserting phase gates into the chain or by using magnetic fields to take advantage of the Aharonov-Bohm effect [80, 180] (assuming that the device consists of actual spins), depending on experimental implementation. To compensate for the unwanted minus signs in $|\psi_2\rangle$, for excitations travelling from spin 1 to spin B an additional phase of $e^{i\frac{\pi}{2}}$ is inserted into channel α and an additional phase of $e^{-i\frac{\pi}{2}}$ into channel β (again, the la-

belling of α and β is irrelevant). If excitations travel the opposite way, from B to 1, this corresponds to a phase of $e^{-i\frac{\pi}{2}}$ in channel α and a phase of $e^{i\frac{\pi}{2}}$ in channel β. This ensures the hermiticity of the Hamiltonian $\widehat{\mathscr{H}}$. Using artificial phases or phase shifts in spin chains has previously also been used to enhance transport qualities of a chain [98, 181, 182]. Where exactly in α and β the phases are added has no effect on the outcome. It is also possible to split a single phase gate of $e^{\pm i\frac{\pi}{2}}$ over several phase gates without affecting the result, as long as their cumulative phase adds up to $e^{\pm i\frac{\pi}{2}}$ within the channel. Adding these phases (taking into account the direction of travel of the excitations) means that instead of $|\psi_2\rangle$, we achieve the state

$$
\begin{aligned}
|\psi_{2'}\rangle &= \frac{1}{2}\left(e^{-i\frac{\pi}{2}}|0\rangle_{p\alpha}|1\rangle_{p\beta} - e^{i\frac{\pi}{2}}|1\rangle_{p\alpha}|0\rangle_{p\beta}\right)\left(-e^{i\frac{\pi}{2}}|0\rangle_{q\alpha}|1\rangle_{q\beta} + e^{-i\frac{\pi}{2}}|1\rangle_{q\alpha}|0\rangle_{q\beta}\right) \\
&= -\frac{1}{2}\left(|0\rangle_{p\alpha}|1\rangle_{p\beta} + |1\rangle_{p\alpha}|0\rangle_{p\beta}\right)\left(|0\rangle_{q\alpha}|1\rangle_{q\beta} + |1\rangle_{q\alpha}|0\rangle_{q\beta}\right)
\end{aligned}
$$

$|\psi_{2'}\rangle$ factorises in a way that does allow for recombination at the hubs 1 and B, therefore resulting in PST of the original two excitation state (see figure 4.2). We have therefore adjusted the basic circular spin chain to allow for two excitation PST by simple addition of two phase gates. It must be noted however that this adapted circular spin chain will no longer allow for PST of a single excitation, unless the phase gates are removed again: If the phase gates were left in, the device would overcompensate for a crossing which does not occur, which would result in interference at the hub and not lead to smooth recombination of the excitations or PST.

4.1.2   Limitations

While the above discussion opens up PST in circular spin chain devices to the two excitation subspace, the method is subject to some strong limitations. First of all, the two channels α and β must be of equal length, and the overall device must contain an even number N of spins. If the channels were of unequal length, recombination at the hubs would be perturbed by the different travelling times of excitations along the channels, similar to the Y-type chain in section 2.1.2. Adjusting the couplings such that the travelling times are the same would lead to a loss of PST conditions. It is also not possible to extend our result for two excitations to higher excitation subspaces: Diagram 4.3 shows the logical next step, a circle with three singled out input sites and hubs A, B and C (analogous to sites 1 and B in diagram 4.1). All three hubs have to have their adjacent couplings adjusted according to the hub rule. As there is now an odd number of channels between hubs in the device, the position
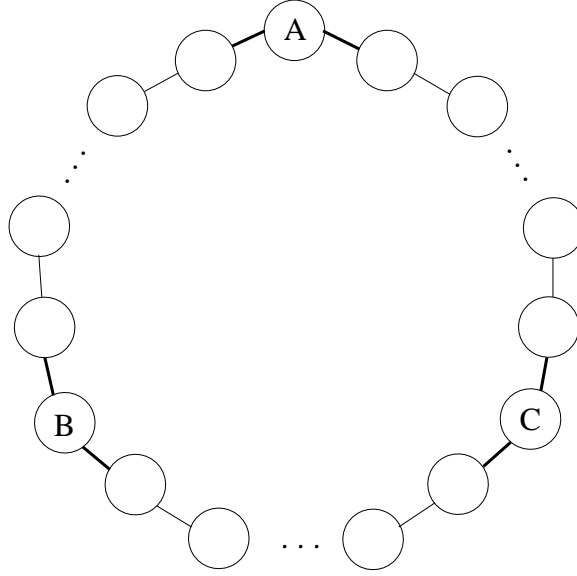
Figure 4.3: Diagram of a circular spin chain with three hubs. Bold lines indicate couplings adjusted for the hub rule ($J_i/\sqrt{2}$).

and number of any phase gates that may be required to compensate for the various crossings is not obvious anymore. With an odd number of hubs and excitations it is also not obvious what the state of the system should ideally be at t_M as the "mirror sites" (so sites a number $\frac{N}{2}$ spins away) are not hubs and may lie between spins. If we were to assume that all three excitations of an input state $|0\cdots1_A\cdots1_B\cdots1_C\cdots0\rangle$ are localised, each excitation would split into two halves, each of which would undergo a total of four crossings with two other half-excitations. Based on this, we investigated whether due to the even number of crossings there might in fact be no artificial phases needed, but the corresponding simulation did not reveal either PST or any type of regular dynamics for this set-up. The same was true for any number of phase gates and changes to the ECL we tried to adjust the system dynamics with, giving strong indication that PST in this device is not possible. Even when setting the ECL such that ECL$=\frac{N}{3}+1$ and initialising the system with 3 excitations (one in each hub), PST was not achievable (regardless of the position and number of phase gates introduced). The largest device of this type that we analysed numerically (without being able to achieve PST) had 27 spins. Transfer of a single excitation between two hubs is not possible in this device as the two separate paths between any two hubs are now not of equal length: One of them will be direct and the other involve twice the distance plus the third hub, leading to different timings and thus no recombination which would lead to PST.

In an attempt to re-introduce more symmetry in a circular device with more than two hubs, we set up a circular spin chain with four equidistant hubs. Un-
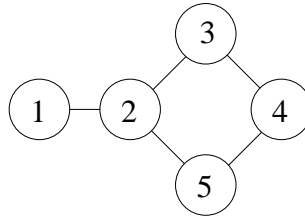
Figure 4.4: Diagram of a circular spin chain consisting of 5 spins with one branch.

fortunately, we encountered similar problems as with the three hub circular spin chain of diagram 4.3: Due to the increased number of excitations and the resulting more complex dynamics, we could not find a combination of phase gates (or lack thereof) and varying ECL that allowed for PST of one, two or four excitation symmetric input (i.e., with excitations initially in the hubs). A likely explanation is that our initial assumption of limited localisation, which allowed us to deduce the necessary phase adjustments for a circular device with two hubs, does not hold since more excitations in a device of similar size leads to more overlap between excitations. It might be possible that in very large devices, sufficient amounts of localisation do occur to allow an adjustment of the dynamics via artificial phase gates, but in general this approach does not lead to the desired results. As such, circular devices with two hubs remain the only circular devices for which PST of more than one excitation can be achieved via phase corrections.

4.2 Circular devices with branches

Having considered the dynamics of basic circular spin chains, we will now analyse a more complex type of device which involves a circle and one or more branches. Adding branches alters the dynamics significantly, making them more complex, but also allows for more flexible devices with potential uses beyond PST.

4.2.1 Case study

Before attempting to analyse the general case of circular devices with branches, we will start by looking at the smallest possible case of this set of devices: a 5-spin device consisting of a 4-spin circle and a single 1-spin branch (see diagram 4.4). The advantage of such a small device is that it is feasible to solve it analytically by computing the eigenvectors of its Hamiltonian instead of ap-
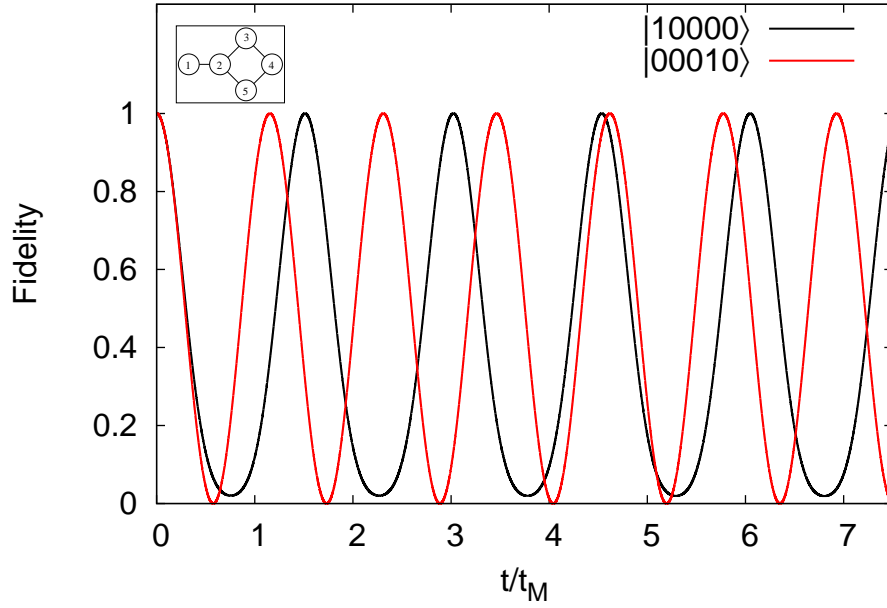
Figure 4.5: Fidelity of the two input states $|10000\rangle$ and $|00010\rangle$ in the device of diagram 4.4 (see inset) vs. rescaled time t/t_M under normal PST couplings and two artificial phase gates.

proximately solving its time-dependent Schrödinger equation, which reduces the potential for computational mistakes. The drawback of considering a devices with only a few spins is that the dynamics do not necessarily scale onto larger systems - see for example the Bell storage device in section 2.3, which only works for exactly four spins.

In the present 5-spin device, we need to first of all establish what possibilities there are for PST. We found numerically that with two artificial phase gates in the device (implemented between on couplings $J_{2,3}$ or $J_{3,4}$ and $J_{5,4}$ or $J_{2,5}$), simple PST of a single excitation from spin 1 to spin 4 (or vice versa) is possible if the usual PST set-up is used (with ECL= 4), with spins 2 and 4 as hubs and their couplings adjusted for the hub rule. This can be seen in figure 4.5, where the fidelities of the two single excitation input states with excitations at spins 1 and 4 are shown to return to perfect fidelity in regular intervals. However, the periods of the two states $|10000\rangle$ and $|00010\rangle$ are different: While $|10000\rangle$ follows a period of approximately $1.5t_M$, the period of $|00010\rangle$ is slightly longer than t_M. This means that if we injected a two excitation state $|10010\rangle$, it would not see perfect revival, at least within the first few periods, despite the phase gate correction.

Due to the device under consideration being so small, we have discovered a
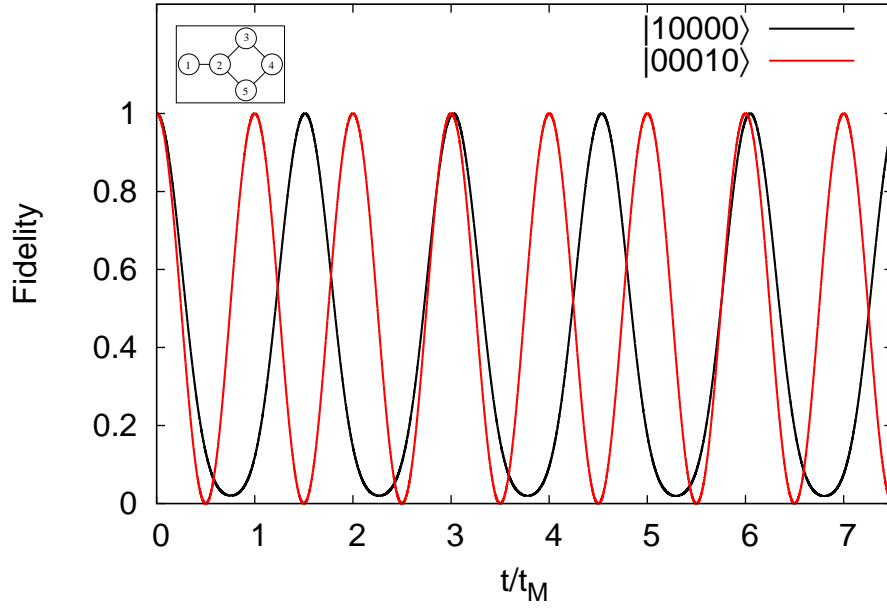
Figure 4.6: Fidelity of the two input states $|10000\rangle$ and $|00010\rangle$ in the device of diagram 4.4 (see inset) vs. rescaled time t/t_M under adjusted PST couplings and two artificial phase gates.

small adjustment which can be made to the couplings of spin 4 which solves this problem. According to the hub rule, the couplings $J_{4,3}$ and $J_{4,5}$ should be $J_1/\sqrt{2}$. If, instead, we adjust these couplings to be $J_2/\sqrt{2}$ (where J_2 is calculated based on the same ECL of 4), the period of $|00010\rangle$ changes to t_M, as is shown in figure 4.6. Note that the period of $|10000\rangle$ does not change and remains approximately $1.5t_M$. The two periods now peak together at $3t_M$ and also to a lesser extent every following $3t_M$, which is due to the period of $|10000\rangle$ being in fact slightly larger than $1.5t_M$. This allows us now to perfectly revive the two excitation state $|10010\rangle$ as well as the single excitation states $|10000\rangle$ and $|00010\rangle$ without having to adjust the device (for example by adding or subtracting artificial phase gates).

As we can now transfer both one and two excitation states between spins 1 and 4, we can also transfer the state $|\psi\rangle = |+\rangle_1|+\rangle_4 = \frac{1}{2}(|00000\rangle + |10000\rangle + |00010\rangle + |10010\rangle)$. This is of interest because, as we have previously seen in chapter 3, this type of input state can lead to maximally entangled states. Figure 4.7 shows that indeed, not only does the state $|\psi\rangle$ revive perfectly at $3t_M$ and with decreasing fidelity also at multiples thereof, the EoF of spins 1 and 4 also shows maximal entanglement at $3t_M$. This demonstrates that we have achieved a state of maximal entanglement (namely $\frac{1}{2}(|00000\rangle + |10000\rangle - |00010\rangle + |10010\rangle)$) between spins 1 and 4 at $3t_M$. This entanglement could then be extracted at this
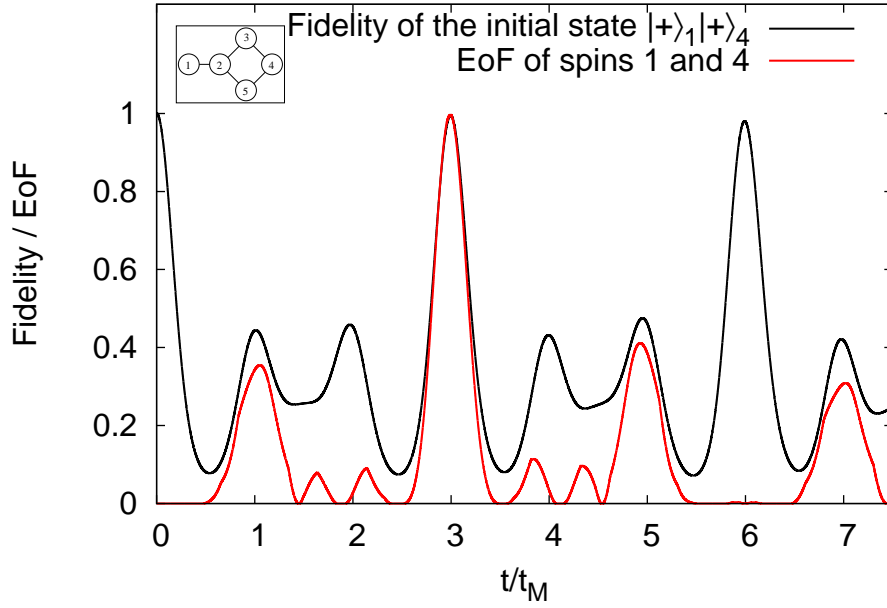
Figure 4.7: Fidelity of the initial state $|+\rangle_1|+\rangle_4$ in the device of diagram 4.4 (see inset) and EoF of spins 1 and 4 vs. rescaled time t/t_M.

time by effecting a SWAP gate between spin 1 and an ancilla and also a SWAP gate between spin 4 and a second ancilla. If the state is not extracted, spins 1 and 4 become unentangled again as the system approximately reverts to its original state $|\psi\rangle$ at $6t_M$. This can be seen by the fidelity almost reaching unity and the EoF dropping to zero at $6t_M$.

While this is a very nice application of a circular device with a single branch, it must be kept in mind that it did require us to adjust the couplings at the hub spin 4 in a way which is different to the usual PST conditions and the hub rule. While it would be possible to solve this particular device analytically to see how the adjustment allows for this serendipitous result, there is no obvious reason to expect that this should generalise to bigger chains, as we will now see in the general case.

4.2.2 General case

The general case of circular devices with branches would be a circle of spins with a number of branches attached, the length of which might vary. Such a device might be used to connect multiple registers within a quantum computer and, if possible, create entanglement between sites with a comparatively large spacial distance between them. We know from our investigations so far that
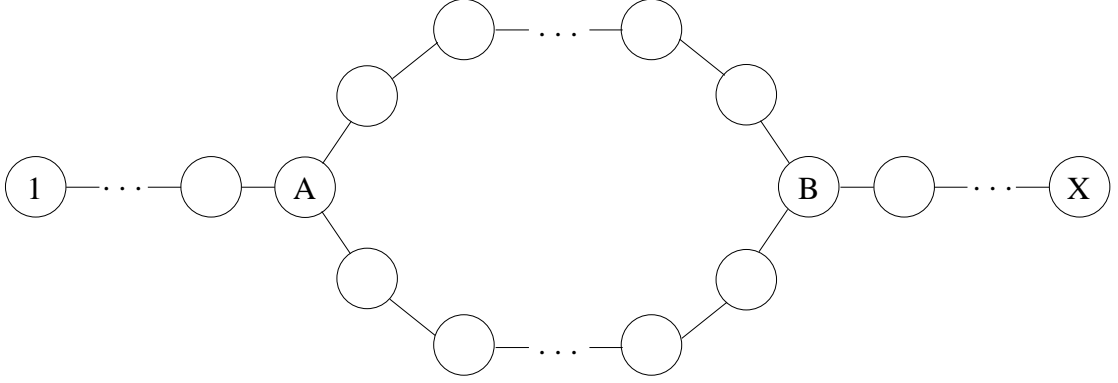
Figure 4.8: Diagram of a circular spin chain with two branches.

symmetric devices (ideally also with symmetric input states) are favourable to PST dynamics and so we will consider a circular chain with two branches of equal length as the simplest general device. A diagram of such a circular device is shown in figure 4.8. Here, we are assuming that the branches $1 - A$ and $B - X$ are of the same length and also that the length of the two paths between the hubs A and B is equal. Beyond this, we do not make any assumptions about the size of the device, but we do assume that it is set up for PST in the usual way (including the hub rule), where the ECL corresponds to the length of the path $1 - X$.

We start off by considering the possibilities of transporting a single excitation across the device. In analogy with section 4.1.1, where PST of a single excitation was only possible without the addition of phases, we find that indeed this is also true for a circular device with two branches. Figure 4.9 demonstrates that an addition of phase gates of $e^{\pm i \frac{\pi}{2}}$ in the two channels of the circle significantly disrupts both the periodicity of the fidelity of the initial state $|\psi_1\rangle = |1_1 0 \cdots 0\rangle$ as well as the quality of the transport.

It is now tempting to think that a circular device with two branches is merely the sum of two types of devices which we know are capable of PST, namely circles with two equidistant hubs and linear chains, but investigations in higher excitation subspaces show that this is not the case. The most favourable two excitation initial input state contains one excitation in spin 1 and one in spin X: $|\psi\rangle = |1_1 0 \cdots 1_X \cdots\rangle$. Figure 4.10 demonstrates the lack of PST of $|\psi\rangle$ in a device of 10 spins with very short branches of length 1. Even when choosing such a relatively small device, it is clear that the evolution of the fidelity of the initial state $|\psi\rangle = |1_1 0 \cdots 1_X \cdots\rangle$ does not follow PST when the usual phase gates are used as the peak heights are irregular. It could be argued that instead of regarding the device as a sum of a circle and two linear chains, it should be viewed as simply a linear chain which is split in the middle and that therefore,
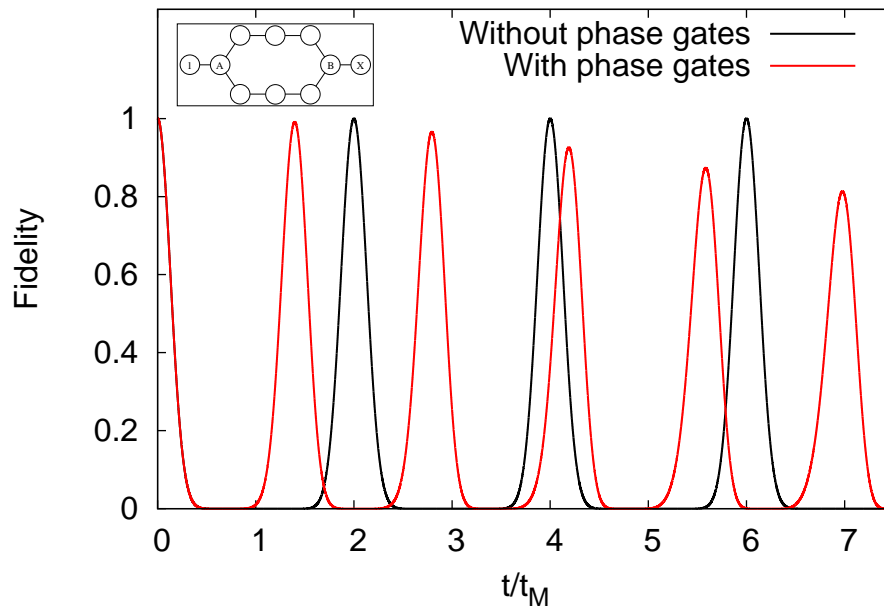
Figure 4.9: Fidelity of the initial one excitation state $|\psi_1\rangle = |1_1 0 \cdots 0\rangle$ in a 10-spin circular device with two branches of length 1 each (see inset for a diagram) with and without use of additional phase gates vs. rescaled time t/t_M.
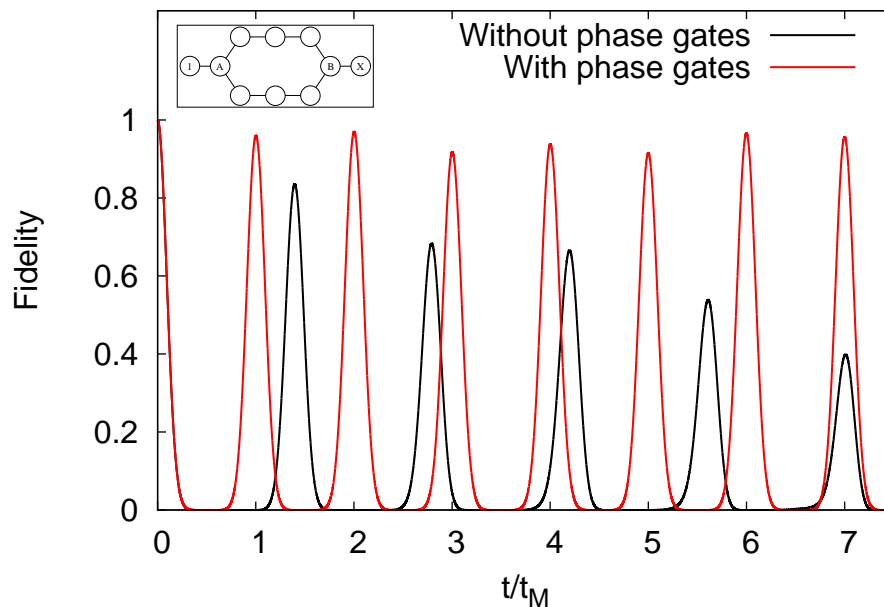
Figure 4.10: Fidelity of the initial two excitation state $|\psi\rangle = |1_1 0 \cdots 1_X \cdots\rangle$ in a 10-spin circular device with two branches of length 1 each (see inset for a diagram) with and without use of additional phase gates vs. rescaled time t/t_M.

the artificial phase gates we used to achieve two excitation PST in circular devices should not be employed. Figure 4.10 shows that this argument does not hold, with the fidelity of $|\psi\rangle$ decaying very quickly when no phase gates are in place. Another difference between the two plots of figure 4.10, showing the evolution with and without phase gates, is their periodicity. Without phase gates, there is a constant period, but it is not a multiple of the characteristic system time t_M. If instead the phase correction of $e^{\pm i\frac{\pi}{2}}$ is added, the period becomes t_M, which is the periodicity to be expected for PST of a state such as $|\psi\rangle$, which is its own mirror twin. This is in keeping with the phase-dependent change in periodicity in figure 4.9, where a set up with phases that do not allow for PST of a given input state also results in a period that is not a multiple of t_M.

This effect is common to circular devices with two branches in general: Regardless of the quality of transfer, the phase correction always adjusts the period to t_M, even in cases where there is no recognisable periodicity without artificial phase gates. Note that the phase correction must be done inside the circle, inserting artificial phases into the branches has no effect on the dynamics. We have investigated a range of these devices, noting the difference in the transfer of state $|\psi\rangle = |1_1 0 \cdots 1_X \cdots\rangle$ with and without phase gates. Since linear spin chains have previously exhibited behaviour repeated as modulo 4 sites, we have considered devices with branch length of 1 to 5 spins and circle size also of 1 to 5 spins, where the circle size is the number of spins between the hubs *A* and *B* (not including the hub spins). In the resulting 25 devices, inserting phases has always lead to an improvement of the dynamics, fixing the period to t_M but also improving the revival fidelity of $|\psi\rangle$. However, in no case did we observe true PST, although some devices (such as the one in figure 4.10, which has branch length 1 and circle size 3) give a good approximation. Contrary to our expectations, there was also no visible modulo 4 sites behaviour, either in circle size or branch length.

A pattern which did emerge was that devices where the circle size was larger than the branch length performed better than those with the opposite arrangement. The larger the circle size and the smaller the branch length, the better was the revival of the initial state $|\psi\rangle$. This indicates that the branches are a perturbation to the circle dynamics, as opposed to our previous idea that the circle might be a split in an otherwise linear chain. A possible reason for this is as explained in section 3.1.3, an excitation travelling through a linear spin chain picks up a phase which depends on the length of the chain. This means that by connecting a linear part to the hub of a circle, the excitation reaching the circle will also have picked up some phase, which makes its dynamics sig-

nificantly different from those of an excitation injected into the hub of a circle with no branches. This additional effect cannot easily be compensated for. It is not sufficient to add a phase gate into the branches of a device, as this would only work if the excitation were to be entirely recovered at the hub spin before moving on, which would require a lot more control over the device than we are currently allowing for.

Aside from symmetric circular devices with branches, we also attempted to generalise the special case of a circular device with a single branch discussed in section 4.2.1. Unfortunately, we could not achieve the same type of result in devices with more than five spins. Attempts to adjust the couplings of the hub not connected to the branch in a similar fashion as before, either by setting the couplings in question to $J_2/\sqrt{2}$ based on the actual chain length or by deriving couplings from an altered ECL, did not lead to PST. In view of our investigations on circular devices with two branches, it is fair to conjecture that in this case too the branch is a perturbation to the circle, but that this perturbation is so small in a 5-spin device that we did not detect it in the timespan we considered.

Overall, we conclude that there is no simple way of achieving multi-excitation PST in branched circular devices. As the simplest device already displayed too complex dynamics to adjust them, it is reasonable to assume that devices with less symmetry or more branches would only suffer from more problems of the same type. This was tested on circular devices with four branches of equal length. Here, in keeping with the above results, perfect transfer of both two or four excitations was not possible.

We will therefore not pursue the idea of circular devices with branches beyond the special case proposed in section 4.2.1 and instead consider devices composed of multiple circles.

4.3   Devices of more than one circle

We have seen in this chapter that PST in circular devices is possible if the right conditions for perfect recombination of the excitation(s) at the hubs are given. As combinations of circles and linear chains did not lead to PST, we will now investigate whether a device consisting of multiple circles is more suitable. To start off, we consider again the smallest possible device, shown in diagram 4.11, which consists of two circles with a total of 7 spins. We set up this device using the usual PST conditions (the ECL here is 5) and hub rule and also insert four phase gates, two in each circle, such that there is a phase of $e^{i\frac{\pi}{2}}$ inserted at

Figure 4.11: Diagram of a spin chain device consisting of two adjacent circles.
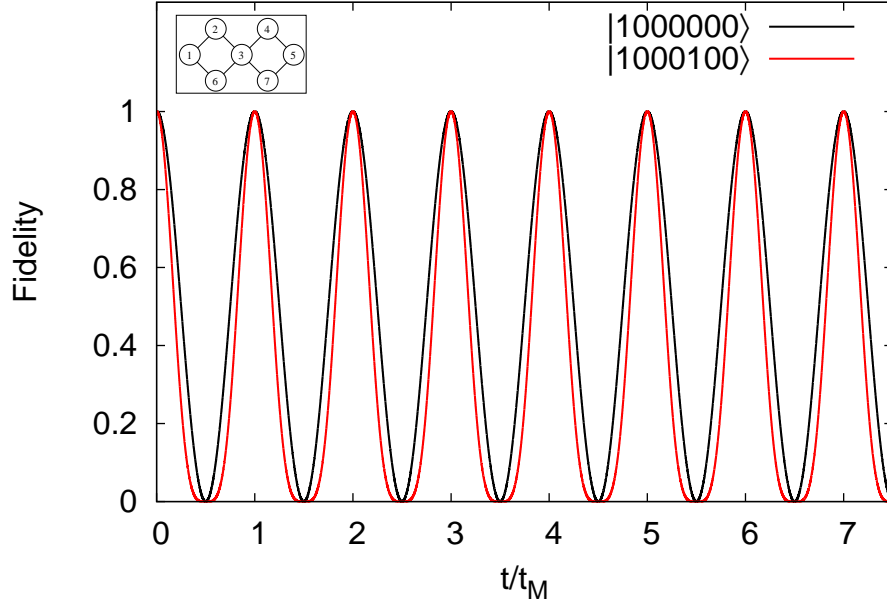
Figure 4.12: Fidelity of the initial states $|\psi_1\rangle = |1000000\rangle$ and $|\psi_2\rangle = |1000100\rangle$ in a circular device with two circles (see inset for a diagram) vs. rescaled time t/t_M.

$J_{1,2}$ and also at $J_{4,5}$, a phase of $e^{-i\frac{\pi}{2}}$ inserted at $J_{1,6}$ and also at $J_{7,5}$ and also the complex conjugates when considering the opposite direction of motion, e.g. $J_{5,7} = J_{7,5}^*$. Again, we will start off by using an initial state which is favourable to the system because of its symmetry and use the two excitation state $|\psi_2\rangle = |1000100\rangle$ which corresponds to injecting an excitation at each "end" of the device, namely at the hub spins 1 and 5. We see in figure 4.12 that $|\psi_2\rangle$ achieves perfect revival at every t_M, which is the period to be expected for a state which is its own "mirror twin". However, we cannot talk about PST in this case. Also in figure 4.12, we have recorded the fidelity of the one excitation state $|\psi_1\rangle = |1000000\rangle$ in the same device (with the same set-up). As $|\psi_1\rangle$ is not its own "mirror twin" but should instead transfer to the state $|0000100\rangle$, we would expects its revival period to be $2t_M$ instead of the period of t_M we observe.

This indicates that instead of being transferred along the chain, the excitation is merely reflected - indeed, given the initial state $|\psi_1\rangle$, only spins 1, 2 and 6 achieve non-zero occupation probability at any point in time. There is therefore destructive interference at spin 3, which prevents the excitation from crossing over to the second circle. Similarly, excitations in state $|\psi_2\rangle$ are not actually perfectly transferred, instead they are perfectly reflected. This is an important distinction to make, as it reveals that the two excitations of state $|\psi_2\rangle$ never interact and in particular never cross through each other. As a result, we cannot expect to generate any entanglement with the device. This was tested by using an initial state $|+\rangle_1|+\rangle_5$ and recording the EoF of spins 1 and 5 with respect to the rest of the device: No entanglement was found at any time.

Due to this destructive interference at spin 3, the actual weight of the couplings at this spin has no effect on the system, as long as $J_{2,3} = J_{3,6}$ and $J_{3,4} = J_{3,7}$. It is also possible to revive a single excitation injected at spin 3, although the period of this revival is faster, at approximately $0.57t_M$. Again, this is due to destructive interference, although this time at the hub spins 1 and 5. Another symmetric input state would be one with three excitations, one at spins 1, 3 and 5 each. This does however not lead to either perfect transfer or revival, as there is now interference due to the crossing of excitations. Asymmetric initial states such as the two excitation state $|0100001\rangle$ are not transferred or revived perfectly and neither are single excitation states with an excitation in a spin that is neither one of the two hub spins nor spin 3.

Expanding this circular device with two circles to a larger device with more spins leads to similar results: Provided that the device is set up for PST and two artificial phase gates are used in each circle, perfect revival of input states involving the two hub spins only can be achieved, but there is no transfer across the device and thus no potential for the generation of entanglement. It is possible to change the artificial phase gates, for example by changing their sign (from $e^{-i\frac{\pi}{2}}$ to $e^{i\frac{\pi}{2}}$ or vice versa), to prevent destructive interference. This does then lead to some entanglement (as recorded via EoF of the two hub spins with respect to the rest of the device), but it also destroys any periodicity of the system and causes irregular dynamics during the time scale we considered.

Circular spin chain devices with more than two circles follow a similar pattern. Diagram 4.13 shows the smallest possible circular device consisting of three adjacent circles. Again, if we set this device up for PST (the ECL here is 7) and insert two artificial phase gates into the two outer circles, we can achieve perfect revival of initial states involving the two outer hubs (here spins 1 and 7) only, but no transfer. A demonstration of the perfect revival of the initial state $|\psi\rangle = |1000001000\rangle$ is given in figure 4.14. Note that due to the destructive
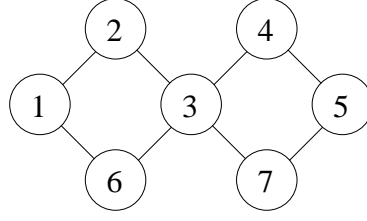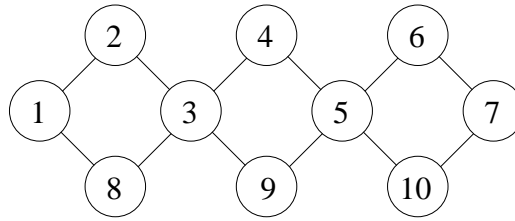
Figure 4.13: Diagram of a spin chain device consisting of three adjacent circles.
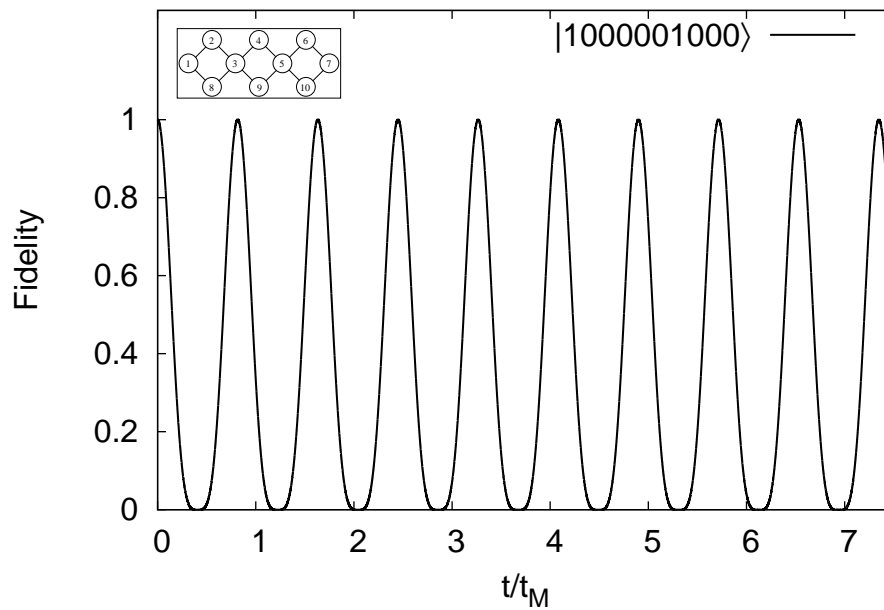
Figure 4.14: Fidelity of the initial state $|\psi\rangle = |1000001000\rangle$ in a circular device with three circles (see inset for a diagram) vs. rescaled time t/t_M.

interference at spins 3 and 5, we do not require any phase gates in the middle circle in order to achieve this revival. However, the addition of another circle compared to the device of diagram 4.11 does have a visible effect on the system dynamics, as the revival period of $|\psi\rangle$ is not t_M but approximately $0.8t_M$. This is due to the excitation travelling a distance shorter than the ECL, which is the distance it would cover in the time t_M.

Attempts to move the artificial phase gates from the two outer circles into the inner circle, either using four or two gates in the inner circle, did not result in excitation transfer but merely in irregular dynamics for the simulation times considered. Similarly, injecting two excitations in spins 3 and 5, which could have resulted in formation of entanglement as two excitations initially present in the same circle will have to interact, does not lead to any sort of ordered dynamics, regardless of the arrangement of artificial phase gates.

4.4   Conclusions

Our investigation of circular spin chain devices has shown that with the addition of phase gates, basic circular spin chains are capable of perfectly transferring two excitation states, which expands the results of [104]. This result is however limited to circular devices of two hubs only, as the more complex dynamics of more hubs and/or more excitations cannot easily be compensated for via phase gates. There is room here for further investigations as not all possibilities were explored and the analytic considerations were not expanded to the general case. Instead, we went on to explore the possibilities offered by devices involving either a combination of one or more linear chains and circles or multiple circles of spins. Circular devices with branches did in general not allow for PST, although the addition of artificial phase gates lead to an improvement in the system dynamics in all cases investigated. The smallest possible device of this category, consisting of a circle and a single one-spin branch, stood out from this as it allows not only PST of both one and two excitation states, but is also capable of generating entanglement. Devices of more than one circle, while allowing for perfect revival of one and two excitation states, were found to be unsuitable for entanglement generation as destructive interference prevents actual transfer, and thus crossing, of excitations. Again, there is scope for further work and analysis here, particularly in the category of circular devices with branches where a more in-depth consideration of the eigenstates of the Hamiltonians describing the systems might lead to more insight.

Chapter 5

Effects of fabrication defects

In this chapter, we will consider the effect of a number of fabrication defects that might affect the performance of a spin chain. As no fabrication process is perfect, these effects will inevitably play a role in the quality of information transfer and any other protocols which we would like to use spin chains for. So far, we have considered different kinds of uses, such as entanglement and cluster state generation, and different kinds of architectures, resulting in a multitude of scenarios which will all be affected by fabrication defects. Some discussions of the effects of perturbations on spin chains can be found in the following references: [135, 156, 183–201]. An analytic approach to this problem is beyond the scope of this thesis and instead a numerical investigation was done on a representative number of samples. This is also in keeping with the numerical analyses done in previous chapters, thus providing a natural extension. As such, we will only consider linear chains in this chapter but investigate the effect of fabrication defects under the form of noise, non-uniform on-site energies and unwanted interactions between excitations. We will do this for a number of input states, including entangled ones and those leading to entanglement, and also look into effects on the cluster state knitting protocol. As a result, we will present simple analytic parametrisations of the effects of these decoherences, providing a simple estimator for experimentalists. The discussions in this chapter are entirely original work, parts of which have been published in [145] and also [42].

5.1   Random noise

First of all, we will consider the effects of random noise in the system. This is arguably the most general representation of fabrication defects, as it is simulated by a direct perturbation of all non-zero elements in the Hamiltonian $\widehat{\mathscr{H}}$

(equation (1.3)). Let us first of all assume that noise is a local disturbance. This means that the effect of this perturbation is not influenced by the state of adjacent sites but represents local fabrication defects. For example, depending on the physical implementation of the spin chain, there might be slight inaccuracies in the profile of the barriers between individual sites, such as physical deviations in barrier height or thickness. As a result, we can think of this noise as a perturbation in the couplings $J_{i,i+1}$ as defined in equation (1.5) such that

$$J_{i,i+1} = J_0\sqrt{i(N-i)} + r_i J_{max} \tag{5.1}$$

where $0 \leq r_i \leq r$ are random numbers generated from a flat distribution and r is the magnitude of the noise perturbation in units of J_{max} (as defined in section 1.2.1). This represents a more unfavourable scenario than using random numbers from for example a Gaussian distribution, which allows us to consider the worst case scenario. While negative values of r_i would also be representative of the perturbation we are simulating, we must ensure that $J_{i,i+1} \geq 0$ (where any $J_{i,i+1} = 0$ corresponds to a breaking of the chain which thus becomes unusable for its original purpose) and so we only allow for $r_i \geq 0$. As we perturb each individual coupling $J_{i,i+1}$ by the same amount, we automatically preserve the hermiticity of $\widehat{\mathscr{H}}$. It could be argued that the coupling noise should be affected by the chain's characteristic coupling J_0, such that $J_{i,i+1} = J_0\sqrt{i(N-i)} + J_0 r_i$. As $J_0 \leq 1$, this would make the influence of r_i much less significant and would also make the influence decrease with N (as J_0 is proportional to $1/N$). As the aim is to simulate noise stemming from the physical implementation of the chain, such a dependence seems unjustified and the resulting simulations would be unnecessarily harder to interpret. We will therefore only use the form of noise given by equation (5.1).

We could also think of noise as a global disturbance and change the Hamiltonian $\widehat{\mathscr{H}}$ accordingly. In this case, we would let the state of nearby sites influence the perturbation experienced by a site, such as for example the presence of a second excitation in a nearby spin (more on this particular fabrication defect is given below in section 5.2.2). Such general noise cannot be expressed simply in terms of the couplings like local noise in equation (5.1). Instead, we would add a random coupling (i.e., a random number r_i, where again, $0 \leq r_i \leq r$ are random numbers generated from a flat distribution) to each non-zero element in the strictly lower (or strictly upper) triangle of $\widehat{\mathscr{H}}$ and adjust the strictly upper (or strictly lower) triangle accordingly, in order to preserve hermiticity.

Even though these two ways of considering noise, either as a local or global disturbance, seem rather different, we have found that their effect on the per-
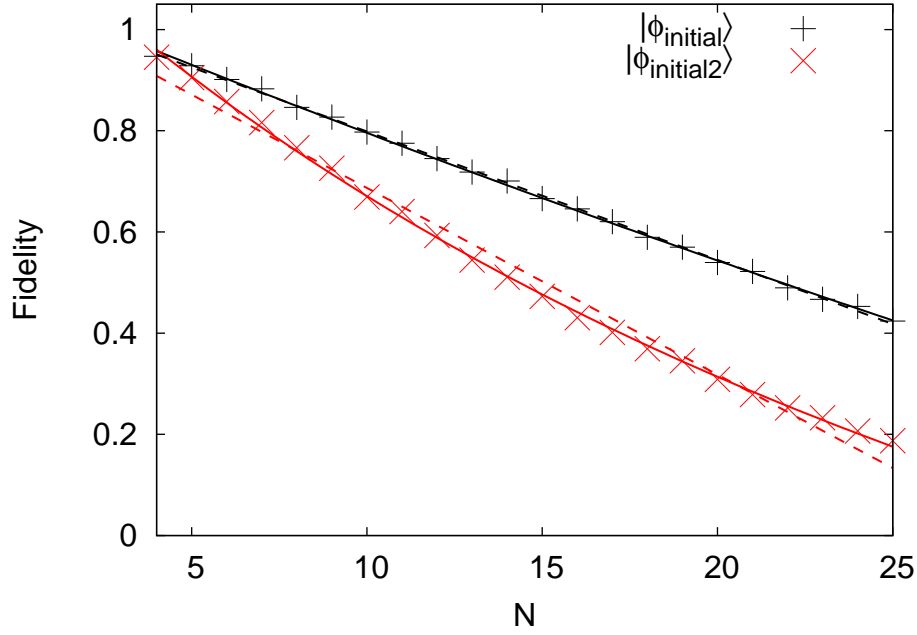
Figure 5.1: Influence of random coupling noise with $r = 0.05$ for unentangled initial states $|\phi_{initial}\rangle = |1\cdots0\rangle$ (one excitation) and $|\phi_{initial2}\rangle = |111\cdots0\rangle$ (three excitations): Fidelity of the first revival peak at $2t_M$ vs. chain length N. Fits are as $1/N$ (solid lines) and linear (dashed lines).

formance of the chain is in fact indistinguishable. This is independent of the length of the chain or the type of input state, and so we will only consider random noise represented by a local disturbance as a representative of random noise in general. Every data point on figures 5.1 to 5.4 is averaged over 1000 random realisations.

5.1.1 Unentangled states

First of all, we will investigate the effect of random noise on unentangled states. Figure 5.1 shows this effect for constant $r = 0.05$, such that $0 \leq r_i \leq 0.05$ for all i, and varying N. For each N, the initial state was set to $|\phi_{initial}\rangle = |1\cdots0\rangle$, so that each initial state contains one and only one excitation. We see that the dependence of the fidelity at the expected revival time $2t_M$ of this state could be fitted as linear decay, with longer chains being more affected. This is in agreement with physical intuition, as longer chains will have more perturbed couplings (i.e., entries in the Hamiltonian) affecting each excitation before revival. However, to be in keeping with $|\phi_{initial2}\rangle$ discussed below, the fit for $|\phi_{initial}\rangle$ as shown in figure 5.1 is in fact $1/N$, which gives an equally adequate fit. As such, the fidelity loss is almost negligible for very short chains but becomes unacceptable for long chains: At a loss of over 50% of the revival fidelity
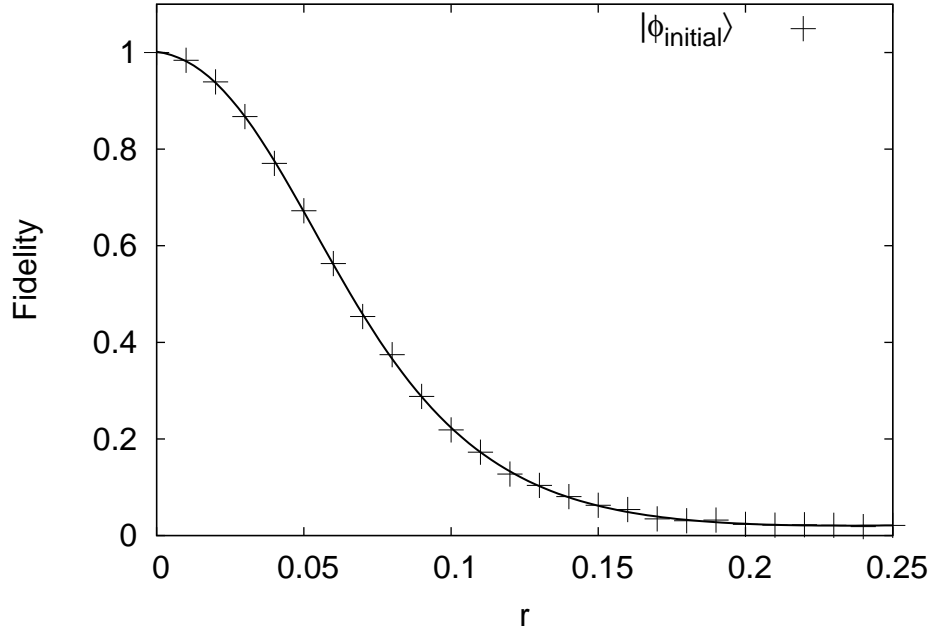
Figure 5.2: Fidelity at $2t_M$ of the single excitation vector $|\phi_{initial}\rangle = |1...0\rangle$ ($N = 15$) vs. random noise term r.

for $N = 25$, the amount of noise in the system has made the chain effectively unusable.

If instead of an initial state in the single excitation subspace we choose $|\phi_{initial2}\rangle = |111\cdots0\rangle$ (so $|\phi_{initial2}\rangle$ contains exactly three excitations), the detrimental effect of random noise becomes all the more visible. We see also in figure 5.1 that the loss in fidelity for the same constant $r = 0.05$ scales as $1/N$ like for $|\phi_{initial}\rangle$, but it does so much more rapidly, to the point where the loss in fidelity which was previously observed at $N = 25$ for one excitation is already attained at $N = 15$ for three excitations. Again, this can be understood intuitively, as there are more excitations involved in $|\phi_{initial2}\rangle$, each of which is affected by every perturbed coupling in the chain.

The fidelity dependence on r is not linear. Figure 5.2 shows the loss of fidelity at the revival time $2t_M$ for $N = 15$ and $0 \leq r \leq 0.25$, given the single excitation input state $|\phi_{initial}\rangle = |1\cdots0\rangle$ as defined above. The decay of fidelity has been fit using a Padé approximant [202] of order [3/2], i.e., of the form $\frac{a+br+cr^2}{1+\beta r+\gamma r^2+\kappa r^3}$. We observe a long tail for $r \gtrsim 0.15$, which tends to zero as indicated by a very large value of κ ($\kappa = 143$). Furthermore, $a = 1.00$ and $b \approx \beta$, which confirms that the fit correctly models the unperturbed case (i.e., unit fidelity for $r = 0$) and also shows that the gradient of the fit at $r = 0$ is ≈ 0. This too is in keeping with physical intuition: For negative values of r such that $\min\left(\frac{J_{i,i+1}}{J_{max}}\right) < r < 0$, we can expect that the perturbative effect of r is similar to that of the range

$\min\left(\frac{J_{i,i+1}}{J_{max}}\right) > r > 0$. As such, it is reasonable to predict the gradient of the fit to be zero at $r = 0$, in order for there to not be a discontinuity. Very small values of r of less than 0.05 allow for fidelities of more than 75%, but beyond this the revival of $|\phi_{initial}\rangle$ is severely perturbed. Since we have seen in figure 5.1 that especially for large values of N, the performance of the single excitation state was less affected than that of the three excitation state, it is safe to assume that figure 5.2 shows the best case scenario for $N = 15$ and for the range of r given and that any other unentangled initial states would perform similarly or worse. As such, it is important that the influence of random noise for chains with unentangled states be restricted to only a few percent ($r < 5\%$) of the maximum coupling J_{max} (as defined in section 1.2.1).

5.1.2 Entangled states

Having considered the effects of random noise on unentangled states, we will now look at entangled states. Since we have already established that states with more excitations suffer more performance decay, we will now focus on states with a single excitation. In particular, we will use the following states: i) $|\psi_1\rangle = \frac{1}{\sqrt{2}}\left(|10\cdots0\rangle + |01\cdots0\rangle\right)$, ii) $|\psi_2\rangle = \frac{1}{\sqrt{2}}\left(|1\cdots0\rangle + |0\cdots1\rangle\right)$ and iii) $|\psi_3\rangle = \frac{1}{2}\left(|0_1 0_N\rangle + |1_1 0_N\rangle + |0_1 1_N\rangle + |1_1 1_N\rangle\right) \otimes |0_2\cdots0_{N-1}\rangle$ (which is initially unentangled but leads to entanglement at t_M, see section 3.1.3). Even though $|\psi_3\rangle$ is a superposition of vectors in three excitation subspaces, the expectation value of $\widehat{\mathscr{T}}$ (as defined in equation (1.2.1.2) and adjusted to also account for the zero and two excitation subspaces) in the state $|\psi_3\rangle$ is $\langle\psi_3|\widehat{\mathscr{T}}\psi_3\rangle = 1$. We therefore expect it to behave similarly to $|\psi_2\rangle$ since in both cases only spins 1 and N are initially excited. $|\psi_3\rangle$ is of particular interest as it is the first step of the cluster state knitting protocol and so the effect on the entanglement resulting from this state at t_M is important for the performance of the protocol.

We see the effect of random noise with $r = 0.05$ (so $0 \leq r_i \leq 0.05$) on all three types of input states mentioned above in figure 5.3. In order to be able to do a fair comparison between the three types of input states and with the unentangled states, we will use the state fidelity as a quality measure. For increasing values of N, there is linear decay in fidelity for $|\psi_1\rangle$, $|\psi_2\rangle$ and $|\psi_3\rangle$. There is however a clear difference in the loss in transport quality between $|\psi_1\rangle$, where the entanglement is split over the first two sites of the chain, and $|\psi_2\rangle$ and $|\psi_3\rangle$, both of which use spins 1 and N to transport or generate entanglement, respectively. While in all cases, serious loss is suffered for a long chain of $N = 15$, $|\psi_1\rangle$ loses less than 25% of its fidelity, while $|\psi_2\rangle$ and $|\psi_3\rangle$ lose over 30%. As we expected, the loss of fidelity of $|\psi_2\rangle$ and $|\psi_3\rangle$ is very similar and differs by
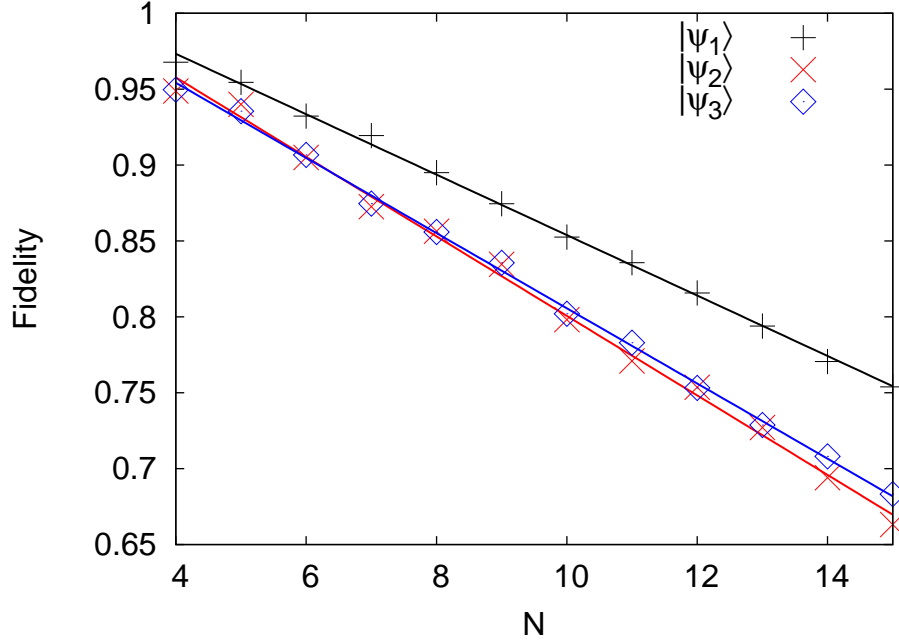
Figure 5.3: Influence of random coupling noise with $r = 0.05$ for entangled initial states $|\psi_1\rangle = \frac{1}{\sqrt{2}}(|10\cdots0\rangle + |01\cdots0\rangle)$, $|\psi_2\rangle = \frac{1}{\sqrt{2}}(|1\cdots0\rangle + |0\cdots1\rangle)$ and the initially unentangled $|\psi_3\rangle = \frac{1}{2}(|0_10_N\rangle + |1_10_N\rangle + |0_11_N\rangle + |1_11_N\rangle) \otimes |0_2\cdots0_{N-1}\rangle$ which leads to entanglement at t_M, fidelity at $2t_M$ vs. chain length N. Fits are linear to guide the eye.

less than 3% for the range of N considered. For very short chains of $N \leq 6$, the amount of fidelity retained is over 90% for all three states, making these chains very stable against random noise. Compared to figure 5.1, where we observed the loss in fidelity under the same amount of noise for an unentangled single excitation chain, the decay observed in figure 5.3 is similar, although $|\psi_1\rangle$ suffers slightly less.

To observe the loss in transport quality against r, we show in figure 5.4 the decay of fidelity of $|\psi_1\rangle$ for $0 \leq r \leq 0.25$. This represents a best case scenario, as $|\psi_1\rangle$ performed best in figure 5.3, but as $|\psi_2\rangle$ and $|\psi_3\rangle$ performed very similarly to the unentangled single excitation state $|\phi_{initial}\rangle$ (as defined in the previous section 5.1.1), it can be expected that their dependence on r is also similar. As in the case of unentangled states (shown in figure 5.2), the dependence of the fidelity decay of $|\psi_1\rangle$ on r is fitted by a Padé approximant [202] of order $[3/2]$. Again, as in figure 5.2, we have a value of a close to 1 ($a = 0.996$) and a near-zero gradient of the fit at $r = 0$, making this fit consistent with the discussions provided for figure 5.2. However, the decay in fidelity is less radical here, as can be seen by the fact that the tail of the graph is not as pronounced and also only starts around $r = 0.15$ instead of $r = 0.1$ as in figure 5.2. The value of κ
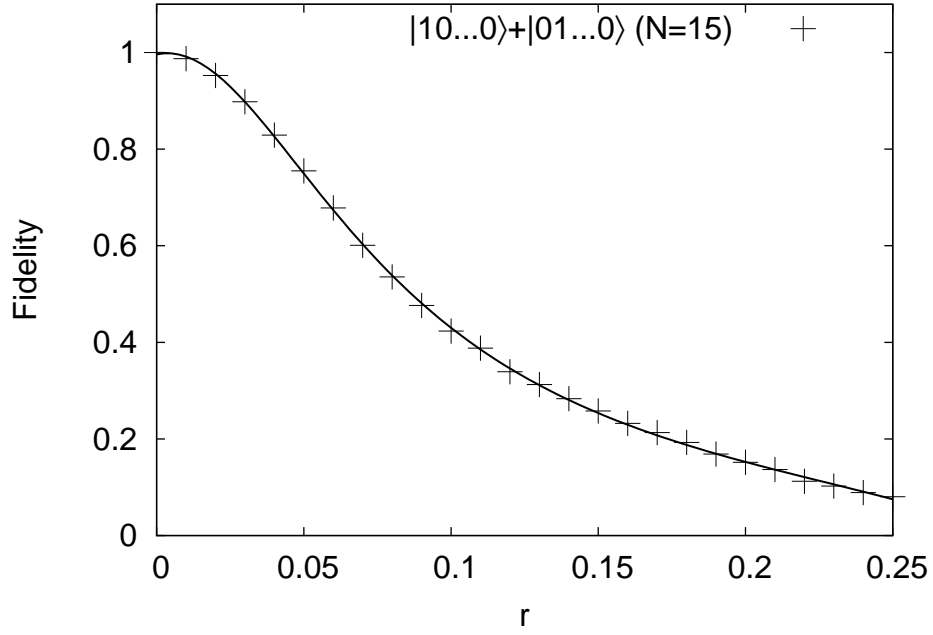
Figure 5.4: Fidelity at $2t_M$ of $|\psi_1\rangle = \frac{1}{2}(|10...0\rangle + |01...0\rangle)$ ($N = 15$) vs. random noise r.

is even larger at $\kappa = 514$, indicating an asymptote very close to zero. As such, again values of r up to 0.05 lead to over 75% retained fidelity. For larger values, although the loss increases less quickly than for the unentangled state, the state is severely perturbed and transport quickly becomes impossible.

Overall, we find that both entangled and unentangled input states behave very similarly under the influence of random noise. While entangled states using adjacent sites for the entanglement are more robust than those where the entanglement is distributed over very distant sites, only values up to about $r = 0.05$ still lead to acceptable amounts of fidelity. For larger values of r, there are then differences in the transfer decay, but as at this stage the transfer has effectively become impossible (as $|\langle \psi | \psi_{ideal} \rangle|$ will be very small), this is of limited relevance.

5.2 Unwanted on-site energies and interactions

Beyond the effect of random perturbations and errors, either due to defects in the couplings between sites or due to global noise induced by imperfect fabrication of the spin chain device, there is also a number of more specific errors which would stem from fabrication defects. In particular, we will now investigate the effect of fluctuating magnetic background fields and also of unwanted interactions between excitations.

5.2.1 On-site energies

First of all, let us consider how any non-uniform on-site energies may have a detrimental effect on the workings of spin chains. To do so, we reintroduce the term $\widehat{\mathcal{H}_1}$:

$$\widehat{\mathcal{H}_1} = \sum_{i=1}^{N} \varepsilon_i J_{max} |1\rangle\langle 1|_i \tag{5.2}$$

($\varepsilon_i \in \mathbb{R}^+$) in the Hamiltonian $\widehat{\mathcal{H}}$ (equation (1.3)), which we had previously dismissed on grounds of the on-site energies ε_i being site-independent and therefore not affecting the system dynamics. $\widehat{\mathcal{H}_1}$ may for example represent random spatial magnetic fluctuations that the system is experiencing, which would lead to the individual sites having different energies. These site-dependent single particle energies may also be due to single-site fabrication imperfections. Just as r_i in equation (5.1), $0 \leq \varepsilon_i \leq \varepsilon$ will be modeled via random numbers from a flat distribution, leading to a more unfavourable setting than a Gaussian distribution. As the additional terms of $\widehat{\mathcal{H}_1}$ are entries on the diagonal of the Hamiltonian $\widehat{\mathcal{H}}$, the hermiticity of $\widehat{\mathcal{H}}$ is not affected.

5.2.1.1 Unentangled states

As in section 5.1, we will first of all consider the effect of $\widehat{\mathcal{H}_1}$ on unentangled states. Christandl et al. claimed that the overall decay in transport quality should be linear in N for small values of ε, based on an estimate of the effect of errors on the energy level spectrum [44]. We see confirmation of this in figure 5.5, which displays the loss in fidelity at $2t_M$ of the initial vector $|\psi_1\rangle = |110\cdots0\rangle$: For small values of $\varepsilon = 0.05, 0.1$ we see that a linear fit to the data (which is averaged over 200 realisations) would be appropriate. However, for the larger energy perturbation of $\varepsilon = 0.5$, the decay in fidelity of the initial state $|\psi_1\rangle$ is not linear. The decay is now instead exponential and we can in fact fit all three sets of data via the same analytic formula $e^{-N\varepsilon^2/\varepsilon_0^2}$ with $\varepsilon_0 = 1.12$, which corresponds to exponential decay with Gaussian damping in ε. For $\varepsilon \leq 0.1$, so in the approximately linear regime of the fidelity decay, the loss in fidelity is small enough ($\leq 15\%$) to allow for good revival of $|\psi_1\rangle$. In particular chains shorter than $N \leq 10$ suffer less than 10% loss, which indicates that these devices are very robust against small energy fluctuations. If the fluctuations are relatively big compared to the maximum coupling J_{max} (see section 1.2.1), i.e., for $\varepsilon = 0.5$, the decay is much more serious. Even the shortest chains considered ($N = 5$) see a revival quality of less than 50%, indicating that the initial state $|\psi_1\rangle$ cannot be reliably recovered anymore. This trend is amplified with increasing N. It is also worth noting that the decay in fidelity
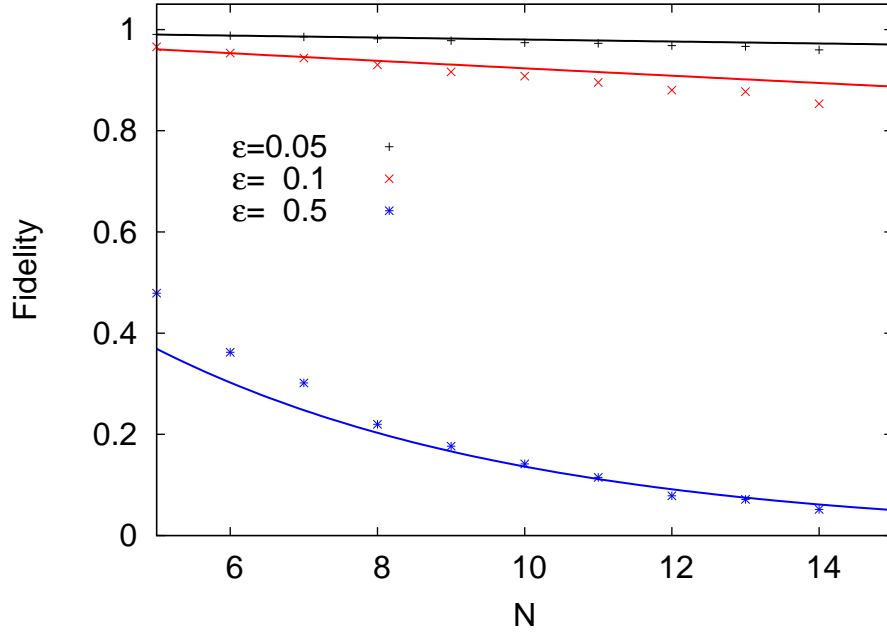
Figure 5.5: Fidelity of initial two excitation state $|\psi_1\rangle = |110\cdots0\rangle$ averaged over 200 realisations at $2t_M$ vs chain length N for three values of ε, as labeled. Fits are according to $e^{-N\varepsilon^2/\varepsilon_0^2}$ with $\varepsilon_0 = 1.12$. Figure adapted from [145].

is not linear in ε, an observation which will be further discussed in section 5.2.2. Overall we confirm that the loss in fidelity is linear for small values of ε, but that the more general decay can be modeled reliably via a simple analytic expression describing exponential decay and Gaussian damping in ε.

5.2.1.2   Entangled states

We observed in section 5.1 that there was no difference in the type of dependence on N between unentangled and entangled states with the same number of excitations, but there was a difference in the magnitude of the effect of random noise. This observation also holds true for random energy fluctuations. In figure 5.6, we observe the decay in EoF at $t = t_M$ of two types of input states, $|\psi_2\rangle = \frac{1}{\sqrt{2}}(|10\cdots0\rangle + |01\cdots0\rangle)$ (frame (a)) and $|\psi_3\rangle = \frac{1}{2}(|0_1 0_N\rangle + |1_1 0_N\rangle + |0_1 1_N\rangle + |1_1 1_N\rangle) \otimes |0_2 \cdots 0_{N-1}\rangle$ (frame (b)). While $|\psi_2\rangle$ is initially entangled, $|\psi_3\rangle$ leads to entanglement at t_M (see discussion in section 3.2). All data points are averaged over 200 random realisations. In both cases, the decay in EoF is fitted by an analytic formula of the form $e^{-N\varepsilon^2/\varepsilon_0^2}$ to a good degree of accuracy. Again, for small values of $\varepsilon = 0.05, 0.1$ a linear fit to the data would also be appropriate, but for larger values of ε the analytic formula works better. The values of ε_0 are different from those used for the fit in figure 5.5 ($\varepsilon_0 = 3.06$ for $|\psi_2\rangle$ and $\varepsilon_0 = 3.01$ for $|\psi_3\rangle$), but our data still shows an exponential decay with Gaussian damp-
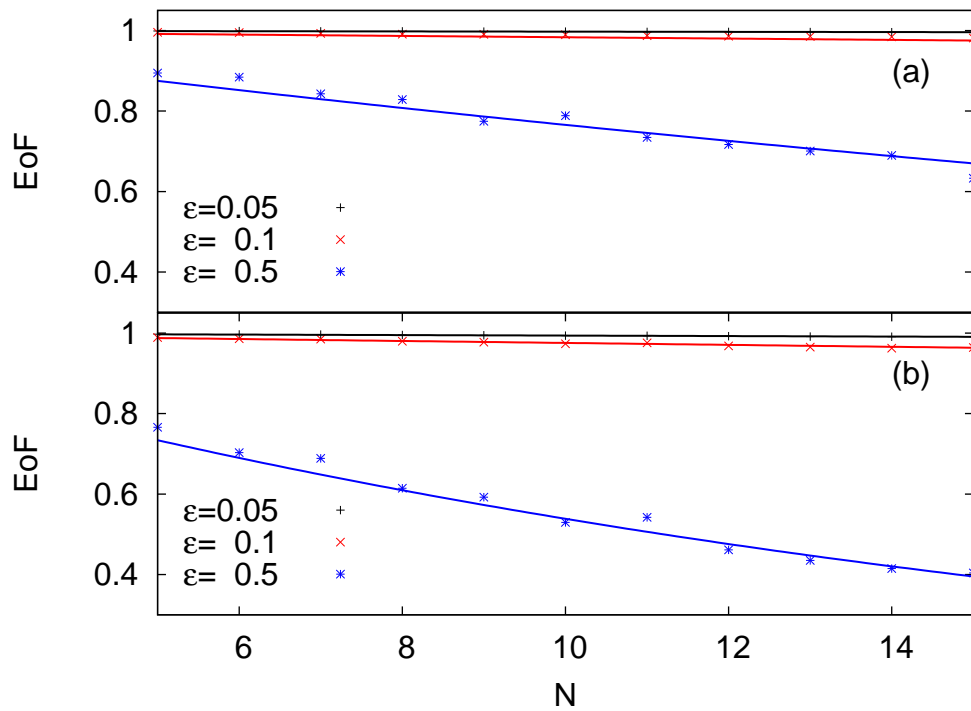
Figure 5.6: EoF calculated at $t = t_M$ averaged over 200 realisations of initial vectors $|\psi_2\rangle$ and $|\psi_3\rangle$ vs chain length N for three values of ε, as labeled. Figure adapted from [145].

(a) $|\psi_2\rangle = \frac{1}{\sqrt{2}}(|10\cdots0\rangle + |01\cdots0\rangle)$, fits are according to $e^{-N\varepsilon^2/\varepsilon_0^2}$ with $\varepsilon_0 = 3.06$.

(b) $|\psi_3\rangle = \frac{1}{2}(|0_1 0_N\rangle + |1_1 0_N\rangle + |0_1 1_N\rangle + |1_1 1_N\rangle) \otimes |0_2 \cdots 0_{N-1}\rangle$, fits are according to $e^{-N\varepsilon^2/\varepsilon_0^2}$ with $\varepsilon_0 = 2.01$.
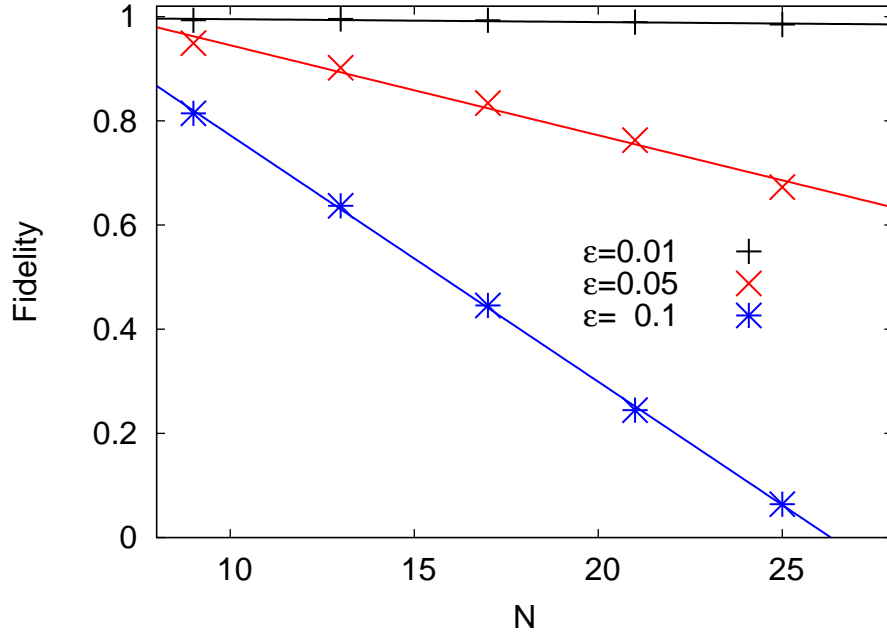
Figure 5.7: Effect of $\widehat{\mathcal{H}_1}$ on the cluster knitting protocol: Fidelity of the desired 4-qubit crossed square cluster state averaged over 100 realisations vs chain length N for three values of ε, as labeled. Fits are linear. Figure adapted from [42].

ing in ε. Similar to the results from figure 5.1, it is the initially entangled state $|\psi_2\rangle$ (with entanglement split over spins 1 and 2) that is least affected. Even for large values of $\varepsilon = 0.5$ and chains up to 10 spins, less than 20% of the EoF is lost. For $\varepsilon = 0.05, 0.1$, even very long chains of $N = 15$ maintain over 98% of the entanglement, making this type of state very robust against energy fluctuations. Compared to $|\psi_1\rangle$ of figure 5.5, $|\psi_2\rangle$ has the advantage of only having one and not two excitations, but a direct comparison between the two graphs is not meaningful as different measures of transport quality are used. In frame (b) of figure 5.6, $|\psi_3\rangle$ shows a similar amount of EoF as $|\psi_2\rangle$ for $\varepsilon = 0.05, 0.1$ but suffers more loss for $\varepsilon = 0.5$, where chains longer than $N = 10$ lose over 40% of their achievable entanglement at t_M.

$|\psi_3\rangle$ is the type of input needed for the cluster state knitting protocol and while the achieved EoF at t_M is very high for $\varepsilon \leq 0.1$, the effect of $\widehat{\mathcal{H}_1}$ on the complete cluster state knitting protocol is much more severe. This is demonstrated in figure 5.7, where we have recorded the fidelity against the desired crossed square cluster state (see section 3.2) at $1.5t_M$ under the influence of $\widehat{\mathcal{H}_1}$ for $\varepsilon = 0.01, 0.05, 0.1$. We have chosen these smaller values of ε as already for $\varepsilon = 0.1$, chains with $N \geq 17$ suffer more than 50% loss in fidelity, down to a 95% loss for $N = 25$. The range of N here is larger to allow for a sufficient number of data points as only every fourth spin chain is suitable for this protocol. To cut

down on the computing time, each data point is averaged over 100 realisations, which still leads to very clear trends. As we are now in the regime of small ε, the fits to the data are linear, as conjectured in [44], and again the dependence on ε is not linear. For very small values of $\varepsilon = 0.01$, even the longest spin chains considered show a very high degree of stability against the influence of $\widehat{\mathscr{H}_1}$ and lose at most 2% of the fidelity of the perfect crossed squared cluster state that the protocol is aiming to achieve. Already for $\varepsilon = 0.05$ however, chains of $N = 25$ suffer more than 30% loss in fidelity and for $\varepsilon = 0.1$, chains as short as $N = 13$ suffer nearly 40% loss. The shortest chain that can be used for the cluster state knitting protocol, which is $N = 9$, maintains over 80% fidelity for $\varepsilon \leq 0.1$ and is therefore still usable even under this relatively high level of perturbation. This demonstrates why very short chains might be desirable for the cluster state knitting protocol, despite the higher risk of imperfect injection that was discussed in section 3.2.4.

5.2.2 On-site energies and interactions between excitations

For spin chain devices of any shape, an additional potential fabrication error arises due to unwanted interaction between excitations. In quantum dots, this might for example be due to biexcitationic interaction [203, 204] or in the case of other nanostructures due to repulsion between electrons [128, 133]. To represent these unwanted interactions, we add to the Hamiltonian $\widehat{\mathscr{H}}$ (1.3) the perturbative term $\widehat{\mathscr{H}_2}$:

$$\widehat{\mathscr{H}_2} = \sum_{i=1}^{N-1} \gamma J_0 |1\rangle\langle 1|_i \otimes |1\rangle\langle 1|_{i+1} \tag{5.3}$$

($\gamma \in \mathbb{R}^+$). Again, as the terms of $\widehat{\mathscr{H}_2}$ are entries on the diagonal of the Hamiltonian $\widehat{\mathscr{H}}$ (1.3), the hermiticity of $\widehat{\mathscr{H}}$ is not affected. The strength of the influence of $\widehat{\mathscr{H}_2}$ is determined by γ and also varies with the chain length as J_0 depends on N (see section 1.2.1). As both $\widehat{\mathscr{H}_1}$ and $\widehat{\mathscr{H}_2}$ add to the diagonal elements of the Hamiltonian $\widehat{\mathscr{H}}$, we expect $\widehat{\mathscr{H}_2}$ to have a similar type of effect on the system dynamics as $\widehat{\mathscr{H}_1}$, but not necessarily the same magnitude. To analyse the overall effect of these two types of fabrication defects, we will investigate the combined influence of $\widehat{\mathscr{H}_1}$ and $\widehat{\mathscr{H}_2}$ in the plots below instead of separately repeating the investigations done in the previous section 5.2.1.
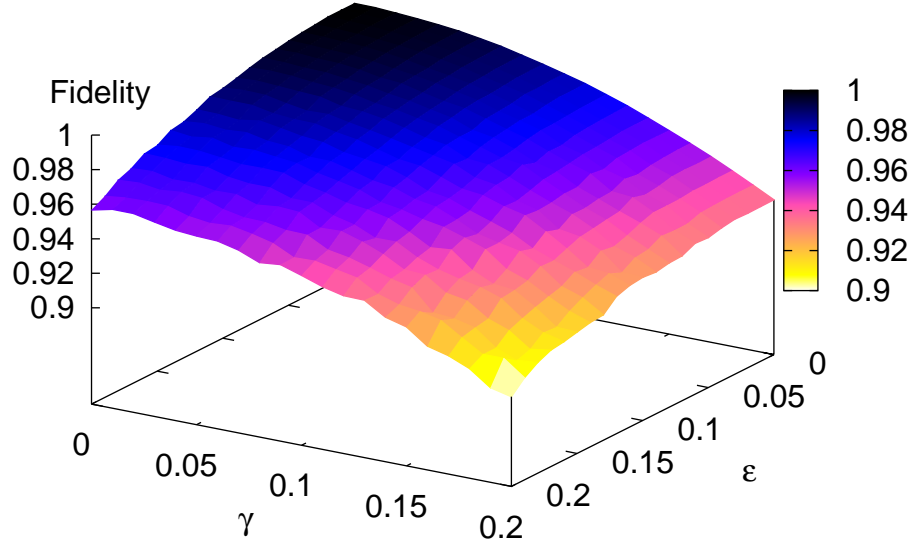
Figure 5.8: Fidelity averaged over 200 realisations of initial vector $|\psi_1\rangle = |111000\rangle$ at $2t_M$ vs ε and γ. Figure published in [145].

5.2.2.1 Unentangled states

In order to observe the effect of $\widehat{\mathcal{H}_2}$ on the quality of state revival of unentangled states, we use an initial vector with multiple excitations, namely $|\psi_1\rangle = |111000\rangle$. Figure 5.8 shows the decay in fidelity of $|\psi_1\rangle$ at the revival time $2t_M$ under the influence of both $\widehat{\mathcal{H}_1}$ (determined by ε) and $\widehat{\mathcal{H}_2}$ (determined by γ). We observe that for this case of a very short chain ($N = 6$) which contains half as many excitations as spins, the effect of $\widehat{\mathcal{H}_2}$ is more severe than that of $\widehat{\mathcal{H}_1}$ and that in both cases, the fidelity does not decay linearly. Nonetheless, even under the combined influence of $\widehat{\mathcal{H}_1}$ and $\widehat{\mathcal{H}_2}$ and values of $\varepsilon = \gamma = 0.2$, $|\psi_1\rangle$ retains more than 90% of its initial fidelity. This demonstrates that even chains which are potentially very prone to the effects of energy fluctuations and interactions between excitations maintain reliable state revival against them and are thus robust against this type of fabrication error.

5.2.2.2 Entangled states

Given previous discussions and the similarities between $\widehat{\mathcal{H}_1}$ and $\widehat{\mathcal{H}_2}$, we will now focus on input states of the type $|\psi_3\rangle = \frac{1}{2}(|0_1 0_N\rangle + |1_1 0_N\rangle + |0_1 1_N\rangle + |1_1 1_N\rangle) \otimes |0_2 \cdots 0_{N-1}\rangle$ which under unperturbed conditions leads to a maximally entangled state which is also the first building block of the cluster state knitting protocol. It is to be expected that unlike in figure 5.8, the influence of $\widehat{\mathcal{H}_1}$ will
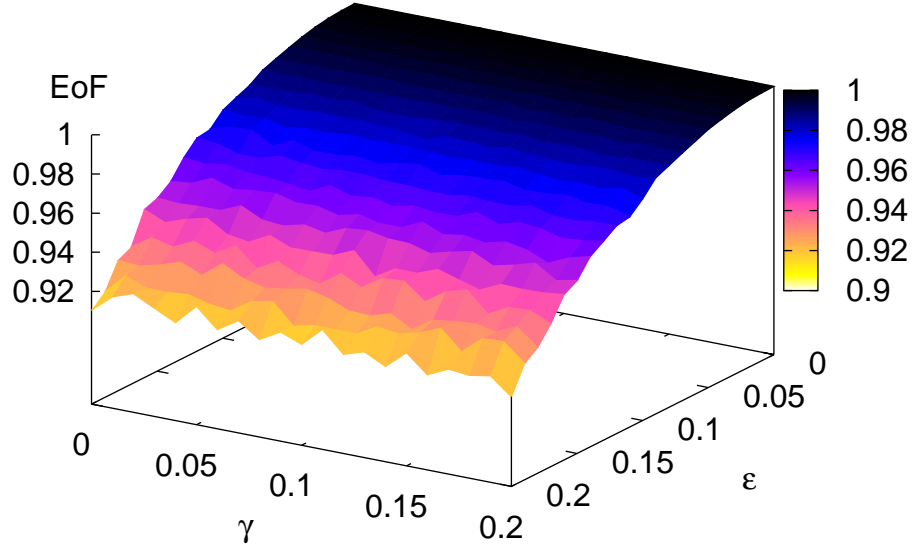
Figure 5.9: EoF averaged over 100 realisations of initial vector $|\psi_3\rangle = \frac{1}{2}(|0_1 0_9\rangle + |1_1 0_9\rangle + |0_1 1_9\rangle + |1_1 1_9\rangle) \otimes |0_2 \cdots 0_8\rangle$ at t_M vs ε and γ. Figure published in [42].

dominate the influence of $\widehat{\mathcal{H}_2}$ as only one out of the four components of $|\psi_2\rangle$ encompasses multiple excitations and will thus be affected by $\widehat{\mathcal{H}_2}$. We see that this is indeed the case in figure 5.9, which shows the amount of entanglement produced by $|\psi_2\rangle$ at t_M for a 9-spin chain. Compared to the loss in EoF due to $\widehat{\mathcal{H}_1}$, the influence of $\widehat{\mathcal{H}_2}$ is effectively negligible. The loss in entanglement even for $\varepsilon = \gamma = 0.2$ is however still very small at less than 9%, which is very promising.

If instead of merely recording the achieved entanglement at t_M, we proceed with a second injection of $|+\rangle$ states to spins 1 and N at $0.5 t_M$ and thus follow the knitting protocol for a 4-qubit crossed square cluster state, the result is dramatically different. Instead of maintaining a high level of transport quality as we observed in figure 5.9, we see in figure 5.10 that the fidelity against the ideal cluster state drops below 75% for $\varepsilon \geq 0.12$, down to less than 40% for $\varepsilon = 0.2$. Once more, the influence of $\widehat{\mathcal{H}_2}$ has become negligible when compared to that of $\widehat{\mathcal{H}_1}$, even for large values of $\gamma = 0.2$. Perturbations due to interactions between excitations are thus of little to no relevance for purposes of cluster state knitting and entanglement generation based on $|\psi_2\rangle$, but for states with a large number of excitations compared to N, they can be a prominent perturbation.
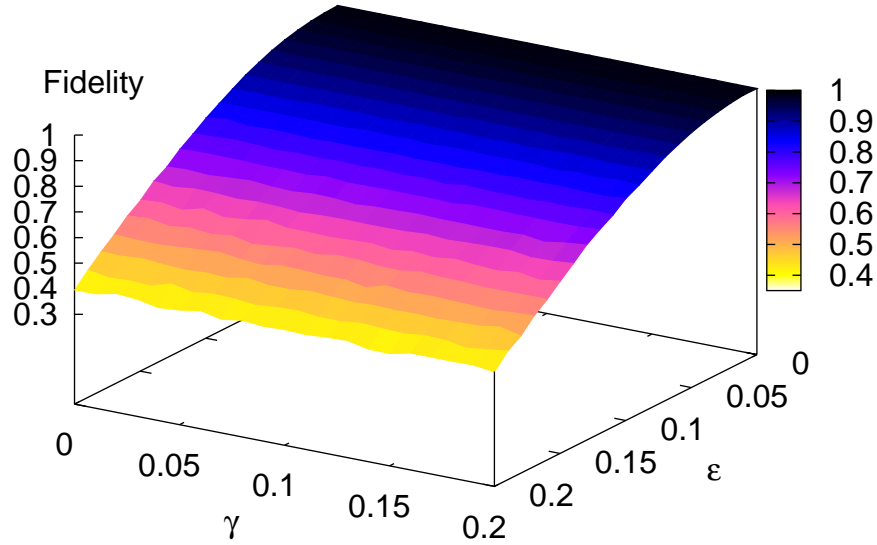
Figure 5.10: Fidelity of the ideal 4-qubit crossed square cluster state achieved from a 9-spin chain averaged over 100 realisations at $1.5t_M$ vs ε and γ. Figure published in [42].

5.3 Conclusions

Having considered three different types of fabrication defects, we have found several similarities in their effects on the performances of spin chains. In all three cases, we found that an increase in the number of excitations in the initial state leads to much more severe perturbations. This is particularly noticeable for perturbations arising from interaction between excitations, where we saw a clear decay in the revival fidelity of a three excitation input state but virtually no effect on the cluster state knitting protocol where the average number of excitations in the chain is lower. Both perturbations due to noise and unwanted on-site energies and interactions have shown non-linear dependences in r, ε and γ respectively. For noise and on-site energies, entangled initial input with entanglement split over adjacent sites was found to be the most robust type of input state. We confirmed the linear decay in transport quality for small energy fluctuations but found that for a larger range of ε, the decay can be modeled via a simple analytic formula representing exponential decay with Gaussian damping in ε. As such, we have shown that a useful parametrisation of the effects of decoherence with N and with perturbation size can be made, which may be a useful tool for experimentalists or quantum circuit designers. Energy fluctuations are also by far the most detrimental fabrication defect with regards to the cluster state knitting protocol, indicating that this will be the

most important perturbation out of those considered so far to eliminate in any physical implementations.

Chapter 6

Other perturbations of information transfer

Having considered the effects of a range of fabrication defects, we are now going to look at the perturbative influence of unwanted additional channels on the one hand and mistimed input operations on the other. The conclusions we draw in this chapter are the result of original work, which has been published in [42, 145, 146]. So far, we have assumed that the only couplings present in the device (perturbed or not) will be those given by the Hamiltonian (equation (1.3)), but this might not necessarily reflect experimental circumstances: Depending on the hardware used to implement the spin chain, excitations may travel along channels which are not part of the Hamiltonian as described so far.

Another assumption we have made, in particular in chapter 3, is that the timing of all external operations, for example swapping excitations in or out, is perfect. In particular, if two sites are to be acted on simultaneously, as is the case in the cluster state knitting protocol, it is assumed that there is a perfect clock. We will therefore also analyse the effects of mistimed input operations, both with respect to multiexcitation initial input states as well as the cluster state knitting protocol.

Throughout this chapter, we will only consider linear spin chains. While more complex architectures are of course also expected to be affected by the perturbations we consider, the analysis of linear chains will allow us to detect dependencies on N (which will for example translate as dependencies on the ECL for branched devices) and other global behaviour. Moreover, longer range interactions will be very dependent on the actual physical realisation as for example the distance between individual sites or the type of interaction might vary a great deal. As there are currently no physical realisations of spin chain

devices beyond linear chains, we have no results against which to compare any models and would therefore not be able to judge the relevance or quality of our results.

6.1   Unwanted additional couplings

Let us first of all consider the effect of additional, unwanted couplings on the information transfer in a spin chain. Unlike some existing studies on longer range interactions [59, 205–211], we strictly consider these to be a perturbation to the system. As such, we will keep the usual PST conditions as given by equation (1.5) and observe the effect of the additional couplings with no other perturbations present.

6.1.1   Next-nearest neighbour coupling

Before looking into additional couplings in general, we will begin by considering next-nearest neighbour interaction. We add to the Hamiltonian (1.3) the perturbative element

$$\widehat{\mathcal{H}_\Delta} = \sum_{i=1}^{N-2} J_{i,i+2} \left[|1\rangle\langle 0|_i \otimes |0\rangle\langle 1|_{i+2} + |0\rangle\langle 1|_i \otimes |1\rangle\langle 0|_{i+2} \right], \tag{6.1}$$

with

$$J_{i,i+2} = \Delta \frac{J_{i,i+1} + J_{i+1,i+2}}{2}, \tag{6.2}$$

where Δ determines the strength of the interaction.

The actual effect of next-nearest neighbour interaction depends on the type of interaction between spin chain sites. Equation (6.2) uses an average over the two nearest neighbour sites, weighted by Δ, a model which we can verify using results for dipole-dipole interaction and also some experimental data on graphene quantum dots.

Let us first of all consider a scenario where the coupling between quantum dots is due to dipole-dipole interactions [143]. An example of an implementation with such couplings are quantum dots with exciton qubits and Förster coupling [212], in which case the coupling $J_{i,j}$ between two sites scales as $1/R_{i,j}^3$ [45], where $R_{i,j}$ is the distance between the sites i and j. Using equa-

Variable description	Variable	Variable value/expression
Onsite Coulomb energy	U	$U = 10$ meV
Width of a quantum dot	W	$W = 30$ nm
Length of a quantum dot	L	$L \approx W = 30$ nm
Distance between quantum dots i and $i+1$ (constant for all i)	$R_{i,i+1}$	$R_{i,i+1} = 10L = 300$ nm
"Forbidden" momentum in the barrier (constant for all i)	k	$\lvert k \rvert R_{i,i+1} = 4$
Ground state energy	ε	$\varepsilon = 30$ meV
Tunnelling (hopping) parameter between sites a and b	$t_{a,b}$	$t_{a,b} = 0.03\varepsilon$ $t_{a,b} = \alpha R_{a,b} e^{-R_{a,b}\lvert k \rvert}$
Coupling between quantum dots i and $i+1$	$J_{i,i+1}$	$J_{i,i+1} = \dfrac{4t_{i,i+1}^2}{U}$

Table 6.1: Experimental data and expressions for variables related to graphene quantum dots used from reference [141].

tion (1.5), we can therefore derive an analytic expression for $R_{i,i+2}$:

$$R_{i,i+2} = R_{i,i+1} + R_{i+1,i+2}$$

$$= \left(\frac{1}{J_0[i(N-i)]^{\frac{1}{2}}} \right)^{\frac{1}{3}} + \left(\frac{1}{J_0[(i+1)(N-(i+1))]^{\frac{1}{2}}} \right)^{\frac{1}{3}}$$

$$= J_0^{-\frac{1}{3}} \left[\{i(N-i)\}^{-\frac{1}{6}} + \{(i+1)(N-(i+1))\}^{-\frac{1}{6}} \right]$$

and since $J_{i,i+2} = 1/R_{i,i+2}^3$,

$$J_{i,i+2} = J_0 \left[\{i(N-i)\}^{-\frac{1}{6}} + \{(i+1)(N-(i+1))\}^{-\frac{1}{6}} \right]^{-3}. \qquad (6.3)$$

The other scenario we consider is a hardware implementation where the couplings in the chain are due to tunnelling, so for example quantum dots with spin qubits [55, 150]. One such hardware implementation is presented in [141], where parameters as well as useful and experimentally reasonable approximations and expressions for the various variables needed are given for graphene quantum dots. In this case, it is not possible to derive an explicit expression for $J_{i,i+2}$ in terms of $J_{i,i+1}$, but it is possible to find numerical values for the next-nearest neighbour couplings nonetheless. To do this, we use the data from [141] presented in table 6.1 to check the agreement of our model (equation (6.2)) with results derived from experimental parameters. First of all, we calculate the value of the constant α, which we need to calculate the next-nearest

neighbour hopping parameter $t_{i,i+2}$:

$$t_{i,i+1} = 0.03\varepsilon = 0.9 = \alpha R_{i,i+1} e^{-R_{i,i+1}|k|}$$

$$= \alpha \times 300 \times e^{-4}$$

$$\alpha = \frac{0.9}{300 \times e^{-4}}$$

$$\approx 0.16 \, \text{meV} \times \text{nm}^{-1}$$

We now proceed to numerically derive values for $J_{i,i+2}$ using the following algorithm:

Algorithm 2 Finding numerical values of the next-nearest neighbour couplings $J_{i,i+2}$, assuming that the interaction between sites is tunnelling. Data and expressions based on [141] (see table 6.1).

1: Using the usual PST condition from equation (1.5) and $J_{i,i+1} = \frac{4t_{i,i+1}^2}{U}$, find values for $t_{i,i+1}$.
2: Using $t_{i,i+1} = \alpha R_{i,i+1} e^{-R_{i,i+1}|k|}$, find values for $R_{i,i+1}$ such that the values for $t_{i,i+1}$ match those found in step 1.
3: Calculate $R_{i,i+2} = R_{i,i+1} + L + R_{i+1,i+2}$.
4: Using $R_{i,i+2}$, find $t_{i,i+2} = \alpha R_{i,i+2} e^{-R_{i,i+2}|k|}$.
5: Using $t_{i,i+2}$, find $J_{i,i+2} = \frac{4t_{i,i+2}^2}{U}$.

We will now observe whether our model (equation (6.2)) matches the expression and values for next-nearest neighbour couplings derived from equation (6.3) (dipole-dipole interaction) and [141] (numerical results for tunnelling based on algorithm 2). Figure 6.1 shows that for both types of interactions, there is near-perfect agreement between the dynamics from our model and the dynamics derived from data for suitably chosen values of Δ.

For the dipole-dipole interaction scenario, we achieve a very good fit by choosing $\Delta = 0.12$, meaning that the next-nearest neighbour couplings are about a tenth of the nearest neighbour couplings. Given that the sites of an 8-spin chain are roughly equidistant, this value is well within the range of what we could expect to find [45, 208]. The information transport itself in this case is however very poor, the influence of $\widehat{\mathcal{H}_\Delta}$ on the system is such that even the fidelity of the mirror twin $|\psi_{twin}\rangle = |00000011\rangle$ of the initial two-excitation input state $|\psi_{in}\rangle = |11000000\rangle$ at the mirror time t_M is reduced by nearly 50%. It is also clear from the graph that the subsequent periodicity is lost as the excitations spread out in the chain.

The scenario assuming couplings due to tunnelling shows very different results. Again, we achieve very good agreement between our model and the data for graphene dots and spin qubits from [141], this time by setting $\Delta = 0.0001$.
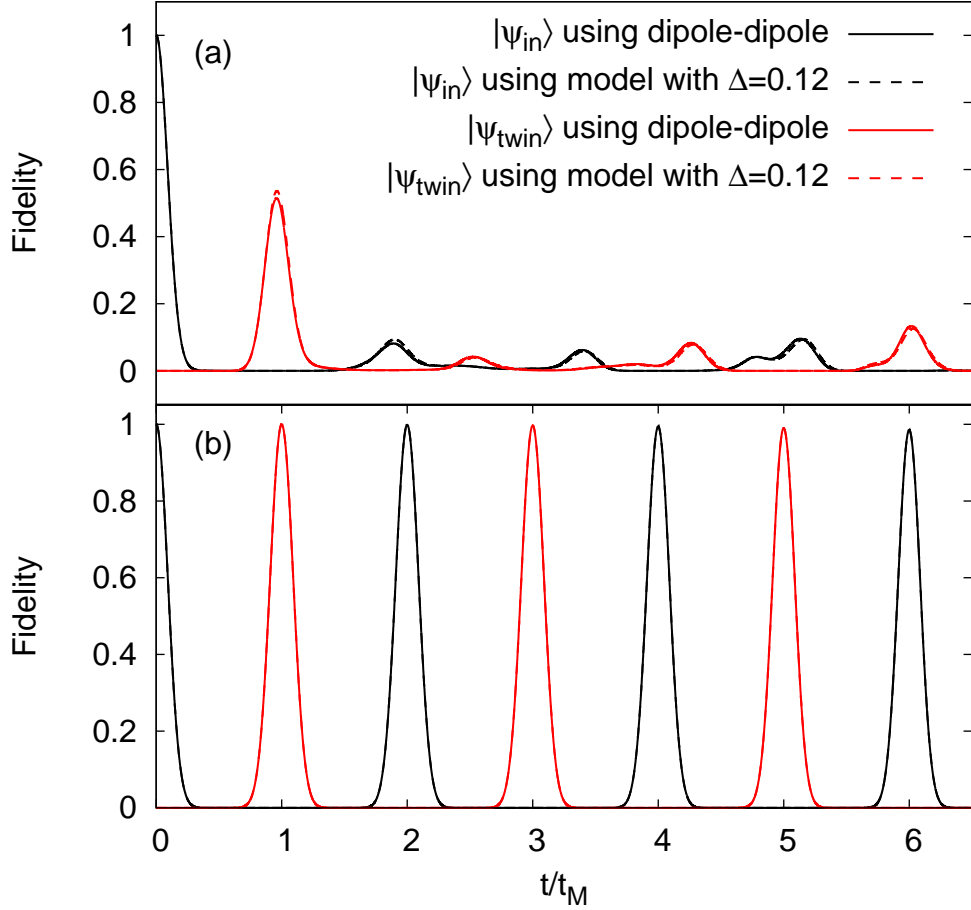
Figure 6.1: (a) Influence of $\widehat{\mathcal{H}_\Delta}$ (equation (6.2)) on the example of an 8-spin chain with initial input state $|\psi_{in}\rangle = |11000000\rangle$ (twin state $|\psi_{twin}\rangle = |00000011\rangle$), fidelity vs. rescaled time t/t_M, according to both equation (6.2) (solid lines) and equation (6.3) (dashed lines; dipole-dipole coupling). The peak of $|\psi_{twin}\rangle$ at t_M is approximately 0.52. As the model of equation (6.2) matches the data derived from equation (6.3) extremely well, the lines of the respective plots are nearly indistinguishable.

(b) As for main panel but for graphene quantum dots and spin qubits, with tunnelling couplings (dashed lines) and couplings according to equation (6.2), $\Delta = 0.0001$ (solid lines). Again results from the two models for the coupling constants are virtually indistinguishable from each other. Figure adapted from [145].

This can be seen in panel (b) of figure 6.1, where the two plots are virtually indistinguishable. As the interaction under tunnelling decays exponentially [141], this very small value of Δ is to be expected. With such a small value of Δ, the system loses less than 2% of fidelity after $6t_M$. This considerable contrast with the dipole-dipole scenario highlights how strongly the effect of $\widehat{\mathscr{H}_\Delta}$ depends on the type of interaction between the spin chain sites and thus the hardware implementation. Where for dipole-dipole interaction, next-nearest neighbour interaction is a serious perturbation and care must be taken to minimise it, transport by tunnelling is hardly affected so that next-nearest neighbour interaction is only of limited importance. As values of Δ below 0.01 have a negligible effect on the system, we will now focus on the range $0.01 \leq \Delta \leq 0.1$. We have shown that this upper bound is of interest to some experimental implementations, but the effect of $\widehat{\mathscr{H}_\Delta}$ on the system for larger values of Δ is so detrimental that information transport is not possible anymore.

In the example of figure 6.1, we have considered an 8-spin chain with a two-excitation unentangled input state under the influence of $\widehat{\mathscr{H}_\Delta}$. It is fair to assume that both an increase in the number of excitations as well as the number of sites in the chain will lead to a decrease in state transfer fidelity as longer chains will contain more unwanted couplings that an excitation could be subject to while travelling between distant sites of the chain. A more subtle question is whether the number of excitations and sites is the only factor in the influence of $\widehat{\mathscr{H}_\Delta}$ on the state transfer, or whether the form of the initial input state also matters. To investigate this, we will consider three different types of input states: i) $|\psi_1\rangle = |110\cdots0\rangle$ (unentangled, two excitations), ii) $|\psi_2\rangle = \frac{1}{\sqrt{2}}(|10\cdots0\rangle + |01\cdots0\rangle)$ (spins 1 and 2 entangled, one excitation) and iii) $|\psi_3\rangle = \frac{1}{2}(|0_1 0_N\rangle + |1_1 0_N\rangle + |0_1 1_N\rangle + |1_1 1_N\rangle) \otimes |0_2 \cdots 0_{N-1}\rangle$ (initially unentangled but leading to entanglement via action of the intrinsic gate defined in equation (3.4), see discussion in section 3.1.3). We see in figure 6.2 that there are significant differences between these three types of input. Type i) (panel (a)) suffers the most loss in fidelity, suffering more than 20% fidelity loss for moderate values of $\Delta = 0.05$ and all chain lengths. By comparison, type ii) (panel (b)) input suffers about 10% EoF loss for $\Delta = 0.05$ and short chains, but again for large values of $\Delta = 0.1$ and long spin chains the loss in EoF is such that most of the entanglement is lost and so the information transport fails. On the other hand, the other type of input which leads to entanglement, type iii) (panel (c)), is much more robust against the influence of $\widehat{\mathscr{H}_\Delta}$: For small and moderate values of $\Delta = 0.01, 0.05$, even very long chains of $N = 15$ suffer an EoF loss of less than 10%. For $\Delta = 0.1$, the loss is up to 30% for the values of N considered, which is significantly different from the results of types i) and ii).
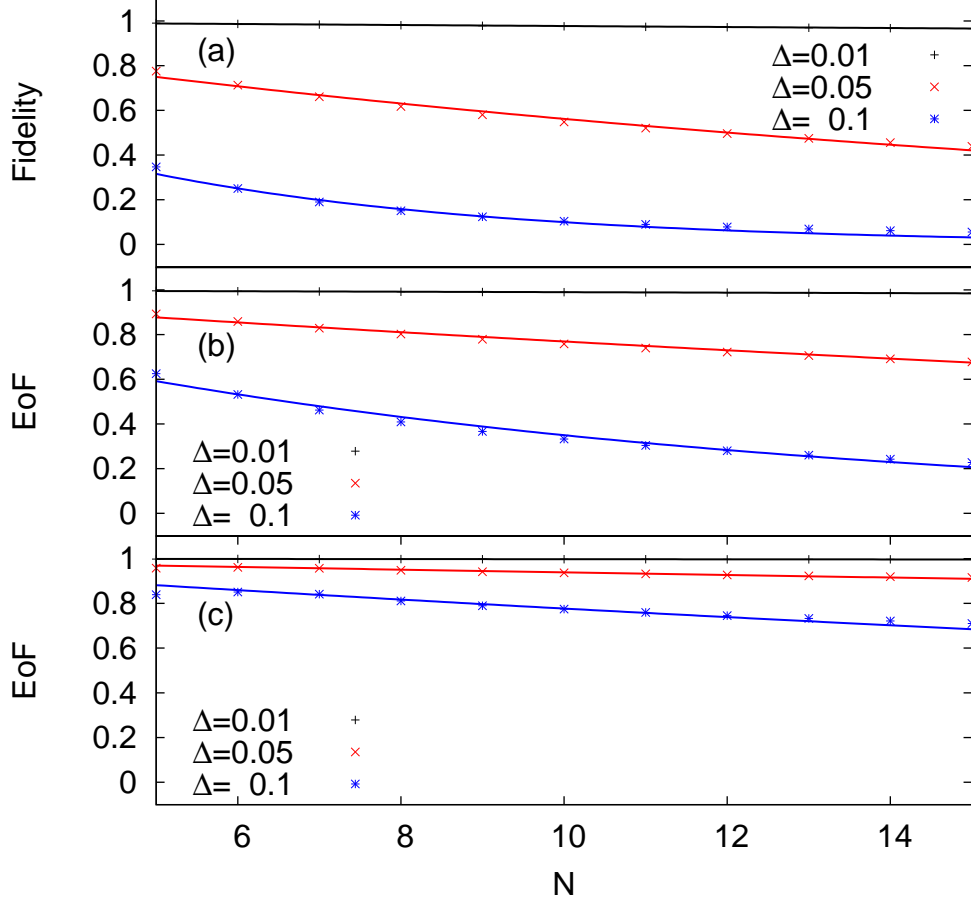
Figure 6.2: Fidelity and EoF under the influence of $\widehat{\mathcal{H}_\Delta}$ (equation (6.2)) vs. N for three values of Δ (as labelled) and the following initial states, all fitted via $e^{-N\Delta^2/\Delta_0^2}$:

(a) $|\psi_1\rangle = |110\cdots0\rangle$, fitted with $\Delta_0 = 0.21$ (recording peak at $2t_M$)

(b) $|\psi_2\rangle = \frac{1}{\sqrt{2}}(|10\cdots0\rangle + |01\cdots0\rangle)$, fitted with $\Delta_0 = 0.31$ (recording peak at $2t_M$)

(c) $|\psi_3\rangle = \frac{1}{2}(|0_1 0_N\rangle + |1_1 0_N\rangle + |0_1 1_N\rangle + |1_1 1_N\rangle) \otimes |0_2 \cdots 0_{N-1}\rangle$, fitted with $\Delta_0 = 0.63$ (recording peak at t_M).

Figure adapted from [145].
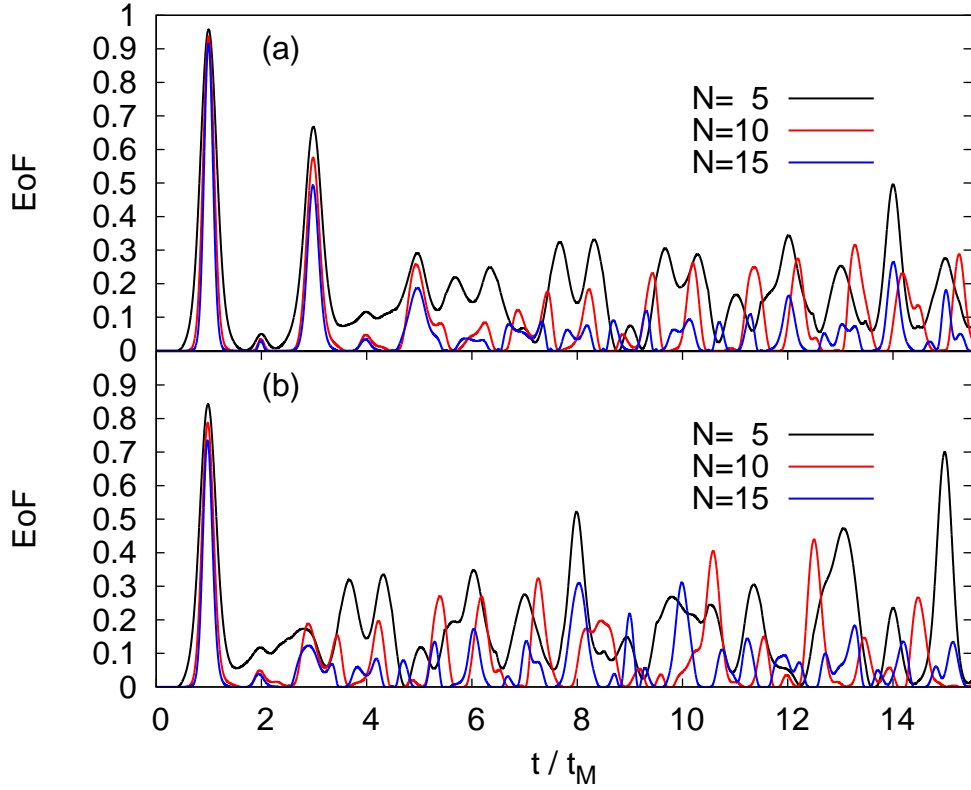
Figure 6.3: Spin chains with input state $|\psi_{in}\rangle = \frac{1}{2}(|0_1 0_N\rangle + |1_1 0_N\rangle + |0_1 1_N\rangle + |1_1 1_N\rangle) \otimes |0_2 \cdots 0_{N-1}\rangle$:
(a) EoF of $|\psi_{in}\rangle$ vs rescaled time t/t_M for $\Delta = 0.05$: The periodicity of the entanglement of formation is completely lost after the second peak at $3t_M$.
(b) EoF of $|\psi_{in}\rangle$ vs rescaled time t/t_M for $\Delta = 0.1$: The periodicity of the entanglement of formation is completely lost after the first peak at t_M. Figure adapted from [145].

Despite these different results, the influence of $\widehat{\mathcal{H}_\Delta}$ is of the same form for all three types on input states. As shown in figure 6.2, in all three cases the data could be fitted via a single analytic formula of the form $e^{-Nf(\Delta)}$, with $f(\Delta) = \Delta^2/\Delta_0^2$ and Δ_0 the characteristic parameter of the influence of $\widehat{\mathcal{H}_\Delta}$ in the specific case. The resulting fits are of sufficient accuracy to deduce that both the loss in fidelity and EoF scale as exponential decay with Gaussian damping in Δ. This means that $\widehat{\mathcal{H}_\Delta}$ is potentially very damaging very quickly, in particular for states which are unentangled and do not lead to entanglement, to the point where it could not just perturb but entirely inhibit information transfer in a chain.

In figure 6.2 we have considered the fidelity and EoF of the first peaks only. There is however another effect of $\widehat{\mathcal{H}_\Delta}$ concerning the periodicity of the system dynamics. Figure 6.3 shows how for type iii) input the initial state $|\psi_3\rangle$ evolves under $\Delta = 0.05$ (panel (a)) and $\Delta = 0.1$ (panel (b)) for $N = 5, 10, 15$. Even though
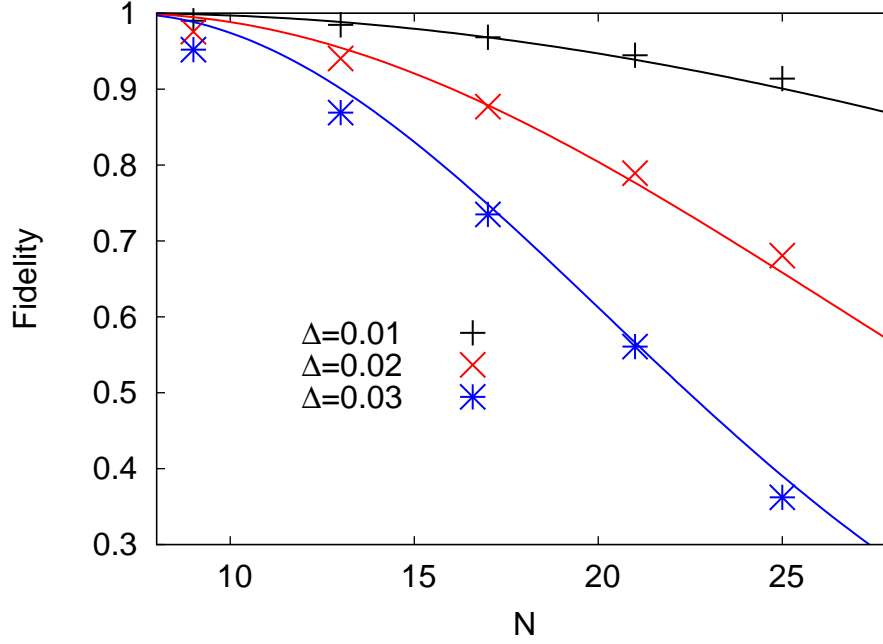
Figure 6.4: Fidelity of the ideal 4-qubit crossed square cluster state at $1.5t_M$ vs N for three values of Δ as labeled. Lines are fitted via $e^{-\frac{\Delta^2 (N-a)^2}{b}}$ with $a = 7$ and $b = 0.31$. Data has previously been published in [42].

for both values of Δ, the first EoF peak is well pronounced, the subsequent dynamics are much more affected: For $\Delta = 0.05$, even the very short chain with $N = 5$ has lost more than 30% of its EoF at the second peak at $3t_M$, after which the dynamics deteriorate completely and the excitations are spread out. For $\Delta = 0.1$, there is no second peak achieved for any chain length. Overall, this indicates that even for settings where the fidelity or EoF of the first peak is of good or acceptable magnitude, there might be a subsequent total loss of periodicity, making the chain unsuitable for protocols which rely on periodicity, such as for example the cluster state knitting protocol presented in chapter 3.

Next-nearest neighbour interaction is in general very detrimental to the cluster state knitting protocol, even when only the smallest 4-qubit crossed square cluster state is knitted. Even very small values of Δ lead to a serious loss of fidelity of the desired 4-qubit state, as is shown in figure 6.4. Good fidelity values of over 90% for all chain lengths considered are only achieved for $\Delta = 0.01$, whereas even for $\Delta = 0.02$ there is a fidelity loss of over 20% for chains longer than $N = 21$. For $\Delta = 0.03$, reliable knitting of the crossed square cluster state with more than 80% fidelity is only possible for chains of length $N = 13$ or less. The decay in fidelity is now of a slightly different form than in figure 6.2 and follows a simple Gaussian decay according to $e^{-\frac{\Delta^2 (N-a)^2}{b}}$. Values of Δ larger than 0.03 still allow for acceptable fidelity peaks at $1.5t_M$ for short and medium

chains, but the subsequent periodicity is lost once more. For longer chains such as $N = 21$, even values of $\Delta = 0.05$ do not allow for formation of this first fidelity peak anymore and so the cluster knitting protocol fails entirely. This increased detrimental effect of $\widehat{\mathscr{H}_\Delta}$ is due both to the increased chain lengths considered (compared to figure 6.2, as only 1 in 4 chains is suitable for the cluster state knitting protocol), and also to the increased number of excitations needed to implement the protocol (four excitations compared to two in panel (c) of figure 6.2). The increased chain length leads to additional perturbative channels and the increased number of excitations leads to an accelerated perturbation of the dynamics, an effect which can also be observed in chains with other types of input. Overall, these results underline the need to control next-nearest neighbour interactions, particularly in long chains and for initial input states containing many excitations, as otherwise not only spin chain protocols but also simple information transfer might be severely affected or become impossible altogether.

6.1.2   Longer range couplings

Having observed and quantified the effect of next-nearest neighbour interaction on linear spin chains with various types on input states, we will now look into the influence of additional, unwanted couplings in general. Again, we strictly consider these additional couplings beyond nearest neighbour interaction as perturbative, so that all nearest neighbour couplings are still set up for PST as per equation (1.5). This is in contrast to previous work, where longer range interactions have been treated as a known feature of the chain such that the couplings can be optimised [206], whereas we treat couplings beyond nearest neighbour interaction as of a priori unknown strength.

To simulate all longer range couplings, we add to all zero entries $\widehat{\mathscr{H}_{l,m}} = 0$ in the Hamiltonian (1.3) a random coupling $\chi d_{l,m} J_{max}$ for $1 \leq l, m \leq k$ and $l \neq m$, with k the number of basis vectors (see equation (2.2)) and χ the strength of the perturbation. $d_{l,m}$ are random numbers generated from a flat distribution such that $0 \leq d_{l,m} \leq 1$. In order to preserve the hermiticity of the Hamiltonian, we impose $d_{l,m} = d_{m,l}$. As the outcome of each simulation will now be dependent on these random numbers, the data points in figure 6.5 are averaged over 100 realisations each.

As in section 6.1.1, we consider three different types of input: i) $|\psi_1\rangle = |110\cdots0\rangle$ (unentangled, two excitations), ii) $|\psi_2\rangle = \frac{1}{\sqrt{2}}(|10\cdots0\rangle + |01\cdots0\rangle)$ (spins 1 and 2 entangled, one excitation) and iii) $|\psi_3\rangle = \frac{1}{2}(|0_1 0_N\rangle + |1_1 0_N\rangle + |0_1 1_N\rangle + |1_1 1_N\rangle) \otimes |0_2 \cdots 0_{N-1}\rangle$ (initially unentangled but leading to entanglement, see discussion
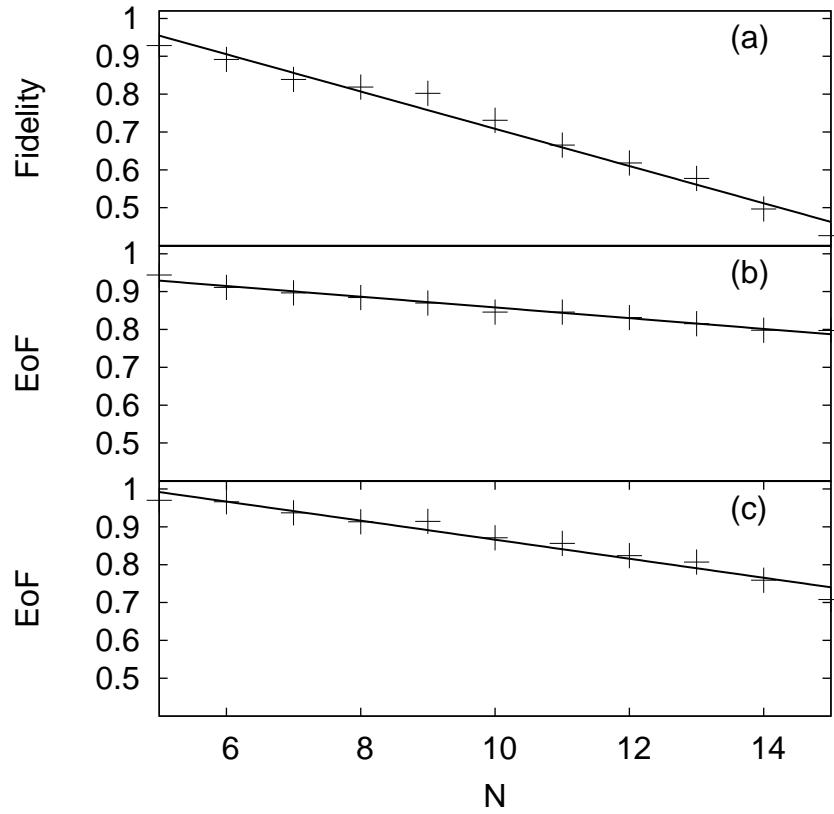
Figure 6.5: Effect of opening up all longer range interactions with $\chi = 0.03$ on first fidelity and EoF peaks (data points have been averaged over 100 realisations):
(a) Fidelity of $|\psi_1\rangle$ (input type i)) vs N at $2t_M$.
(b) EoF of $|\psi_2\rangle$ (input type ii)) vs N at $2t_M$.
(c) EoF resulting from $|\psi_3\rangle$ (input type iii)) vs N at t_M.

in section 3.1.3). We see in figure 6.5 that, similar to figure 6.2, it is the unentangled input type i) (panel(a)) that suffers the most dramatic loss. Even for a small value of $\chi = 0.03$, the longest chain of $N = 15$ loses more than 50% fidelity at its first peak at $2t_M$. In comparison, type ii) input (panel(b)) suffers less than 25% EoF loss at t_M for $\chi = 0.03$ and $N = 15$. Type iii) input (panel(c)) follows a similar decay to type ii), although shorter chains are less affected while longer chains of $N = 15$ suffer slightly more loss in EoF. It is also worth noting that unlike figure 6.2, the fits to the numerical data are straight line fits and cannot be achieved using exponential fits. This is a strong indication that opening up all possible channels for excitations to travel along the chains leads to much more erratic dynamics than the opening up of an additional regular pattern of channels, such as the next-nearest neighbour interactions. Again, this is due to the larger number of degrees of freedom, which makes any transfer of excitations more prone to using undesired channels, thereby disrupting the desired dynamics.

Having observed a loss of periodicity for next-nearest neighbour interactions, even for settings where the first revival/entanglement peak was close to unity, we observe in figure 6.6 the decline in periodicity for $\chi = 0.03, 0.1$ on the example of a 10-spin chain. In frame (a), we see that even for $\chi = 0.03$, the excitations are completely spread out along the chain, with no significant revival of the initial state $|\psi_1\rangle$ after the first peak at $2t_M$. For larger values of $\chi = 0.1$, the excitations are quickly spread out without the occurrence of any revival peaks. For the entangled input types ii) and iii) of frames (b) and (c) in figure 6.6 respectively, the loss of periodicity does not appear quite as dramatic: For $\chi = 0.03$ type ii) input displays two pronounced EoF peaks at $2t_M$ and $4t_M$ before becoming unpredictable. For $\chi = 0.1$, the behaviour appears however entirely erratic and no meaningful EoF peaks are formed. The initially unentangled type iii) input performs slightly better, showing three EoF peaks over 0.5 at $t_M, 3t_M$ and $5t_M$ for $\chi = 0.03$ and a small EoF peak of 0.31 at t_M for $\chi = 0.1$. Any following peaks are not only of smaller magnitude, but also not occurring at multiples of t_M anymore, indicating that the system dynamics do not follow any PST pattern anymore. Overall, figures 6.5 and 6.6 demonstrate that opening up all longer range interaction channels leads to linear decay in fidelity and EoF, as well as a quick loss of periodicity for all three types of input considered. Initially unentangled input leading to entanglement (type iii)) is most robust against this, which is in-keeping with the effect of next-nearest neighbour interaction, where type iii) input was also least affected.
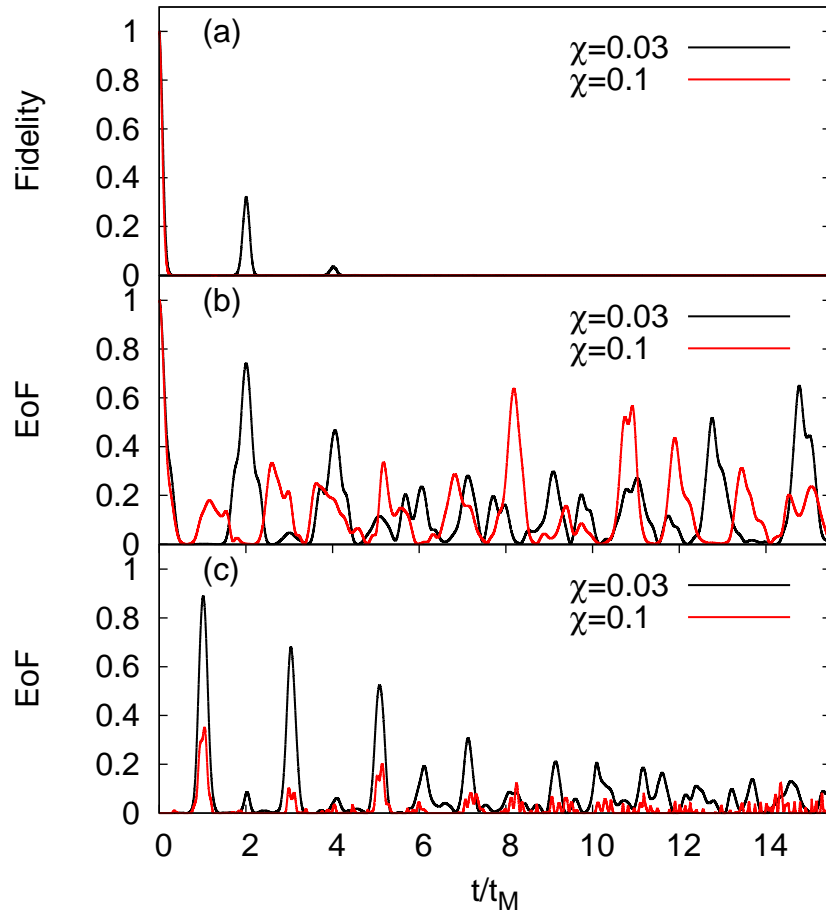
Figure 6.6: Effect of opening up all longer range interactions of a 10-spin chain with $\chi = 0.03, 0.1$ on periodicity:
(a) Fidelity of $|\psi_1\rangle$ (input type i)) vs t/t_M.
(b) EoF of $|\psi_2\rangle$ (input type ii)) vs t/t_M.
(c) EoF resulting from $|\psi_3\rangle$ (input type iii)) vs t/t_M.

6.2   Mistimed operations of spin chains

Both in chapter 5 and in section 6.1, we have discussed the effects of defects and perturbations which are either the result of imperfect initial set-up of the hardware (such as fabrication defects) or due to insufficiently controlled environmental variables (such as fluctuating magnetic fields). In this section, we will now analyse the effects of operational errors on linear spin chains with respect to timing. It goes without saying that there are many possible errors resulting from operations on the spin chain: Dependent on the actual hardware protocols used, states might be improperly initialised or not fully injected or extracted or there might be various degrees of unwanted entanglement with the environment as a result of the operation. For example, a SWAP operation might be imperfect as the excitation could be partially reflected back into the wire used for injection, for instance because of an imperfect lowering of the potential barrier between the desired injection site and the wire. Here, we will only consider the effects of mistimed operations, so input and output operations which are effected at a slight delay compared to the ideal case but otherwise perfect.

In previous chapters, we have already implied the assumption that both ends of a spin chain have access to the same clock since PST can only be achieved if the transferred state is actually also read out at the correct time. For a single unentangled excitation, it is straight-forward to predict the effect of mistimed input or output, i.e., a delay with respect to this clock, as we can simply look at the fidelity of the twin state and note the sub-unity fidelity at any time other than odd multiples of t_M. On the other hand, multiple excitation states pose a more interesting problem as here the time evolution of the initial state is not merely shifted in time (as is the case for the single excitation state) but changes altogether. This would happen for example if not all input sites are accessed simultaneously, so that for example a system which should be initialised in a two excitation state might start evolving as a single excitation state before the second excitation is injected. The effects of such a delay scenario are strongly dependent on the type of injection mechanism used. In this work, we will consider two such possible mechanisms: injection by Rabi flopping and injection by SWAP operation, as defined in section 1.2.3.2.

The main issue with mistimed input operations is that especially for injection sites which are not very far from each other, there arises a probability that the second, delayed input site might already be occupied by the first injected excitation: Instead of being initialised as the two excitation state $|\psi_{ideal}\rangle = |1_i\rangle|1_j\rangle \bigotimes_{k=1}^{N}|0_k\rangle$ ($k \neq i, j$), the system is in fact initialised in the single exci-

tation state $|\psi_1\rangle = |1_i\rangle \bigotimes_{k=1}^{N} |0_k\rangle$ $(k \neq i)$ and evolves into some superposition $|\psi_{temp}\rangle = \sum_{m=1}^{N} \left(c_m |1_m\rangle \bigotimes_{k=1}^{N} |0_k\rangle \right)$ $(k \neq m$ and $\sum_{m=1}^{N} |c_m|^2 = 1)$ before the second injection takes place. Should this be the case, the dynamics that follow are dependent on which injection mechanism is used.

Let us first of all consider the case of injection by Rabi flopping (scenario I). As outlined in section 1.2.3.2, Rabi flopping "inverts" the excitation state of a site, such that $|0\rangle \rightarrow |1\rangle$ and $|1\rangle \rightarrow |0\rangle$. In the case of delayed input of a two excitation state, where the first excitation was injected into site i and a second excitation is injected into site $j \neq i$ at a later time, this will lead to the following:

$$|\psi_{temp}\rangle \rightarrow \sum_{m=1}^{N} \left(c_m |1_m\rangle |1_j\rangle \bigotimes_{k=1}^{N} |0_k\rangle \right) + c_j \bigotimes_{l=1}^{N} |0_l\rangle \tag{6.4}$$

with $k \neq m, j$. The first term of the right-hand side of equation (6.4) represents the vectors resulting of Rabi flopping of an empty site j (so a successful input operation), whereas the second term represents the probability $|c_j|^2$ of performing Rabi flopping on site j when it is occupied, leaving the chain without excitations after the operation. Since a failed injection corresponds to the system containing no excitations afterwards, it is possible to refocus the chain and eliminate this probability. To do so, we assume that the injection succeeded, in which case we know that the mirror twin state of $|\psi_{ideal}\rangle$ should achieve unit fidelity at t_M, meaning that there should be excitations in spins $(N - i + 1)$ and $(N - j + 1)$. By measuring either of these sites at $2t_M$, we will either detect no excitation (collapsing $|\psi_{temp}\rangle$ into the zero excitation subspace), in which case we know that the entire chain is empty and thus also reset for us to re-attempt initialisation, or we will detect an excitation, indicating that the injection was successful (collapsing $|\psi_{temp}\rangle$ into the two excitation subspace). The ability to reliably eliminate all excitations from the chain could also be desirable as a protocol to reinitialise the chain. As we are detecting an excitation at a time when the state of the (ideal) system is known, we are not changing the system state.

In the case of injection by SWAP operation (scenario II)), the result of a mistimed injection of a second injection into what has by then become the evolved single excitation state $|\psi_{temp}\rangle$ is rather different. We described in section 1.2.3.2 how a SWAP operation exchanges the states of a target site i and an external register R, such that $|\phi_i\rangle|\psi_R\rangle \rightarrow |\psi_i\rangle|\phi_R\rangle$. If we therefore inject a delayed second excitation into $|\psi_{temp}\rangle$ at site $j \neq i$, this will lead to the state

$$|\psi_{temp}\rangle \rightarrow \sum_{m=1}^{N} c_m |1_m\rangle |1_j\rangle \bigotimes_{k=1}^{N} |0_k\rangle \otimes |0_R\rangle + c_j |1_j\rangle \bigotimes_{l=1}^{N} |0_l\rangle \otimes |1_R\rangle \tag{6.5}$$

with $k \neq m, j$ and $l \neq j$. Again, the first term on the right-hand side corresponds to the states resulting from a successful injection protocol, while the second term represents the probability $|c_j|^2$ of failed injection due to an excitation having been present at site j. We see from equation (6.5) that there is now unwanted entanglement between the chain and the register. This entanglement can however be lifted by simply measuring the register after the injection to check whether an excitation is present or not: If there is no excitation in the register, it has successfully been injected into the spin chain, which means that $|c_j|^2 = 0$ and leads to a refocussing of the chain. On the other hand, if after injection it is found that the register does contain an excitation, we can deduce that the injection failed and also that the state of the spin chain at the time of the second attempted injection was in fact $|1_j\rangle \otimes_{k=1}^{N} |0_k\rangle$ ($k \neq j$), which gives us renewed knowledge about the state of the chain, allowing for a possible renewed attempt at injection.

The difference between scenarios I) and II) is illustrated in figure 6.7 on the example of a 6-spin chain with $|\psi_{ideal}\rangle = |110000\rangle$. In both cases, the effect of the refocussing at $2t_M$ is clearly visible and leads to an improvement of the fidelity of the desired two excitation state $|\psi_{ideal}\rangle$ while the error terms are eliminated, up to some numerical noise. Despite the rather large delay of $0.1t_M$ between the injections of the two excitations, the fidelity peaks after $2t_M$ for the Rabi flopping in panel (a) still reach nearly 80% while the SWAP fidelity peaks in panel (b) reach over 98%. In both cases, the fidelity peaks now occur at multiples of $2t_M$ plus delay, so in this case $2.1t_M$. In panel (a), we see that the error term, which in the case of Rabi flopping is the zero vector $|000000\rangle$, is eliminated at $2t_M$, when a refocussing measurement was done and an excitation found. Even though the desired vector $|\psi_{ideal}\rangle$ does not reach perfect fidelity, we now know that the system is entirely confined to the two excitation subspace. Had refocussing failed and we had detected no excitation, the zero vector would have reached unit fidelity as in this case we can deduce that the chain is in fact entirely empty and has thus been reinitialised. In panel (b), the error term stemming from input by SWAP operation is the single excitation vector $|100000\rangle$. Again, this vector is eliminated at $2t_M$ due to refocussing, projecting the chain into the two excitation subspace only. The entanglement with the register is now lifted and very high fidelity of $|\psi_{ideal}\rangle$ is achieved. In the case of failed refocussing, where we would detect an excitation in the register, we also disentangle the chain from the register. In this case, we now know that the chain is still in the one excitation subspace, which implies that we also know its dynamics and can re-attempt injection at a later time. This illustrates that refocussing is a very powerful tool in both scenarios, but also that it is
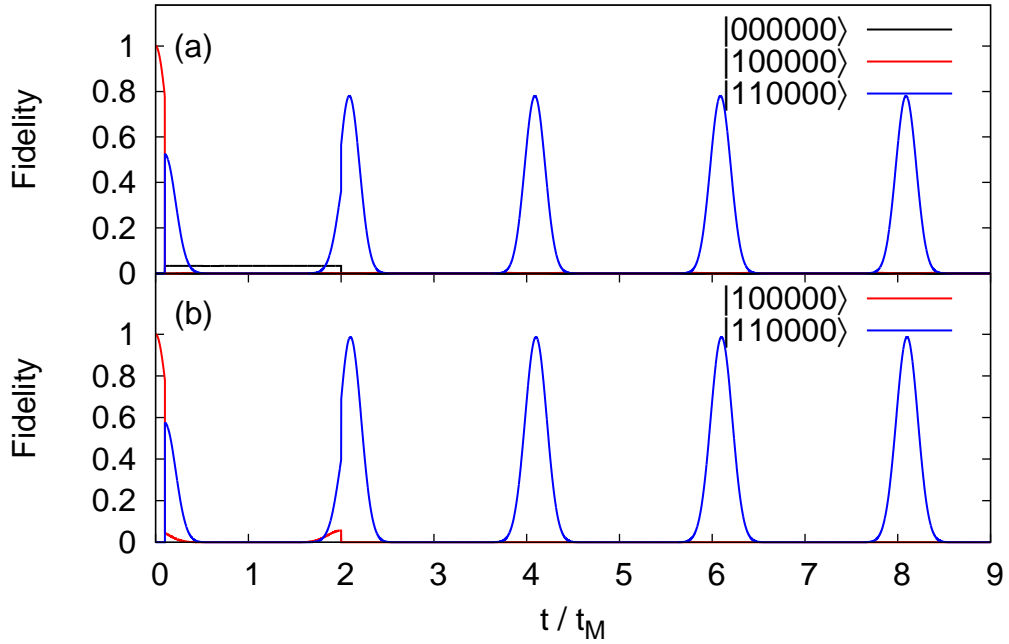
Figure 6.7: Fidelity of $|110000\rangle$ as well as intermediate states with input of the second excitation in a 6-spin chain with $0.1t_M$ delay vs. rescaled time t/t_M:
(a) Injection by Rabi-flopping: The resulting error remains in the system as the zero vector $|000000\rangle$. At $2t_M$ the state of the first spin is measured and an excitation is found, the system is refocused in the two excitation subspace only. The peak of $|110000\rangle$ at $2.1t_M + 2nt_M$ ($n \in \mathbb{Z}^+$) is 0.7807. If at $2t_M$ the second spin is measured instead, the peak fidelity becomes 0.7203.
(b) Injection by SWAP operation: The error remaining in the system is in the one excitation subspace. At $2t_M$ the state of the register is measured and no excitation is found, refocussing to the two excitation subspace only and disentangling the chain from the register. The peak of $|110000\rangle$ at $2.1t_M + 2nt_M$ ($n \in \mathbb{Z}^+$) is 0.9870. Figure adapted from [145].

much more successful in the case of injection by SWAP operation, which is why we will now focus on this type on injection.

If for some reason it is not possible to access two sites simultaneously but the system clock is otherwise known and perfect, it is still possible to achieve a given input state. Provided that the system has a stable period, delayed input might even lead to a wider range of input states using a limited number of input sites. The various effects that delayed input can have on a system are illustrated in figure 6.8 on the example of a 6-spin chain with $|\psi_{ideal}\rangle = |110000\rangle$. In panel (a), there is a rather large delay of $0.15t_M$ between the injection at sites 1 and 2. Despite immediate refocussing after the second injection, the fidelity of $|\psi_{ideal}\rangle$ is henceforth capped at 0.9313, as is the fidelity of its mirror twin, and the peaks are shifted forwards by the delay time. The larger the delay (up to t_M), the lower this cap will be set. If the situation is such that it becomes known that only one excitation has been injected so far, it is possible to salvage the creation of $|\psi_{ideal}\rangle$. This is illustrated in panel (b) of figure 6.8, where there is a delay of $2t_M$ between the two injections. Since we effectively wait for the first excitation to return to its injection site (which it does perfectly, according to the mirroring rule (see [148])), a second injection at this time leads to unit fidelity of both $|\psi_{ideal}\rangle$ and its mirror twin in the following time evolution. It is therefore possible to create multiexcitation input states even if it is only possible to inject a single excitation at a time, provided that the system clock is known and any injections after the first can be done accurately in time. By contrast, panel (c) of figure 6.8 shows the opposite scenario: Here, the second injection is made at the worst possible time, namely t_M. As a result, the occurrence of $|\psi_{ideal}\rangle$ or its mirror twin are negligible (the observed imperfections are due to numerics), the generation of the desired input state has completely failed since the excitation initially injected has been swapped out. This also resets the chain, so that this might be a desirable protocol. However, if again we have sufficient control over the system and are able to inject a second excitation *exactly* delayed by an odd multiple of t_M, we are in fact producing a different input state to the original $|\psi_{ideal}\rangle$, which will then propagate with perfect fidelity. This is illustrated in panel (d) of figure 6.8, where instead of $|\psi_{ideal}\rangle = |110000\rangle$ the new state $|\psi'\rangle = |10010\rangle$ is achieved after a second injection at $3t_M$. Using the same two input sites, we have therefore created two distinct two excitation states, $|\psi_{ideal}\rangle$ and $|\psi'\rangle$, both experiencing PST, which is a useful feature for example in the case that not all sites are suitable for input.

Comparing panel (b) from figure 6.7 and panel (a) of figure 6.8, we see that an increase in the delay time leads to a decrease in the fidelity of the desired state. This decrease is however not linear and depends on the type of injection
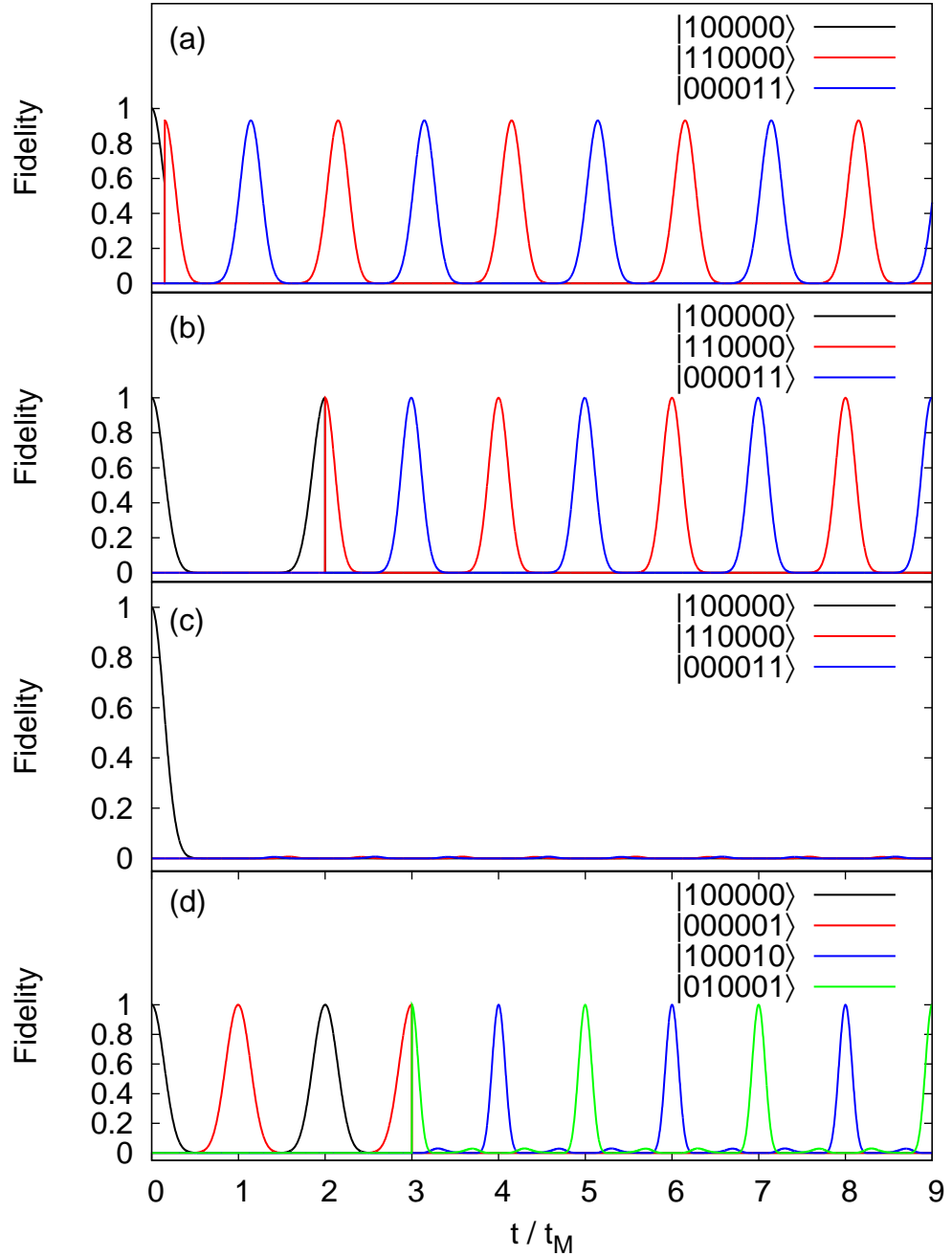
Figure 6.8: Effects of delayed input of a second excitation on a 6-spin chain with SWAP operation given by fidelity vs. rescaled time t/t_M.
(a) input delayed by $0.15 t_M$.
(b) input delayed by an even multiple of t_M (here: $2t_M$).
(c) input delayed by an odd multiple of t_M (here: $1t_M$).
(d) input delayed by an odd multiple of t_M (here: $3t_M$): Creation of a different input state.
For (a) the maximum recurring fidelity of $|000011\rangle$ is 0.9313, at odd integer multiples of t_M plus the delay. For (b), due to the complete period delay, $|000011\rangle$ emerges with unit fidelity, whereas for (c) the occurrence is negligible (observed imperfections are due to numerics). For (d), the occurrence of $|000011\rangle$ is also negligible but instead $|010001\rangle$ and its mirror twin $|100010\rangle$ emerge with unit fidelity. Figure adapted from [145].
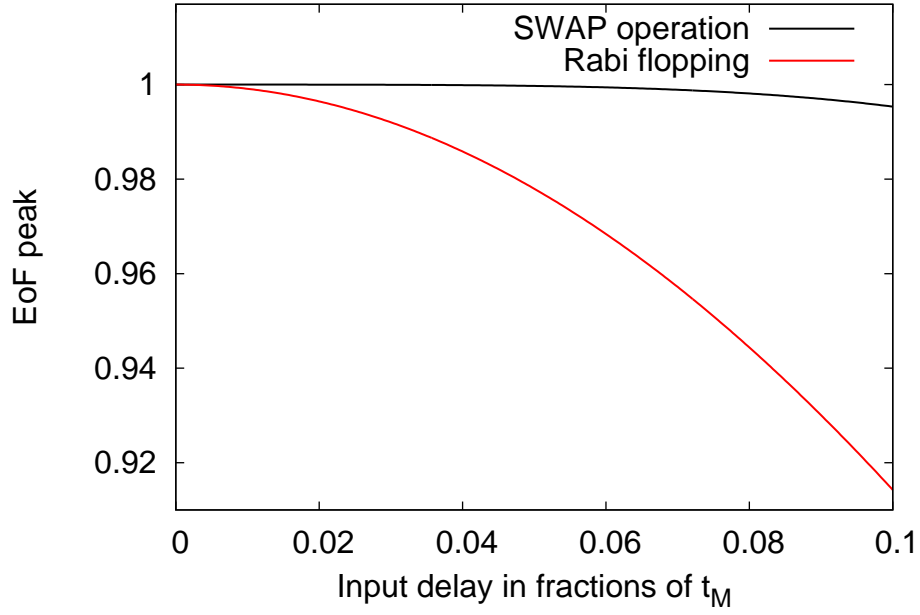
Figure 6.9: Maximum value of the first EoF peak at $2t_M$ vs input delay for a 6-spin chain with type ii) initially entangled input state $|\psi_A\rangle = \frac{1}{\sqrt{2}}(|100000\rangle + |010000\rangle)$ for injection by both Rabi flopping and SWAP operation. Figure published in [145].

protocol used. We see in figure 6.9 that there is a significant difference in the decay of the EoF peak for the input state $|\psi_A\rangle = \frac{1}{\sqrt{2}}(|100000\rangle + |010000\rangle)$ between injection by SWAP operation and Rabi flopping. It is crucial to note that refocussing is not possible in the Rabi flopping protocol here, as the two injection sites are entangled and measurement of either would destroy $|\psi_A\rangle$. This problem does not occur for injection by SWAP operation, as here the register is measured so there is no effect on the chain other than disentanglement from the register. We assume that the refocussing for the SWAP operation is effected immediately after injection. As the two input sites are next to each other, there is a larger probability that the first excitation will have spread to an adjacent site and so there is a clear discrepancy between input by Rabi flopping, where refocussing is not possible, and the SWAP operation, where refocussing is instantaneous. While the EoF peak under Rabi flopping falls off quadratically, the delayed injection by SWAP operation has very little effect on the EoF, to the extent where the EoF peak still reaches more than 99% of its possible entanglement for delays as large as $0.1t_M$. Nonetheless, the effect of delay by Rabi flopping is also relatively small, with the EoF peak losing less than 10% for a serious delay of $0.1t_M$.

If the two input sites are further apart, such as is the case for type iii) input
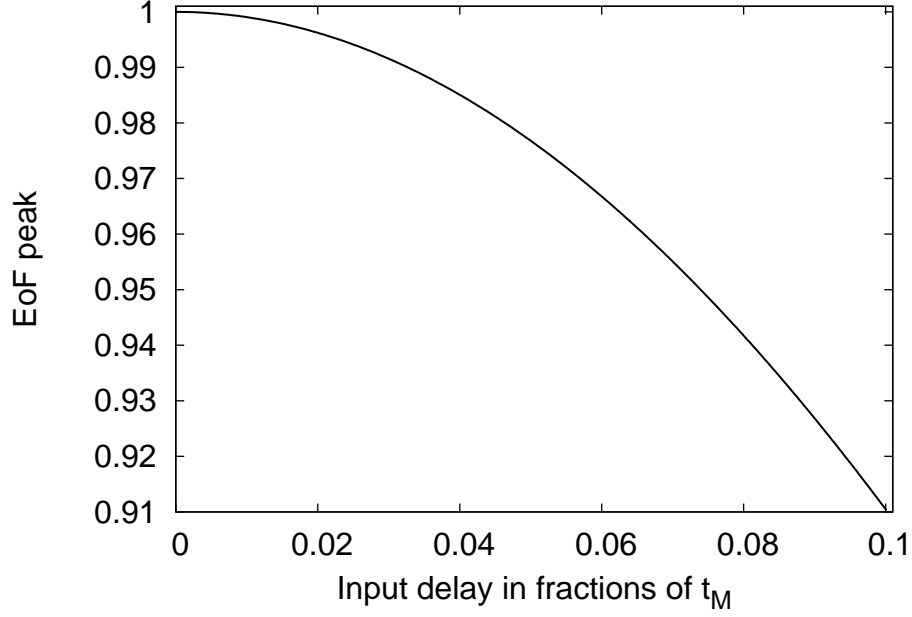
Figure 6.10: Maximum value of the first EoF peak at t_M vs input delay for an 8-spin chain with type iii) initially unentangled input state $|\psi_B\rangle = \frac{1}{2}(|0_1 0_N\rangle + |1_1 0_N\rangle + |0_1 1_N\rangle + |1_1 1_N\rangle) \otimes |0_2 \cdots 0_{N-1}\rangle$ for injection by both Rabi flopping and SWAP operation. Figure published in [145].

where the initial state is of the form $|\psi_B\rangle = \frac{1}{2}(|0_1 0_N\rangle + |1_1 0_N\rangle + |0_1 1_N\rangle + |1_1 1_N\rangle) \otimes |0_2 \cdots 0_{N-1}\rangle$ where only spins 1 and N are non-empty, this discrepancy between injection by Rabi flopping and SWAP operation becomes very small. This is shown in figure 6.10 on the example of an 8-spin chain. Again, due to the entanglement between sites, refocussing is not possible in the case of Rabi flopping and we are assuming that injection by SWAP operation is followed by instantaneous refocussing. We see now that there is virtually no difference between the loss in EoF between injection by Rabi flopping or SWAP operation, as the $|+\rangle$ state injected at the first site will not have spread out sufficiently to have a major effect on the second injection site, provided that the delay is small compared to the transfer time t_M. The more complex input state does make the system more fragile against delay, but the loss in EoF is similar to that of the Rabi flopping in figure 6.9 and the system still achieves more than 90% of its ideal entanglement, even for delay as large as $0.1 t_M$.

This also has consequences on the cluster state knitting protocol of chapter 3, where even for the smallest 4-qubit crossed square cluster state, various delay scenarios arise. Assuming that in the ideal scenario excitations 1 and 2 are injected at $t = 0$ and excitations 3 and 4 are injected at $0.5 t_M$, such that excitations 1 and 3 are injected at site 1 and excitations 2 and 4 are injected at site N (see figure 3.5), the following delay scenarios arise:
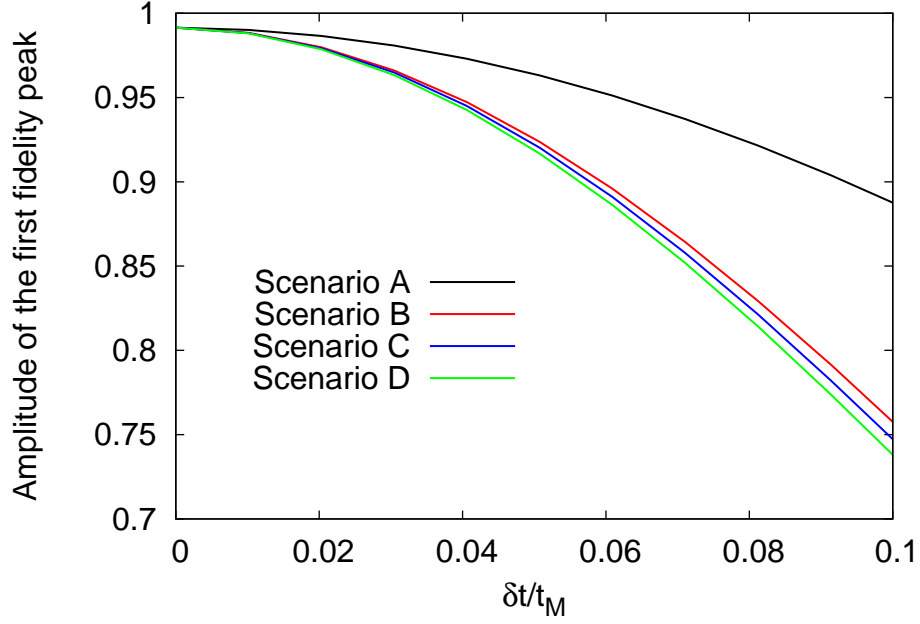
Figure 6.11: Maximum value of the first fidelity peak at $1.5t_M + \delta t$ vs input delay for a 9-spin chain used to knit a 4-qubit crossed square cluster state (using SWAP operation) under delay scenarios A-D. Figure adapted from [42].

- (A): Excitations 3 and 4 are both injected at $t_M/2 + \delta t$

- (B): Excitation 4 is injected at $t_M/2 + \delta t$ (while excitation 3 is on time)

- (C): Excitation 2 is injected at δt and excitation 4 is injected at $t_M/2 + \delta t$ (this corresponds to all injections on one side of the chain being delayed by the same amount)

- (D): Excitation 1 is injected at δt and excitation 4 is injected at $t_M/2 + \delta t$

where δt is the delay in fractions of t_M that the system is subjected to. We assume here that the injections are done by SWAP input, such that refocussing immediately after each injection can be done by measuring the register. The effect of the delay scenarios A-D is summarised in figure 6.11. For moderate values of δt up to $0.05t_M$, the loss in fidelity is less than 10% in all four scenarios. There is a very clear difference between scenario A, where nearly 90% of the fidelity are maintained even for $\delta t = 0.1t_M$, and the other three scenarios, which lose around 25% of the fidelity under the same conditions. This underlines that the system is more reliant on symmetry than on perfect timing. As such, delay of just excitation 4 (scenario B) is much more detrimental to the formation of the desired cluster state than the delay of excitations 3 and 4 together (scenario A), so that if a 10% loss were acceptable, this corresponds to a maximum delay of $0.06t_M$ for scenario B, but $0.095t_M$ for scenario A. This

trend can also be observed when comparing scenarios C and D, where delay
on just one side of the chain is slightly less detrimental than delay on both
sides. Overall, we can confirm that the cluster state knitting protocol is robust
against delayed input for moderate delay values up to $0.05t_M$, with symmetric
delay of the second set of excitations even allowing for delay as large as $0.1t_M$.
It is also worth noting that in all delay scenarios the periodicity of the system
is preserved, so that subsequent fidelity peaks are capped at the value of the
first fidelity peak after completed injections but do not experience further loss
and occur with reliable periodicity.

6.3   Conclusions

We have presented a model for next-nearest neighbour interaction in linear
spin chains and checked its validity against an analytic expression for dipole-
dipole interaction as well as numerical data for graphene quantum dots [141],
finding excellent agreement for the two types of interaction considered. The
effect of $\widehat{\mathcal{H}_\Delta}$ scales as exponential decay with Gaussian damping in Δ for short
spin chains and few excitations, but decays as a simple Gaussian for longer
chains with more excitations, as seen on the example of the chains used for
cluster state knitting. Overall, we have seen that information transfer and the
generation of entanglement are both robust for small values of Δ up to about
0.05 for short and medium chains with few excitations, but that larger values
of Δ (or $\Delta \gtrsim 0.02$ for long chains or chains with many excitations) lead to a
quick decay of the desired states and ultimately also a loss of periodicity. This
poses a severe problem for some protocols, such as cluster state knitting. Sim-
ilarly, longer range couplings, where the perturbation is such that all possible
channels of the spin chain are opened up, result in loss in fidelity and entan-
glement linear in N. Initially unentangled input states leading to entanglement
are most robust against this perturbation; on the whole there are similar effects
regarding loss of periodicity as observed for the next-nearest neighbour inter-
actions, such that experimental implementations should take great care to limit
the influence of this type of perturbation as much as possible, in particular in
longer chains.

We have also considered the effect of delayed input of excitations, both under
Rabi flopping and input by SWAP operation. Both protocols allow for refo-
cussing after injection, unconditionally so for injection by SWAP operations
and for unentangled input states for Rabi flopping. Using refocussing, very
good results can be achieved even for delays of a significant fraction of t_M and
deliberate or controlled delay can even lead to a new range of input states us-

ing only a limited set of input sites. It was found that the effect of delayed input on spin chains with any type of input is limited, making spin chains very robust against this type of operation timing errors. Even in scenarios where multiple rounds of excitations are injected, such as the cluster state knitting protocol, very good state fidelity can be achieved, particularly when the delay is such that it does not disrupt the symmetry of the input.

Chapter 7

Summary and outlook

Over the course of this thesis, we have carried out an extensive investigation into the potential of spin chains as quantum communication devices and also analysed potential uses for spin chains in quantum computation. In addition to the established conditions for PST in linear and Y-type devices, we have presented further PST requirements for a number of additional architectures, as well as their capacities for quantum communication and their elemental limitations. We have discovered that only linear spin chains are capable of perfectly transferring arbitrary input states, i.e., containing any number of excitations and any form of entanglement. While this is a desideratum in any attempt to use the natural dynamics of spin chains for quantum communication, linear spin chains also present a number of additional features which could be of great interest in a quantum computational context.

We found that linear chains with exactly 4 spins are capable of storing Bell states when a simple phase-flip operation is effected, but also that this property does not extend to longer or shorter devices. By contrast, all linear chains contain intrinsic phase gates [171–174] and we found that any chain of length $N = 4k + 1$ ($k \in \mathbb{N}$ and $k \geq 2$) can be used to fabricate a cluster state ladder of arbitrary length [42]. For the cluster state knitting protocol that we have proposed, we require no further tools beyond a linear spin chain of suitable length set up for PST. Using the natural dynamics of the chain alone, we were able to demonstrate the fabrication of a crossed square cluster state and explained how this four-qubit cluster state can reliably be expanded to a cluster state ladder of variable length. We highlighted potential issues with errors resulting from the use of very short chains ($N = 9$) and also found that these imperfect injection errors are very small indeed ($< 2\%$).

Non-linear spin chains were found to be more limited in their potential as quantum communication devices but do in turn open up other uses for spin

chains. We expanded the known results for Y-type chains [74, 132, 157, 158] to double branched chains and found that both of these types of branched devices only support PST for states containing a single excitation. Nonetheless, these devices support the transport of unentangled states as well as entangled states. Compared to linear spin chains, we found that branched spin chain devices are very well suited for both the generation as well as the storage of entangled states. Again, state storage is achieved via a simple phase flip of an individual site, with no modification of the natural dynamics of the spin chain device required.

Another class of non-linear spin chains that we analysed were circular spin chains, where we demonstrated how the addition of two phase gates to a circular chain with two hubs allows for PST of two-excitation states. This represents an important development from single excitation PST [104] but does not permit generalisation to higher excitation subspaces. Furthermore, there are severe restrictions on the type of input state which can be transferred. Expanding on circular devices, we did a limited investigation into circular devices with branches, which we found to be incapable of PST of any type of state with the remarkable exception of the smallest possible, single-branched device: This device was capable of not just transferring both one-excitation and two-excitation states, but also of generating entanglement. Devices consisting of a number of circles without branches also allowed for both one-excitation and two-excitation PST but were found to be incapable of generating any entanglement.

Focussing on linear chains once more, we provided an analysis of several types of perturbations to the dynamics of spin chains [145, 146]. It was found that states containing more excitations are more prone to suffering from loss of transport quality. This was the case for all perturbations observed, and particularly strong for the influence of unwanted interactions between excitations, as well as longer range couplings. The effects of random noise, unwanted on-site energies and unwanted interactions were all found to be non-linear, in particular the effect of large unwanted on-site energies could be modeled using a general analytic formula showing exponential decay with Gaussian damping in the perturbation parameter. For random noise and unwanted interactions between excitations, it was found that entangled initial states with an excitation split over adjacent sites were the most robust.

With regards to the cluster state knitting protocol, on-site energies proved to have the most detrimental effect, which is comparable to the effect of unwanted next-nearest neighbour couplings for very short chains ($N = 9$). For longer chains however, next-nearest neighbour couplings are a far bigger threat

to the generation of cluster states and we concluded that great care should be taken to control these unwanted couplings in any physical implementation.

We demonstrated that our model of next-nearest neighbour couplings is in very good agreement both with an analytic model of dipole-dipole interaction as well as a model based on experimental data of graphene quantum dots [141]. Similar to the influence of unwanted on-site energies, the influence of next-nearest neighbour couplings can be modeled using an analytic formula for exponential decay with Gaussian damping in the perturbation parameter. For very long chains used for the cluster state knitting protocol, the decay in the quality of the achieved crossed square cluster state evolves as a simple Gaussian function. In general, next-nearest neighbour couplings were found to be highly detrimental to any state transfer and can also lead to a very quick loss of periodicity, which is again a serious concern for the cluster state knitting protocol.

Finally, we also considered the possibility of mistimed operations on spin chains as a perturbation, both in the form of Rabi-flopping and SWAP operations. For both these operations, it is however possible to refocus the spin chain after injection. While refocussing does not allow for renewed PST, it significantly enhances the transport quality and thus allows chains to tolerate moderately mistimed operations. This is also true for the generation of a crossed square cluster state, where we analysed a number of delayed input scenarios. Furthermore, we explained how delayed input may also be used intentionally to generate a variety of input states when the number of injection sites is limited.

Based on the investigations we performed, we conclude that spin chains set up for PST and their natural dynamics are an important tool in quantum communication, and also in quantum computing in a wider context, thanks to their varied capacities and uses. While we found that most of the non-linear devices we considered were only of limited potential, an analytic approach might reveal more interesting features. In particular, an analysis of the energy eigenstates of circular devices could be interesting to perform in order to discover any further symmetries or patterns. Similarly, an extended investigation into bigger devices or devices with more excitations could be very useful, in particular with regards to the cluster state knitting protocol, where larger systems would allow for a more extensive error analysis. This was not possible with the simulation code used, but several improvements could be made here: Parallelisation of the core routines would save on computing time, so that a different method for solving the time-independent Schrödinger equation could be used, thus further decreasing the demand of computational resources. Another possibility could be to implement a density-matrix renormal-

isation group method [213].

These improvements are interesting challenges for the future and would enable some still open questions to be pursued. This includes for example the proposed larger cluster state topologies in chapter 3, such as the 6-spin building block to the cluster state knitting protocol or the idea of an additional injection site in the middle of a very long chain.

Beyond the investigation of larger systems with more excitations, there is also scope for research employing spin chains in other fields of quantum information. One such possibility is a demonstration of Anderson localisation, where a linear spin chain could potentially be used to temporarily confine a state to one end of the chain through the systematic use of on-site energies. This is a proposal which we are currently exploring. On the whole, there is a diversity of further possibilities and paths for the study of the natural dynamics of spin chains, and we hope to see many of them examined.

Appendix A

Outline of simulation code

Throughout this thesis, the same code was continuously developed to accommodate all needed features. A basic outline of the structure of the code is given in algorithm 3 below:

Algorithm 3 Basic overall structure of the simulation code used throughout this work.

 1: Initialise the system
 2: Calculate the ECL, J_0 and the PST couplings $J_{i,i+1}$ (as defined in chapter 1)
 3: Write the Hamiltonian $\widehat{\mathscr{H}}$ according to the geometry given
 4: Adjust $\widehat{\mathscr{H}}$ for any perturbations
 5: Use a finite incrementation method to solve the time-dependent Schrödinger equation at every finite time step (see algorithm 4 below)
 6: Renormalise the system to minimise any errors
 7: If relevant, do adjustments for cluster state protocol or simulation of delayed input of excitations
 8: Compute desired measure(s) of information transport quality
 9: Write output

To initialise the system, we need the following information: number of spins, geometry of the device, timing parameters (number of periods the system should run for and number of time steps), initial state of the system and the strength of any perturbations, if present.

When writing the Hamiltonian, we take a crucial computational shortcut: Instead of simulating the entire Hilbert space $\mathfrak{H}$, which has dimension 2^N (see section 1.1.1.1), we only compute the excitation subspaces of $\mathfrak{H}$ which are relevant to the current simulation. This can be justified on the one hand by observing the natural decomposition of $\mathfrak{H}$ into excitation subspaces (see section 1.2.1.2) and on the other hand by noting that the number of excitations is conserved by the natural dynamics, such that any initial state cannot leave the excitation subspace(s) it is initially confined to. Exceptions to this are scenarios such as

the cluster state knitting protocol or simulations of mistimed input operations, where we manually inject and extract excitations. In this case, we compute all subspaces that will be needed over the course of the simulation, instead of simply those of the initial state. The Hamiltonian $\widehat{\mathcal{H}}$ is then accordingly smaller, which leads to a significant saving in computing power.

The core of the code is the solver of the time-dependent Schrödinger equation. The method used for this solver is a finite incrementation method, i.e., one that is based on discrete time steps. If we write $H(j,k)$ for the array storing the Hamiltonian $\widehat{\mathcal{H}}$ and $c(j)$ for the coefficients c_j in the state decomposition $|\psi\rangle = \sum_{j=1}^{q} c_j |\phi\rangle_j$ (with $q = \dim(H)$), we can find the coefficients $c(j, t + \delta t)$ (where δt is a small but finite increment of the time t) according to:

$$i * c(j, t + \delta t) = i * c(j, t) + \delta t * \sum_{k=1}^{q} H(j, k) * c(k, t)$$

$$= i * c(j, t) + \delta t * \Delta c(j, t)$$

$$c(j, t + \delta t) = c(j, t) - i * \delta t * \Delta c(j, t)$$

where $*$ designates multiplication and $i = \sqrt{-1}$. An outline of the pseudo-code describing the implementation of this method is given in algorithm 4. This method for solving the time-dependent Schrödinger equation does not

---

Algorithm 4 Pseudo-code for the solver of the time-dependent Schrödinger equation.

1: **for** all time steps in the simulation **do**
2:   Set storage array Δc to zero
3:   **for** j and k running from 1 to q **do**
4:     $\Delta c(j) = \Delta c(j) + H(j, k) * c(k)$ (update Δc according to the coefficients c)
5:   **end for**
6:   **for** n running from 1 to q **do**
7:     $c(n) = c(n) - i * \delta t * \Delta c(n)$ (update coefficients c)
8:   **end for**
9: **end for**

---

change with the initialisation of the system or the type of analysis we wish to do. While there are other methods for evolving the system in time, this method has the great advantage that it does not require us to find any eigenvalues, a computationally expensive task.

Bibliography

[1] J. Von Neumann. *Mathematical foundations of quantum mechanics*. Princeton University Press, 1955. Translated from "Mathematische Grundlagen der Quantenmechanik" (1932).

[2] T. P. Spiller, W. J. Munro, S. D. Barrett, and P. Kok. An introduction to quantum information processing: applications and realizations. *J. Contemp. Phys.*, 46(6):407, Nov 2005.

[3] S. Wiesner. Conjugate coding. *SIGACT News*, 15(1):78, Jan 1983.

[4] J. Eisert and M. Wilkens. Quantum games. *J. Mod. Opt.*, 47(14-15):2543, Jul 2000.

[5] S. C. Benjamin and P. M. Hayden. Multiplayer quantum games. *Phys. Rev. A*, 64(3):030301(R), Aug 2001.

[6] J. Du, H. Li, X. Xu, M. Shi, J. Wu, X. Zhou, and R. Han. Experimental realization of quantum games on a quantum computer. *Phys. Rev. Lett.*, 88(13):137902, Mar 2002.

[7] P. W. Shor. Polynomial-time algorithms for prime factorization and discrete logarithms on a quantum computer. *SIAM J. Comput.*, 26(5):1484, 1997.

[8] D. Deutsch and R. Jozsa. Rapid solution of problems by quantum computation. *Proc. R. Soc. Lond. A*, 439(1907):553, Dec 1992.

[9] L. K. Grover. A fast quantum mechanical algorithm for database search. In *Proceedings of the twenty-eighth annual ACM symposium on Theory of computing*, STOC '96, page 212, May 1996.

[10] C. H. Bennett, G. Brassard, C. Crépeau, R. Jozsa, A. Peres, and W. K. Wootters. Teleporting an unknown quantum state via dual classical and Einstein-Podolsky-Rosen channels. *Phys. Rev. Lett.*, 70(13):1895, Mar 1993.

[11] D. Bouwmeester, J.-W. Pan, K. Mattle, M. Eibl, H. Weinfurter, and A. Zeilinger. Experimental quantum teleportation. *Nature*, 390(6660):575, Dec 1997.

[12] D. Boschi, S. Branca, F. De Martini, L. Hardy, and S. Popescu. Experimental realization of teleporting an unknown pure quantum state via dual classical and Einstein-Podolsky-Rosen channels. *Phys. Rev. Lett.*, 80(6):1121, Feb 1998.

[13] A. Furusawa, J. L. Sørensen, S. L. Braunstein, C. A. Fuchs, H. J. Kimble, and E. S. Polzik. Unconditional quantum teleportation. *Science*, 282(5389):706, Oct 1998.

[14] P. R. Halmos. *Introduction to Hilbert space and the theory of spectral multiplicity*. Chelsea Publishing Company, New York, 1951.

[15] C. Di Franco, M. Paternostro, and M. S. Kim. Perfect state transfer on a spin chain without state initialization. *Phys. Rev. Lett.*, 101(23):230502, Dec 2008.

[16] C. Di Franco, M. Paternostro, and M. S. Kim. Bypassing state initialisation in perfect state transfer protocols on spin-chains. In *Proceedings of the 5th conference on Theory of quantum computation, communication, and cryptography*, TQC'10, page 168, Berlin, Heidelberg, Feb 2011. Springer-Verlag.

[17] M. Markiewicz and M. Wiesniak. Perfect state transfer without state initialization and remote collaboration. *Phys. Rev. A*, 79(5):054304, May 2009.

[18] M. A. Nielsen and I. Chuang. *Quantum Computation and Quantum Information*. Cambridge University Press, 2000.

[19] L. Amico, A. Osterloh, F. Plastina, R. Fazio, and G. M. Palma. Dynamics of entanglement in one-dimensional spin systems. *Phys. Rev. A*, 69(2):022304, Feb 2004.

[20] W. K. Wootters. Entanglement of formation of an arbitrary state of two qubits. *Phys. Rev. Lett.*, 80(10):2245, Oct 1998.

[21] Z.-H. Ma, Z.-H. Chen, J.-L. Chen, C. Spengler, A. Gabriel, and M. Huber. Measure of genuine multipartite entanglement with computable lower bounds. *Phys. Rev. A*, 83(6):062325, Jun 2011.

[22] X.-H. Gao, S.-M. Fei, and K. Wu. Lower bounds of concurrence for tripartite quantum systems. *Phys. Rev. A*, 74(5):050303, Nov 2006.

[23] R. Blume-Kohout, J. O. S. Yin, and S. J. van Enk. Entanglement verification with finite data. *Phys. Rev. Lett.*, 105(17):170501, Oct 2010.

[24] O. Gühne, B. Jungnitsch, T. Moroder, and Y. S. Weinstein. Multiparticle entanglement in graph-diagonal states: Necessary and sufficient conditions for four qubits. *Phys. Rev. A*, 84(5):052319, Nov 2011.

[25] B. Coecke and A. Kissinger. The compositional structure of multipartite quantum entanglement. In *Proceedings of the 37th international colloquium conference on Automata, languages and programming: Part II*, ICALP '10, page 297, Berlin, Heidelberg, 2010. Springer-Verlag.

[26] A. I. Solomon and C.-L. Ho. Condition for tripartite entanglement. *arXiv:1111.4903*, Nov 2011. To appear in the Proceedings of "Quantum Theory and Symmetries 7", Prague, Aug 7-13, 2011.

[27] Y. S. Weinstein, J. Feldman, J. Robins, J. Zukus, and G. Gilbert. Superoperator analysis of entanglement in a four-qubit cluster state. *arXiv/1011.6336*, Nov 2010.

[28] P. Lougovski, S. J. van Enk, K. S. Choi, S. B. Papp, H. Deng, and H. J. Kimble. Verifying multi-partite mode entanglement of w states. *New J. Phys.*, 11(6):063029, Jun 2009.

[29] V. Viguié, K. Maruyama, and V. Vedral. Work extraction from tripartite entanglement. *New J. Phys.*, 7(1):195, Sep 2005.

[30] S. Tamaryan, A. Sudbery, and L. Tamaryan. Duality and the geometric measure of entanglement of general multiqubit w states. *Phys. Rev. A*, 81(5):052319, May 2010.

[31] H. Zhu, L. Chen, and M. Hayashi. Additivity and non-additivity of multipartite entanglement measures. *New J. Phys.*, 12(8):083002, Aug 2010.

[32] P. Facchi, G. Florio, U. Marzolino, G. Parisi, and S. Pascazio. Classical statistical mechanics approach to multipartite entanglement. *J. Phys. A: Math. Theor.*, 43(22):225303, May 2010.

[33] A. Bayat, S. Pasquale, and S. Bose. Negativity as the entanglement measure to probe the Kondo regime in the spin-chain Kondo model. *Phys. Rev. B*, 81(6):064429, Feb 2010.

[34] G. Vidal and R. F. Werner. Computable measure of entanglement. *Phys. Rev. A*, 65(3):032314, Feb 2002.

[35] V. Coffman, J. Kundu, and W. K. Wootters. Distributed entanglement. *Phys. Rev. A*, 61(5):052306, Apr 2000.

[36] C. H. Bennett, D. P. DiVincenzo, J. A. Smolin, and W. K. Wootters. Mixed-state entanglement and quantum error correction. *Phys. Rev. A*, 54(5):3824, Nov 1996.

[37] Y.-C. Ou and M. S. Byrd. Computable constraints on entanglement-sharing of multipartite quantum states. *Quantum Inf. Comput.*, 10(3&4):0223, Mar 2010.

[38] J. Pipek and I. Nagy. Measures of spatial entanglement in a two-electron model atom. *Phys. Rev. A*, 79(5):052501, May 2009.

[39] Y. S. Weinstein. Entanglement sudden death as an indicator of fidelity in a four-qubit cluster state. *Phys. Rev. A*, 79(5):052325, May 2009.

[40] X. Q. Su, A. M. Wang, X. S. Ma, and L. Qiu. Entanglement sudden death in a spin channel. *J. Phys. A: Math. Theor.*, 40(37):11385, Sep 2007.

[41] T.-Z. Wei, K. Nemoto, P. M. Goldbart, P. G. Kwiat, W. J. Munro, and F. Verstraete. Maximal entanglement versus entropy for mixed quantum states. *Phys. Rev. A*, 67(2):022110, Feb 2003.

[42] R. Ronke, I. D'Amico, and T. P. Spiller. Knitting distributed cluster-state ladders with spin chains. *Phys. Rev. A*, 84(3):032308, Sep 2011.

[43] S. Bose. Quantum communication through spin chain dynamics: an introductory overview. *Contemp. Phys.*, 48(1):13, Jan 2007.

[44] M. Christandl, N. Datta, T. C. Dorlas, A. Ekert, A. Kay, and A. J. Landahl. Perfect transfer of arbitrary states in quantum spin networks. *Phys. Rev. A*, 71(3, Part A):032312, Mar 2005.

[45] I. D'Amico. *Relatively short spin chains as building blocks for an all-quantum dot quantum computer architecture*, chapter 9, page 281. Nova Science Publishers, 2007.

[46] F. Bloch. Nuclear induction. *Phys. Rev.*, 70(7-8):460, Oct 1946.

[47] S. Filippov, V. Vyurkov, and L. Gorelik. Quantum computing based on space states without charge transfer. *Phys. Lett. A*, 374(33):3285, Jul 2010.

[48] A. Kay. Perfect, efficient, state transfer and its application as a constructive tool. *Int. J. Quantum Inf.*, 8(4):641, Mar 2010.

[49] A. Kay. Basics of perfect communication through quantum networks. *Phys. Rev. A*, 84(2):022337, Aug 2011.

[50] S. Bose. Quantum communication through an unmodulated spin chain. *Phys. Rev. Lett.*, 91(20):207901, Nov 2003.

[51] M. Wiesniak. Heisenberg chains cannot mirror a state. *Phys. Rev. A*, 78(5):052334, Nov 2008.

[52] C. Di Franco, M. Paternostro, and M. S. Kim. Quantum state transfer via temporal kicking of information. *Phys. Rev. A*, 81(2):022319, Feb 2010.

[53] L. Banchi, T. J. G. Apollaro, A. Cuccoli, R. Vaia, and P. Verrucchi. Optimal dynamics for quantum-state and entanglement transfer through homogeneous quantum wires. *arXiv/1006.1217*, Jun 2010.

[54] J. Fitzsimons and J. Twamley. Globally controlled quantum wires for perfect qubit transport, mirroring and computing. *Phys. Rev. Lett.*, 97(9):090502, Sep 2006.

[55] G. M. Nikolopoulos, D. Petrosyan, and P. Lambropoulos. Electron wavepacket propagation in a chain of coupled quantum dots. *J. Phys. Condens. Matter*, 16(28):4991, Jul 2004.

[56] M. Christandl, N. Datta, A. Ekert, and A. J. Landahl. Perfect state transfer in quantum spin networks. *Phys. Rev. Lett.*, 92(18):187902, May 2004.

[57] X. Q. Xi, J. B. Gong, T. Zhang, R. H. Yue, and W. M. Liu. Explicit designs of spin chains for perfect quantum state transfer. *Eur. Phys. J. D*, 50(2):193, Dec 2008.

[58] V. Kostak, G. M. Nikolopoulos, and I. Jex. Perfect state transfer in networks of arbitrary topology and coupling configuration. *Phys. Rev. A*, 75(4):042319, Apr 2007.

[59] G. Gualdi, V. Kostak, I. Marzoli, and P. Tombesi. Perfect state transfer in long-range interacting spin chains. *Phys. Rev. A*, 78(2):022325, Aug 2008.

[60] J.-L. Chen and Q.-L. Wang. Perfect transfer of entangled states on spin chain. *Int. J. Theor. Phys.*, 46(3):614, Mar 2007.

[61] M. A. Jafarizadeh and R. Sufiani. Perfect state transfer over distance-regular spin networks. *Phys. Rev. A*, 77(2):022315, Feb 2008.

[62] M. A. Jafarizadeh, R. Sufiani, M. Azimia, and F. Eghbali Fama. Perfect state transfer over interacting boson networks associated with group schemes. *Quantum Inf. Process.*, 11(1):1, Feb 2012.

[63] Y. Li, Z. Song, and C. P. Sun. Perfect transfer of many-particle quantum state via high-dimensional systems with spectrum-matched symmetry. *Commun. Theor. Phys.*, 48(3):445, Sep 2007.

[64] R. Chakrabarti and J. Van der Jeugt. Quantum communication through a spin chain with interaction determined by a Jacobi matrix. *J. Phys. A: Math. Theor.*, 43(8):085302, Feb 2010.

[65] A. Salimi, S. Ghoraishipour, and A. Sorouri. Perfect state transfer via quantum probability theory. *arXiv/1007.3002*, Jul 2010.

[66] Y. Wang and F. Shuang. All possible schemes in XY spin chains for perfect state transfer. *Phys. Rev. A*, 84(1):012307, Jul 2011.

[67] T. Brougham, G. M. Nikolopoulos, and I. Jex. Perfect transfer of multiple excitations in quantum networks. *Phys. Rev. A*, 83(2):022323, Feb 2011.

[68] L. Vinet and A. Zhedanov. How to construct the spin chains with perfect state transfer. *Phys. Rev. A*, 85(1):012323, Jan 2012.

[69] R. J. Angeles-Canul, R. M. Norton, M. C. Opperman, C. C. Paribello, M. C. Russell, and C. Tamon. Perfect state transfer, integral circulants and join of graphs. *Quantum Inf. Comput.*, 10(3):325, Mar 2010.

[70] A. Bernasconi, C. Godsil, and S. Severini. Quantum networks on cube-like graphs. *Phys. Rev. A*, 78(5):052320, Nov 2008.

[71] H. Kobayashi, F. Gall, H. Nishimura, and M. Rötteler. General scheme for perfect quantum network coding with free classical communication. In *ICALP '09: Proceedings of the 36th International Colloquium on Automata, Languages and Programming*, page 622, Berlin, Heidelberg, 2009. Springer-Verlag.

[72] Y. Ge, B. Greenberg, O. Perez, and C. Tamon. Perfect state transfer, graph products and equitable partitions. *Int. J. Quantum Inf.*, 9(3):823, Apr 2010.

[73] C. Godsil. State transfer on graphs. *Discrete Mathematics*, 312(1):129, Jan 2011.

[74] I. D'Amico, B. W. Lovett, and T. P. Spiller. Branching spin chain dynamics. *J. Magn. Magn. Mater.*, 321(8):949, Apr 2009.

[75] D. Burgarth, K. Maruyama, and F. Nori. Coupling strength estimation for spin chains despite restricted access. *Phys. Rev. A*, 79(2):020305, Feb 2009.

[76] N. Y. Yao, L. Jiang, A. V. Gorshkov, Z.-X. Gong, A. Zhai, L.-M. Duan, and M. D. Lukin. Robust state transfer in random unpolarized spin chains. *Phys. Rev. Lett.*, 106(4):040505, Jan 2011.

[77] D. Burgarth, K. Maruyama, M. Murphy, S. Montangero, T. Calarco, F. Nori, and M. B. Plenio. Scalable quantum computation via local control of only two qubits. *Phys. Rev. A*, 81(4):040303(R), Apr 2010.

[78] A. Wójcik, T. Łuczak, P. Kurzyński, A. Grudka, T. Gdala, and M. Bednarska. Unmodulated spin chains as universal quantum wires. *Phys. Rev. A*, 72(3):034303, Sep 2005.

[79] T. Shi, Y. Li, Z. Song, and C. P. Sun. Quantum-state transfer via the ferromagnetic chain in a spatially modulated field. *Phys. Rev. A*, 71(3, Part A):032309, Mar 2005.

[80] S. Bose, B.-Q. Jin, and V. E. Korepin. Quantum communication through a spin-ring with twisted boundary conditions. *Phys. Rev. A*, 72(2):022345, Feb 2005.

[81] S. Oh, Y.-P. Shim, M. Friesen, and X. Hu. Effect of randomness on quantum data buses of heisenberg spin chains. *arXiv/1012.0288*, Dec 2010.

[82] A. Wójcik, T. Łuczak, P. Kurzyński, A. Grudka, T. Gdala, and M. Bednarska. Multiuser quantum communication networks. *Phys. Rev. A*, 75(5):022330, Feb 2007.

[83] S. Yang, Z. Song, and C. P. Sun. Quantum dynamics of tight-binding networks coherently controlled by external fields. *Front. Phys. China*, 2(1):1, Oct 2007.

[84] T. Linneweber, J. Stolze, and G. S. Uhrig. Perfect state transfer in xx chains induced by boundary magnetic fields. *arXiv/1111.2686*, Nov 2011.

[85] P. Cappellaro, L. Viola, and C. Ramanathan. Coherent state transfer via highly mixed quantum spin chains. *Phys. Rev. A*, 83(3):032304, Mar 2011.

[86] M. B. Plenio, J. Hartley, and J. Eisert. Dynamics and manipulation of entanglement in coupled harmonic systems with many degrees of freedom. *New J. Phys.*, 6(1):36, Mar 2004.

[87] T. S. Cubitt and J. I. Cirac. Engineering correlation and entanglement dynamics in spin systems. *Phys. Rev. Lett.*, 100(18):180406, May 2008.

[88] S. G. Schirmer and P. J. Pemberton-Ross. Fast high-fidelity information transmission through spin-chain quantum wires. *Phys. Rev. A*, 80(3):030301(R), Sep 2009.

[89] H. Wichterich and S. Bose. Exploiting quench dynamics in spin chains for distant entanglement and quantum communication. *Phys. Rev. A*, 79(6):060302(R), Jun 2009.

[90] L. F. Santos. Creation of stable multipartite entangled states in spin chains with defects. *Int. J. Quantum Inf.*, 4(3):563, 2006.

[91] K. Maruyama and F. Nori. Entanglement purification without controlled-not gates by using the natural dynamics of spin chains. *Phys. Rev. A*, 78(2):022312, Aug 2008.

[92] L. Dai, Y. P. Feng, and L. C. Kwek. Engineering quantum cloning through maximal entanglement between boundary qubits in an open spin chain. *J. Phys. A: Math. Theor.*, 43(3):035302, Dec 2009.

[93] H.-H. Tu and M. Sanz. Exact renormalisation in quantum spin chains. *Phys. Rev. B*, 82(10):104404, Sep 2010.

[94] A. Kay. Interfacing with Hamiltonian dynamics. *Phys. Rev. A*, 79(4):042330, Apr 2009.

[95] A. V. Gorshkov, J. Otterbach, M. Fleischhauer, T. Pohl, and M. D. Lukin. Photon-photon interactions via Rydberg blockade. *Phys. Rev. Lett.*, 107(13):133602, Sep 2011.

[96] E. Safonov and O. Lychkovskiy. Spin dynamics in finite cyclic xy model. *arXiv/1109.4127*, Sep 2011.

[97] D. Burgarth and S. Bose. Conclusive and arbitrarily perfect quantum-state transfer using parallel spin-chain channels. *Phys. Rev. A*, 71(5):052315, May 2005.

[98] Z.-M. Wang, B. Shao, and J. Zou. Enhanced entanglement transfer by phase-shift control in two parallel Heisenberg spin chains. *J. Phys. A: Math. Theor.*, 40(30):9067, Jul 2007.

[99] A. Perales and M. B. Plenio. Manipulating quantum information by propagation. *J. Opt. B: Quantum Semiclassical Opt.*, 7(12):S601, Dec 2005.

[100] M.-H. Yung. Spin star as switch for quantum networks. *J. Phys. B: At. Mol. Opt. Phys.*, 44(13):135504, Jun 2011.

[101] Z. Jiang, Q. Chen, and S. Wan. Optimal $1 \to m$ universal quantum cloning via spin networks. *Phys. Rev. A*, 76(3):034302, Sep 2007.

[102] A. Kay. Unifying quantum state transfer and state amplification. *Phys. Rev. Lett.*, 98(1):010501, Jan 2007.

[103] S. Yang, Z. Song, and C. P. Sun. Beam splitter for spin waves in quantum spin network. *Eur. Phys. J. B*, 52(3):377, Aug 2006.

[104] A. Kay and M. Ericsson. Geometric effects and computation in spin networks. *New J. Phys.*, 7(1):143, Jun 2005.

[105] T. Tufarelli and V. Giovannetti. High-fidelity state transfer in binary-tree spin networks. *Phys. Rev. A*, 79(2):022313, Feb 2009.

[106] S. Perseguers. Fidelity threshold for long-range entanglement in quantum networks. *Phys. Rev. A*, 81(1):012310, Jan 2010.

[107] M.-H. Yung, S. C. Benjamin, and S. Bose. Processor core model for quantum computing. *Phys. Rev. Lett.*, 96(22):220501, Jun 2006.

[108] G. De Chiara, R. Fazio, C. Macchiavello, S. Montangero, and G. M. Palma. Quantum cloning in spin networks. *Phys. Rev. A*, 70(6):062308, Dec 2004.

[109] H. L. Deng and X. M. Fang. Quantum cryptography in spin networks. *Chin. Phys. Lett.*, 24(11):3051, Mar 2007.

[110] A. Casaccino, S. Mancini, and S. Severini. Entanglement manipulation via dynamics in multiple quantum spin systems. *Quantum Inf. Process.*, 10(1):107, Feb 2011.

[111] P. J. Pemberton-Ross and A. Kay. Perfect quantum routing in regular spin networks. *Phys. Rev. Lett*, 106(2):020503, Jan 2011.

[112] P. Xue and B. C. Sanders. Nearest-neighbour coupling asymmetry in the generation of cluster states. *Phys. Rev. B*, 82(8):085326, Aug 2010.

[113] F. Troiani. Entanglement in finite spin rings with noncollinear ising interaction. *Phys. Rev. A*, 83(2):022324, Feb 2011.

[114] A. Soeda, Y. Kinjo, P. Turner, and M. Murao. Quantum computation over the butterfly network. *Phys. Rev. A*, 84(1):012333, Jul 2011.

[115] D. Leung, J. Oppenheim, and A. Winter. Quantum network communication - the butterfly network and beyond. *IEEE Trans. Inf. Theory*, 56(7):3478, Jan 2010.

[116] M. Hayashi, K. Iwama, H. Nishimura, R. Raymond, and S. Yamashita. Quantum network coding. In W. Thomas and P. Weil, editors, *STACS 2007*, volume 4393 of *Lecture Notes in Computer Science*, page 610. Springer-Verlag, Feb 2007.

[117] M. Hayashi. Prior entanglement between senders enables perfect quantum network coding with modification. *Phys. Rev. A*, 76(4):040301(R), Oct 2007.

[118] T. J. Osborne and N. Linden. Propagation of quantum information through a spin system. *Phys. Rev. A*, 69(5):052315, May 2004.

[119] Y. Yang, X. P. Xu, and S. Q. Zhu. Entanglement storage through a spin ladder with cyclic interaction. *Eur. Phys. J. D*, 61(3):751, Jul 2011.

[120] B. Roubert, P. Braun, and D. Braun. Large effects of boundaries on spin amplification in spin chains. *Phys. Rev. A*, 82(2):022302, Aug 2010.

[121] V. Srinivasa, J. Levy, and C. S. Hellberg. Flying qubits: A method for encoding and transporting qubits within a dimerized Heisenberg spin-1/2 chain. *Phys. Rev. B*, 76(9):094411, Sep 2007.

[122] S. Bose and V. Korepin. Quantum gates between flying qubits via spin-independent scattering. *arXiv/1106.2329*, Jun 2011.

[123] A. S. Darwaman and S. D. Bartlett. An optical spin-1 chain and its use as a quantum-computational wire. *Phys. Rev. A*, 82(1):012328, Jul 2010.

[124] I. Affleck, T. Kennedy, E. H. Lieb, and H. Tasaki. Rigorous results on valence-bond ground states in antiferromagnets. *Phys. Rev. Lett.*, 59(7):799, Aug 1987.

[125] J. Tejada, E. M. Chudnovsky, E. del Barco, J. M. Hernandez, and T. P. Spiller. Magnetic qubits as hardware for quantum computers. *Nanotechnology*, 12(2):181, Jun 2001.

[126] J. Simon, W. S. Bakr, R. Ma, Tai M. E., P. M. Preiss, and M. Greiner. Quantum simulation of an antiferromagnetic spin chain in an optical lattice. *Nature*, 472(7343):307, Apr 2011.

[127] J. Twamley. Quantum-cellular-automata quantum computing with endohedral fullerenes. *Phys. Rev. A*, 67(5):052318, May 2003.

[128] W. Harneit. Fullerene-based electron-spin quantum computer. *Phys. Rev. A*, 65(3):032322, Feb 2002.

[129] J. Zhang, N. Rajendran, X. Peng, and D. Suter. Iterative quantum-state transfer along a chain of nuclear spin qubits. *Phys. Rev. A*, 76(1):012317, Jul 2007.

[130] C.-Y. Lu, X.-Q. Zhou, O. Gühne, W.-B. Gao, J. Zhang, Z.-S. Yuan, A. Goebel, T. Yang, and J.-W. Pan. Experimental entanglement of six photons in graph states. *Nat. Phys.*, 3(2):91, Jan 2007.

[131] S. M. Giampaolo and F. Illuminati. Long-distance entanglement and quantum teleportation in coupled-cavity arrays. *Phys. Rev. A*, 80(5):050301(R), Nov 2009.

[132] I. D'Amico, B. W. Lovett, and T. P. Spiller. Freezing distributed entanglement in spin chains. *Phys. Rev. A*, 76(3):030302, Sep 2007.

[133] L. Hofstetter, S. Csonka1, J. Nygård, and C. Schönenberger. Cooper pair splitter realized in a two-quantum-dot y-junction. *Nature*, 461(7266):960, Oct 2009.

[134] P. M. Petroff, A. Lorke, and A. Imamoglu. Epitaxially self-assembled quantum dots. *Phys. Today*, 54(5):46, May 2001.

[135] S. Yang, A. Bayat, and S. Bose. Spin state transfer in laterally coupled quantum dot chains with disorders. *Phys. Rev. A*, 82(2):022336, Sep 2010.

[136] P. Cappellaro, C. Ramanathan, and D. G. Cory. Simulations of information transport in spin chains. *Phys. Rev. Lett.*, 99(25):250506, Dec 2007.

[137] J. Zhang, G. L. Long, W. Zhang, Z. Deng, W. Liu, and Z. Lu. Simulation of Heisenberg XY interactions and realization of a perfect state transfer in spin chains using liquid nuclear magnetic resonance. *Phys. Rev. A*, 72(1):012331, Jul 2005.

[138] P. Neumann, R. Kolesov, B. Naydenov, J. Beck, F. Rempp, M. Steiner, V. Jacques, G. Balasubramanian, M. L. Markham, D. J. Twitchen, S. Pezzagna, J. Meijer, J. Twamley, F. Jelezko, and J. Wrachtrup. Quantum register based on coupled electron spins in a room-temperature solid. *Nat. Phys.*, 6(4):249, Apr 2010.

[139] A. Ardavan and G. A. D. Briggs. Quantum control in spintronics. *arXiv/1102.1546*, Feb 2011.

[140] I. D'Amico. Quantum buses and quantum computer architecture based on quantum dots. *arXiv:cond-mat/0511470v1*, Nov 2005.

[141] B. Trauzettel, D. V. Bulaev, D. Loss, and G. Burkard. Spin qubits in graphene quantum dots. *Nat. Phys.*, 3(3):192, Mar 2007.

[142] A. Bertoni, P. Bordone, R. Brunetti, C. Jacoboni, and S. Reggiani. Quantum logic gates based on coherent electron transport in quantum wires. *Phys. Rev. Lett.*, 84(25):5912, Jun 2000.

[143] R. P. Feynman, R. B. Leighton, and M. Sands. *The Feynman lectures on physics*, volume 2. Addison-Wesley Reading, MA, 1964.

[144] A. Peruzzo, A. Laing, A. Politi, T. Rudolph, and J.L. O'Brien. Multimode quantum interference of photons in multiport integrated devices. *Nat. Commun.*, 2:224, 2011.

[145] R. Ronke, T. P. Spiller, and I. D'Amico. Effect of perturbations on information transfer in spin chains. *Phys. Rev. A*, 83(1):012325, Jan 2011.

[146] R. Ronke, T. P. Spiller, and I. D'Amico. Long-range interactions and information transfer in spin chains. *J. Phys: Conf. Ser.*, 286(1):012020, 2011.

[147] C. Bing and S. Zhi. Controlling quantum state transfer in spin chain with confined field. *Commun. Theor. Phys.*, 46(4):749, Oct 2006.

[148] C. Albanese, M. Christandl, N. Datta, and A. Ekert. Mirror inversion of quantum states in linear registers. *Phys. Rev. Lett.*, 93(23):230502, Dec 2004.

[149] P. Karbach and J. Stolze. Spin chains as perfect quantum state mirrors. *Phys. Rev. A*, 72(3):030301, Sep 2005.

[150] F. Bodoky and M. Blaauboer. Production of multipartite entanglement for electron spins in quantum dots. *Phys. Rev. A*, 76(5):052309, Nov 2007.

[151] Y.-C. Ou and H. Fan. Decoherence of a central quantum system coupled to an xy spin chain. *J. Phys. A: Math. Theor.*, 40(10):2455, Feb 2007.

[152] M. L. Hu and H. L. Lian. State transfer in intrinsic decoherence spin channels. *Eur. Phys. J. D*, 55(3):711, Dec 2009.

[153] C. Zhang, S. Zhu, and J. Ren. Entanglement creation and storage in two qubits coupling to an anisotropic Heisenberg spin chain. *Phys. Lett. A*, 373(39):3522, 2009.

[154] T. J. G. Apollaro and F. Plastina. Quantum information storage in the localized state of a spin chain. *Open Systems & Information Dynamics*, 14(1):41, Mar 2007.

[155] Z. Song and C. P. Sun. Quantum information storage and state transfer based on spin systems. *Low Temp. Phys.*, 31(8):686, Aug 2005.

[156] S. M. Giampaolo, F. Illuminati, A. Di Lisi, and S. De Siena. Engineering massive quantum memories by topologically time-modulated spin rings. *Laser Phys.*, 16(10):1411, May 2006.

[157] I. D'Amico, B. W. Lovett, and T. P. Spiller. Creating, distributing and freezing entanglement with spin chains. *arXiv:quant-ph/0702269v2*, Mar 2007.

[158] I. D'Amico, B. W. Lovett, and T. P. Spiller. Creating and preserving multipartite entanglement with spin chains. In *Physica Status Solidi C*, volume 5, page 2481, 2007.

[159] C. Di Franco, M. Paternostro, and M. S. Kim. Nested entangled states for distributed quantum channels. *Phys. Rev. A*, 77(2):020303(R), Feb 2008.

[160] H. J. Briegel and R. Raussendorf. Persistent entanglement in arrays of interacting particles. *Phys. Rev. Lett.*, 86(5):910, Jan 2001.

[161] S. Bartlett and T. Rudolph. Simple nearest-neighbor two-body Hamiltonian system for which the ground state is a universal resource or quantum computation. *Phys. Rev. A*, 74(4):040302(R), Oct 2006.

[162] W. Dür, G. Vidal, and J. I. Cirac. Three qubits can be entangled in two inequivalent ways. *Phys. Rev. A*, 62(6):062314, Nov 2000.

[163] D. M. Greenberger, M. A. Horne, and A. Zeilinger. *Going Beyond Bell's Theorem*, page 69. Kluwer Academic, 1989.

[164] R. Raussendorf and H. J. Briegel. A one-way quantum computer. *Phys. Rev. Lett.*, 86(22):5188, May 2001.

[165] R. Raussendorf, D. E. Browne, and H. J. Briegel. Measurement-based quantum computation on cluster states. *Phys. Rev. A*, 68(2):022312, Aug 2003.

[166] H. J. Briegel, D. E. Browne, W. Dür, R. Raussendorf, and M. Van den Nest. Measurement-based quantum computation. *Nat. Phys.*, 5:19, Jan 2009.

[167] M. A. Nielsen. Cluster-state quantum computation. *Rep. Math. Phys.*, 57(1):147, Jun 2006.

[168] F. Meier, J. Levy, and D. Loss. Quantum computing with spin cluster qubits. *Phys. Rev. Lett.*, 90(4):047901, Jan 2003.

[169] E. Knill, R. Laflamme, and G. J. Milburn. A scheme for efficient quantum computation with linear optics. *Nature*, 409(6816):46, Jan 2001.

[170] T. P. Spiller, K. Nemoto, S. L. Braunstein, W. J. Munro, P. van Loock, and G. J. Milburn. Quantum computation by communication. *New J. Phys.*, 8(2):30, Feb 2006.

[171] M.-H. Yung, D. W. Leung, and S. Bose. An exact effective two-qubit gate in a chain of three spins. *Quantum Inf. Comput.*, 4(3):174, May 2004.

[172] M.-H. Yung and S. Bose. Perfect state transfer, effective gates, and entanglement generation in engineered bosonic and fermionic networks. *Phys. Rev. A*, 71(3):032310, Mar 2005.

[173] S. R. Clark, C. M. Alves, and D. Jaksch. Efficient generation of graph states for quantum computation. *New J. Phys.*, 7(1):124, May 2005.

[174] S. R. Clark, A. Klein, M. Bruderer, and D. Jaksch. Graph state generation with noisy mirror-inverting spin chains. *New J. Phys.*, 9(6):202, Jun 2007.

[175] A. M. Basharov, V. N. Gorbachev, A. I. Trubilko, and E. S. Yakovleva. One-way gates based on EPR, GHZ and decoherence-free states of W class. *Phys. Lett. A*, 373(38):3410, Sep 2009.

[176] A. Cabello, L. E. Danielsen, A. López-Tarrida, and J. R. Portillo. Optimal preparation of graph states. *Phys. Rev. A*, 83(4):042314, Apr 2011.

[177] P. J. Blythe and B. T. H. Varcoe. A cavity-QED scheme for cluster-state quantum computing using crossed atomic beams. *New J. Phys.*, 8(10):231, Oct 2006.

[178] N. B. Lovett and B. T. H. Varcoe. Generation of topologically useful entangled states. *arXiv:1101.1220*, Jan 2011. Accepted for publication in International Journal of Unconventional Computing - special issue: New Worlds of Computation.

[179] M. B. Plenio and F. L. Semiao. High efficiency transfer of quantum information and multiparticle entanglement generation in translation-invariant quantum chains. *New J. Phys.*, 7(1):73, Feb 2005.

[180] Y. Aharonov and D. Bohm. Significance of electromagnetic potentials in the quantum theory. *Phys. Rev.*, 115(3):485, Aug 1959.

[181] K. Maruyama, T. Iitaka, and F. Nori. Enhancement of entanglement transfer in a spin chain by phase-shift control. *Phys. Rev. A*, 75(1):012325, Jan 2007.

[182] C. S. Castro and M. S. Sarandy. Entanglement dynamics via geometric phases in quantum spin chains. *Phys. Rev. A*, 83(4):042334, Apr 2011.

[183] D. Liu and J.-F. Zhang. Effect of disturbance in perfect state transfer. *Chin. Phys.*, 15(2):0272, Feb 2006.

[184] G. De Chiara, D. Rossini, S. Montangero, and R. Fazio. From perfect to fractal transmission in spin chains. *Phys. Rev. A*, 72(1):012323, Jul 2005.

[185] D. Burgarth and S. Bose. Universal destabilization and slowing of spin-transfer functions by a bath of spins. *Phys. Rev. A*, 73(6):062321, Jun 2006.

[186] B. Corn and T. Yu. Modulated entanglement evolution via correlated noises. *Quantum Inf. Process.*, 8(6):565, Dec 2009.

[187] J.-Y. Cai, V. Choudhary, and P. Lu. On the theory of matchgate computations. In *CCC '07: Proceedings of the Twenty-Second Annual IEEE Conference on Computational Complexity*, page 305, Washington, DC, USA, 2007. IEEE Computer Society.

[188] D. X. Kong and A. M. Wang. Quantum-state transfer on spin-chain channels with random imperfections. *Eur. Phys. J. D*, 55(1):211, Oct 2009.

[189] Z.-H. Wang, B.-S. Wang, and Z.-B. Su. Entanglement evolution of a spin chain bath in driving the decoherence of a coupled quantum spin. *Phys. Rev. B*, 79(10):104428, Mar 2009.

[190] D. Petrosyan, G. M. Nikolopoulos, and P. Lambropoulos. State transfer in static and dynamic spin chains with disorder. *Phys. Rev. A*, 81(4):042307, Apr 2010.

[191] C. Di Franco, M. Paternostro, D. I. Tsomokos, and S. F. Huelga. Control-limited perfect state transfer, quantum stochastic resonance, and many-body entangling gate in imperfect qubit registers. *Phys. Rev. A*, 77(6):062337, Jun 2008.

[192] A. O. Lyakhov, D. Braun, and C. Bruder. Role of interference in quantum state transfer through spin chains. *Phys. Rev. A*, 76(2):022321, Aug 2007.

[193] J. Reslen and S. Bose. End-to-end entanglement in Bose-Hubbard chains. *Phys. Rev. A*, 80(1):012330, Jul 2009.

[194] D. I. Tsomokos, M. J. Hartmann, S. F. Huelga, and M. B. Plenio. Entanglement dynamics in chains of qubits with noise and disorder. *New J. Phys.*, 9(3):79, Mar 2007.

[195] F. Galve, D. Zueco, G. M. Reuther, S. Kohler, and P. Hänggi. Creation and manipulation of entanglement in spin chains far from equilibrium. *Eur. Phys. J. Special Topics*, 180(1):237, Jun 2009.

[196] Y.-B. Sheng and F.-G. Deng. Efficient quantum entanglement distribution over an arbitrary collective-noise channel. *Phys. Rev. A*, 81(4):042332, Apr 2010.

[197] D. Burgarth. Quantum state transfer and time-dependent disorder in quantum chains. *Eur. Phys. J. Special Topics*, 151(1):147, 2007.

[198] D. S. Wang, A. G. Fowler, and L. C. L. Hollenberg. Quantum computing with nearest neighbour interactions and error rates over 1%. *Phys. Rev. A*, 83(2):020302(R), Feb 2011.

[199] A. Zwick, G. A. Álvarez, J. Stolze, and O. Osenda. Robustness of spin-coupling distributions for perfect quantum state transfer. *Phys. Rev. A*, 84(2):022311, Aug 2011.

[200] A. Deschner and E. S. Sørensen. Impurity entanglement in the $j - j\_2 - \delta$ quantum spin chain. *J. Stat. Mech: Theory Exp.*, 2011(10):P10023, Oct 2011.

[201] M. Wiesniak. Decoherence through spin chains: toy model. *arXiv/1108.4289*, Aug 2011.

[202] G. A. Baker and P. R. Graves-Morris. *Padé approximants*. Cambridge University Press, 1996.

[203] S. De Rinaldis, I. D'Amico, and F. Rossi. Exciton–exciton interaction engineering in coupled GaN quantum dots. *Appl. Phys. Lett.*, 81(22):4236, Sep 2002.

[204] I. D'Amico and F. Rossi. Field-induced coulomb coupling in semiconductor macroatoms: Application to single-electron quantum devices. *Appl. Phys. Lett.*, 79(11):1676, Jul 2001.

[205] M. Paternostro, G. M. Palma, M. S. Kim, and G. Falci. Quantum-state transfer in imperfect artificial spin networks. *Phys. Rev. A*, 71(4):042311, Apr 2005.

[206] A. Kay. Perfect state transfer: Beyond nearest-neighbor couplings. *Phys. Rev. A*, 73(3):032306, Mar 2006.

[207] T. Bargheer, N. Beisert, and F. Loebbert. Boosting nearest-neighbour to long-range integrable spin chains. *J. Stat. Mech: Theory Exp.*, (11):L11001, Nov 2008.

[208] M. E. Gouvêa and A. S. T. Pires. One-dimensional XY antiferromagnetic Heisenberg model with nearest and next nearest neighbour exchange interactions. *Phys. Status Solidi B*, 242(12):2530, Oct 2005.

[209] C. J. Mewton and Z. Ficek. The characteristic polynomial of the next-nearest-neighbour qubit chain for single excitations. *J. Phys. A: Math. Theor.*, 41(44):445201, Oct 2008.

[210] D. J. J. Farnell and J. B. Parkinson. A coupled-cluster treatment of spin-1/2 systems with nearest and next-nearest neighbour interactions. *J. Phys. Condens. Matter*, 6(28):5521, Jul 1994.

[211] M. Avellino, A. J. Fisher, and S. Bose. Quantum communication in spin systems with long-range interaction. *Phys. Rev. A*, 74(1):012321, Jul 2006.

[212] T. P. Spiller, I. D'Amico, and B. W. Lovett. Entanglement distribution for a practical quantum-dot-based quantum processor architecture. *New J. Phys.*, 9(1):20, Jan 2007.

[213] S. R. White. Density matrix formulation for quantum renormalization groups. *Phys. Rev. Lett.*, 69(19):2863, Nov 1992.